NORTHROP CORPORATION
NORAIR DIVISION
HAWTHORNE, CALIFORNIA

REPORT NUMBER NOR-63-46
(BLC-148)

EXPERIMENTAL AND THEORETICAL INVESTIGATION OF A REICHARDT BODY OF REVOLUTION WITH LOW DRAG SUCTION IN THE NASA-AMES 12 FT. PRESSURE WIND TUNNEL

July 1963

DOWNGRADED AT 3 YEAR INTERVALS
DECLASSIFIED AFTER 12 YEARS
DOD DIR 5200.10

Classification (canceled) (~~changed to~~) by authority of
OCD-065
on 5-14-74 (Date) (Signature) (Rank)
NAVAL ORDNANCE SYSTEMS COMMAND
Department of the Navy

PREPARED BY

Lloyd W. Gross

W. Pfenninger

RETURN TO
BUR. OF NAVAL WEAPONS
TECHNICAL LIBRARY
Dept. of the Navy
Washington 25, D. C.

BHA 55780
COPY NO. 2

REVISIONS

CHANGE	DATE	ENGINEER	PAGES AFFECTED OR REMARKS

ACKNOWLEDGEMENTS

The support of the NASA Ames Research Center during the experiments is greatly appreciated. The authors are indebted, in particular, to G. G. Kenyon and C. Q. Allen, Ames project aerodynamicists, and to the staff of the Ames 12-foot tunnel. In addition, the authors express their appreciation for the help of V. L. Tucker of the Noratr Boundary layer Research Section in the data reduction and preparation of this report.

SUMMARY

Full length laminar flow with very low friction and equivalent total drags was maintained on an 8 to 1 fineness ratio Reichardt body of revolution of 12-foot length by means of boundary layer suction through 113 fine slots up to a length Reynolds number $R_L = 57.76 \times 10^6$. The lowest coefficient of equivalent total drag (based on body wetted area and including the equivalent suction drag) at an angle of attack $\alpha = 0°$ was $C_{D_t} = 2.63 \times 10^{-4}$ at $R_L = 57.76 \times 10^6$ with a corresponding total suction flow coefficient (based on wetted area) $C_{Q_t} = 1.77 \times 10^{-4}$. This value of equivalent total drag is 12 percent of the friction coefficient of a turbulent flat plate at this length Reynolds number.

TABLE OF CONTENTS

		Page
	ACKNOWLEDGEMENTS	i
	SUMMARY	ii
	NOTATION	iv
I.	INTRODUCTION	1
II.	EXPERIMENTAL STUDY	3
	A. Experimental Setup	3
	B. Measurements and Evaluation	6
	C. Experimental Results	10
III.	THEORETICAL STUDY	13
	A. Computation Procedure	13
	B. Theoretical Results	14
IV.	DISCUSSION	15
	REFERENCES	18
	LIST OF TABLES AND FIGURES	20

NOTATION

$c_p(\varphi)$ local drag contribution of boundary layer momentum thickness at a given radial angle φ

C_D $= \frac{D}{q_\infty S}$; coefficient of drag, based on body wetted area S

C_{D_s} $= \sum_{\substack{\text{all}\\ \text{chambers}}} C_{Q_a}(1 - C_{p_a})$; coefficient of drag due to suction power required to accelerate the suction air without losses to undisturbed velocity and pressure

C_{D_t} $= C_{D_s} + C_{D_w}$; coefficient of equivalent total drag

$C_{D_{t\,min}}$ minimum equivalent total drag coefficient

C_{D_w} $= \int_0^{2\pi} c_{D_w}\, d\varphi$; coefficient of wake drag

C_f laminar flat plate friction coefficient

C_p $= \frac{p - p_\infty}{q_\infty}$; pressure coefficient with respect to ambient static pressure p_∞

C_{p_a} $= \frac{p_a - p_\infty}{q_\infty}$; pressure coefficient of individual suction chamber with respect to ambient static pressure p_∞

C_{Q_a} $= \frac{Q_a}{U_\infty S}$; suction coefficient of individual suction chamber based on body wetted area S

C_{Q_t} = $\sum_{\substack{\text{all}\\ \text{chambers}}} C_{Q_a}^*$; total suction coefficient

$C_{Q\ opt}$ optimum total suction coefficient corresponding to minimum equivalent total drag

D drag (lb)

H = $\frac{\delta^*}{\theta}$; boundary layer shape parameter

$\bar{H}$ average boundary layer shape parameter between the value at the boundary layer rake position and the value at infinity

H_{TE} boundary layer shape parameter at the boundary layer rake position of the model

L model length = 12.0 ft.

p_a pressure in the individual suction chamber (lb/ft^2)

p_∞ undisturbed freestream static pressure (lb/ft^2)

q_∞ = $(1/2)\rho U_\infty^2$; undisturbed freestream dynamic pressure (lb/ft^2)

Q_a suction quantity of individual suction chamber (ft^3/sec)

r body radius at axial station x (ft)

r_{TE} body radius at the boundary layer rake position of the model = 3.345 in.

R_L = $\frac{U_\infty L}{\nu}$; Reynolds number based on model length L

R_θ = $\frac{U\theta}{\nu}$; Reynolds number based on boundary layer momentum thickness θ

s distance along the surface of the model (ft.)

S wetted surface area of model = 46.23 ft^2

u velocity in the boundary layer at height y (ft/sec)

U	velocity at the outer edge of the boundary layer (ft/sec)
U_{TE}	potential flow velocity at the boundary layer rake position of the model (ft/sec)
U_∞	undisturbed freestream velocity (ft/sec)
v_o	suction inflow velocity for equivalent area suction (ft/sec)
v_o^*	$= \frac{v_o}{U_\infty}\sqrt{R_L}$; nondimensional suction inflow velocity for equivalent area suction
x	distance along axis of model (ft)
y	distance normal to the surface of the model (ft)
α	angle of attack (degrees)
δ	boundary layer thickness (ft)
δ^*	$= \int_0^\delta (1 - \frac{u}{U})(1 + \frac{y}{r})\,dy$; boundary layer displacement thickness (ft)
δ^*_{TE}	boundary layer displacement thickness at the boundary layer rake position of the model
θ	$= \int_0^\delta \frac{u}{U}(1 - \frac{u}{U})(1 + \frac{y}{r})\,dy$; boundary layer momentum thickness (ft)
θ_{TE}	boundary layer momentum thickness at the boundary layer rake position of the model
θ_∞	wake momentum thickness far behind the model
μ	absolute viscosity (lb - sec / ft^2).

ν $= \frac{\mu}{\rho}$; kinematic viscosity (ft^2/sec)

ρ density ($lb - sec^2/ft^4$)

φ radial angle (degrees)

1. INTRODUCTION

Substantial performance increases of underwater bodies would be possible if extensive or completely laminar boundary layer flow could be maintained over their surfaces by means of boundary layer suction (reference 2 through 5). The question therefore arises as to whether laminar flow can be maintained on underwater bodies of revolution up to the length Reynolds numbers encountered by such bodies cruising at high speeds. In addition, it is desirable to establish data from which the limits of the parameters significant to boundary layer stability on a body of revolution can be deduced for design purposes.

Low drag suction experiments are generally considerably easier to conduct in low turbulence wind tunnels than in water. Since similar flows develop in water and air for the same Reynolds numbers, as long as effects from a free surface and cavitation can be neglected, it was decided to investigate a Reichardt body of revolution of fineness ratio 8, with low drag suction applied through 113 slots, in the Ames 12-foot low turbulence high pressure tunnel. The low level of turbulence and noise of the Ames 12-foot tunnel at high tunnel pressures (reference 6) should enable the maintenance of full length laminar flow on the Reichardt suction body up to considerably higher length Reynolds numbers than the maximum value of 18×10^6 which was observed during the first experiments on the same suction body in the Norair 7- by 10-foot atmospheric low turbulence tunnel (reference 1).

II EXPERIMENTAL STUDY

A. EXPERIMENTAL SETUP

The body shape was an 8:1 fineness ratio Reichardt body of revolution (reference 8) and was chosen to allow comparison with a test model built by the U.S. Naval Ordnance Test Station (NOTS), Pasadena, California, and described in reference 4. The diameter of the Norair model was 18 inches and the body length 144 inches. At the rear of the body was a 6.5 inch diameter sting which served to support the model and provide a passage for ducting suction air out of the model. The body shape was faired smoothly into the sting from 94 to 103% of the body length, using an algebraic equation with five unknowns to allow matching of the ordinate and first and second derivatives of the body shape as well as the ordinate and first derivative of the sting. The final model contour is illustrated in Figure 1 and the coordinates of the shape are given as Table I.

The potential pressure distribution of the body (without sting and at $\alpha = 0°$ angle of attack) was computed for NOTS by A.M.O. Smith, using the method of reference 9, and was experimentally checked by Norair with a nonsuction Reichardt body of revolution utilizing a sting (reference 1, appendix A). The theoretical pressure distribution is shown in Figure 5.

Based on previous low drag suction experiments on a 30° swept laminar suction wing (reference 7) in the Norair 7- by 10-foot and in the Ames 12-foot tunnel and other low drag suction investigations in the Norair 7- by 10-foot tunnel it was estimated that full length laminar

flow should be feasible on the Reichardt body with low drag suction in the Ames 12-foot tunnel up to 40×10^6 to 50×10^6 length Reynolds number. Accordingly, the model was laid out for a design length Reynolds number $R_L = \frac{U_\infty L}{\nu} = 49 \times 10^6$. The boundary layer development along the body was calculated (Figure 6) by means of Raetz' method (reference 10), using the potential flow pressure distribution and the theoretical suction distribution (for equivalent area suction) shown in Figure 6.

On the front part of the body the boundary layer is rather unstable due to the stretching of disturbance vortices in the boundary layer in the region of increasing body radius. In order to rapidly stabilize the boundary layer in this forward area relatively strong suction was applied far forward, followed by decreasing suction in the region of the flat pressure distribution. In order to avoid an excessive thickening of the boundary layer and laminar separation and transition in the region of the rear pressure rise and decreasing body radius, considerably stronger suction was applied in this area of the body. Area suction, being optimum aerodynamically, was closely approached by means of suction through 113 0.003" wide slots located from 2.75% to 99.6% of the body length. The position of the first slot was selected on the basis of transition experiments on a nonsuction Reichardt body of revolution (appendix A of reference 1) extrapolated to high Reynolds numbers. Figure 1 shows the model and details of the suction system. The slot spacing was determined from the theoretical boundary layer development (Figure 6) to be two inches in the region of the flat pressure distribution from 2.75% to 80% of the body

length and one-half inch in the region of the rear pressure rise from 80% to 99.6% of the length where strong suction is required. In order to avoid local flow decelerations at the slot inlets which might lead to flow instabilities in the boundary layer the slot width was chosen approximately equal to the thickness of the sucked boundary layer at the design length Reynolds number of $49 \cdot 10^6$. The suction air passed through the slots and circumferential grooves or small plenum chambers, through holes, drilled in a thicker continuous inner skin, into 13 individual suction chambers. These holes at the same time acted as suction flow metering holes. In addition, in order to avoid any local flow separation at the inlet of the sharp edged suction slots and suction holes located underneath the slots the Reynolds numbers in these slots and holes (based on slot width or hole radius and mean velocity through the slots or holes) was restricted to such low values that the flow through the slots and holes was purely viscous.

The model was built up of an inner shell composed of seven machined tubes bolted together, a nose piece, and outer rings shrunk-fit to the inner shell. Details of the slot and hole system are given in Table II. Suction plenum chambers were turned into the outer rings. During assembly, the outer rings were forced together as they were shrunk-fit onto the inner shell and the slots were subsequently turned into the joint between rings to provide positive control of the slot width. Compartmentation of the model into thirteen suction chambers was accomplished by means of sealed bulkheads. Calibrated suction flow measuring nozzles were mounted in the face of the bulkheads.

Figure 2 is a schematic drawing of the model as it was installed in the NASA-Ames 12-foot pressure wind tunnel and Figure 3 shows the model as it appeared in the wind tunnel test section. Disturbances from the model support system were minimized. The model was held by a tubular sting extension which, in turn, fitted into the body of revolution of the wind tunnel high-speed support system. Streamline sway braces, extending from the sting extension to the wind tunnel walls, were provided as a guard against flutter and could be used to make slight adjustments of the angle of yaw of the model.

From the suction chambers, the suction air passed through calibrated suction flow measuring nozzles mounted in the various bulkheads, and through aluminum tubes to the exterior of the model. Flexible tubing led the suction air out of the test section through fairings fixed to the high-speed support system and to a common suction box located in the wind tunnel balance chamber. Since the experiments were conducted at tunnel pressures varying from two to five atmospheres, suction could be operated by bleeding the suction air into the atmosphere through a sonic throat. The individual suction quantities of the various suction chambers were varied by means of remotely adjustable needle valves located at the inlets to the common suction box and the total rate of suction was controlled by remotely varying the area of the sonic throat.

Flow disturbances from the internal ducting system which might adversely affect the boundary layer on the external surface were minimized by avoiding local flow separations and flow pulsations in the ducting system and by maintaining a steady and uniquely defined duct flow.

B. MEASUREMENTS AND EVALUATION

The objective of this investigation was the study of the behavior of the laminar boundary layer on a Reichardt body of revolution with suction through many fine slots and the determination of the drag characteristics and suction requirements of this body at various Reynolds numbers R_L. At each Reynolds number the suction quantities were varied over a range that included the point of minimum drag.

The pressure drop across the calibrated flow measuring nozzles located at the downstream end of the various suction chambers was measured to evaluate the suction quantities Q_a of the individual suction chambers. The corresponding chamber static pressures were taken at the downstream end of the suction chambers. The lengthwise pressure distribution was recorded by means of twenty-one static pressure orifices located from 2 to 95% of the length. The location of the static pressure orifices is given in Table III. In order to properly set the model at an angle of attack $\alpha = 0°$, four pressure taps arranged 90 degrees from each other were provided at a station 3% of the body length from the nose.

For the determination of the wake drag of the model, the boundary layer velocity profiles at the aft end of the body were measured by means of six boundary layer rakes. The rakes were located at radial stations $\varphi = 0°$ (top of model), 30°, 60°, 180°, 225° and 270° (see Figure 4). Four of the rakes ($\varphi = 0°$, 30°, 180° and 225°) each consisted of twelve flattened total pressure tubes whereas the remaining two ($\varphi = 60°$ and 270°)

consisted of twelve 0.010-inch diameter round total pressure tubes apiece. Round total pressure tubes, which are less sensitive to angle of attack, were used for the side rakes to minimize errors at angles of attack. Each of the rakes had two static pressure tubes displaced one-half inch from the plane of the total pressure tubes.

The state of the boundary layer was observed from the boundary layer measurements at the aft end of the body.

The static pressures in the measuring nozzles, suction chambers and on the external body surface were displayed on a first U-tube manometer panel. The boundary layer rake readings (total and static pressures) were recorded on a second, separate U-tube manometer board. In this manner fluctuations of the total pressure readings from the rakes did not influence the remaining pressure readings. The pressure data were recorded photographically on 70-mm film, which was then read on a filmreading machine. The recording was on punched cards suitable for use on an IBM 7090 digital computer.

The undisturbed freestream static and dynamic pressures p_∞ and q_∞ were determined from wind tunnel calibration curves and calculations of the tunnel wall corrections by the wind tunnel staff. The resultant minimum pressure coefficients showed a scatter of $\pm$ 0.6% of freestream dynamic pressure.

From the measured suction quantities Q_a in the various suction chambers the suction quantity coefficients $C_{Q_a} = \frac{Q_a}{U_\infty S}$ of the individual chambers

and the coefficient $C_{p_a} = 1 - \frac{p_a - p_\infty}{q_\infty} = 1 - C_{p_a}$ of the isentropic pressure rise across a suction compressor necessary to accelerate the suction air to freestream velocity and ambient static pressure without losses, the equivalent suction drag coefficient is

$$C_{D_s} = \sum_{\substack{\text{all} \\ \text{chambers}}} C_{Q_a} (1 - C_{p_a}).$$

Due to the surface curvature of the body at the rake location, a pressure gradient normal to the body existed and was measured by the two static pressure probes mounted on each rake. A linear variation of static pressure was assumed for the determination of the velocity distribution in the boundary layer at the rake location.

For the evaluation of the wake drag, it was assumed that the measured boundary layer profile is first accelerated over a short distance to a constant static pressure equal to the value at the edge of the boundary layer at the rake location. This new fictitious boundary layer profile at constant static pressure can be determined from the continuity and Bernoulli equations (i.e., assuming constant total pressure along streamlines). The wake momentum loss at infinity, which determines the wake drag, can then be evaluated from the momentum thickness of this fictitious boundary layer at constant static pressure according to Squire and Young:

$$C_{D_w} = \frac{2}{S} \int_0^{2\pi} r\, \theta_\infty d\varphi = \left(\frac{U_{TE}}{U_\infty}\right)^{\bar{H}+2} \int_0^{2\pi} \frac{2\, r_{TE}\, \theta_{TE}}{S}\, d\varphi$$

where r_{TE} is the body radius at the measuring station, U_{TE} is the potential

flow velocity at the edge of the boundary layer, $\bar{H}$ is the value of $H = \frac{\delta^*}{\theta}$ in the wake between the boundary layer rake position and infinity and

$$\theta_{TE} = \int_0^{\delta} \frac{u}{U} \left(1 - \frac{u}{U}\right) \left(1 + \frac{y}{r_{TE}}\right) dy$$

$$\delta^*_{TE} = \int_0^{\delta} \left(1 - \frac{u}{U}\right) \left(1 + \frac{y}{r_{TE}}\right) dy$$

Shortly downstream of the rear end of the model $H_{TE} = 1.4$ (turbulent) and $H = 1.0$ at infinity; therefore, $\bar{H} + 2 = 3.2$, and

$$C_{D_W} = \left(\frac{U_{TE}}{U_\infty}\right)^{3.2} \int_0^{2\pi} 2 \frac{r_{TE}\,\theta_{TE}}{S}\, d\varphi$$

For the determination of the total wake drag the momentum thickness as measured by each boundary layer rake (at radial position φ) was determined and a "local" wake drag $c_{D_W}(\varphi)$ was defined as

$$c_{D_W} = \left(\frac{U_{TE}}{U_\infty}\right)^{3.2} \times 2 \frac{r_{TE}\,\theta_{TE}}{S}$$

At an angle of attack $\alpha = 0°$ the total wake drag was then determined from the average value of the local wake drags so that

$$C_{D_W} = 2\pi \times \frac{\left[c_{D_W}(0) + c_{D_W}(30) + c_{D_W}(60) + c_{D_W}(180) + c_{D_W}(225) + c_{D_W}(270)\right]}{6}$$

The equivalent total drag is then the sum of the wake and equivalent suction drags:

$$C_{D_t} = C_{D_W} + C_{D_S}$$

C. EXPERIMENTAL RESULTS

The experimentally determined lengthwise potential flow velocity distribution is shown in Figure 5 and compared with the theoretical potential flow velocity distribution as calculated by the method of reference 9. The experimental and theoretical potential flow velocity distributions agree within 0.2 percent of the freestream velocity. The experimental curve is consistently higher than the theoretical curve in the region from 25 to 70 percent of the length indicating a slight error in the determination of the freestream velocity.

Figures 7 through 52 show the variation of the wake drag coefficient C_{D_w}, the equivalent suction drag coefficient C_{D_s} and the equivalent total drag coefficient C_{D_t} as a function of the total suction flow coefficient C_{Q_t}. At low suction rates, increasing suction moves transition back towards the end of the body, causing a rapid decrease in wake drag and total drag. As suction is increased further, and turbulent bursts are eliminated entirely, the fully laminar boundary layer is merely thinned by additional suction. Since the corresponding decrease of wake drag due to thinning of the laminar boundary layer with increased suction is smaller than the corresponding increase in equivalent suction drag, the equivalent total drag then increases. Thus, a minimum equivalent total drag coefficient $C_{D_{t_{min}}}$ occurs at an optimum total suction flow coefficient $C_{Q_{opt}}$.

The local drag coefficients $c_{D_w}(\varphi)$ as measured by the individual rakes are not shown. Their variation was the same as that of C_{D_w}, their magnitude was approximately $1/2\pi$ that of C_{D_w} and their total deviation from the average was less than 10 percent in most cases.

Figure 53 shows the variation of minimum equivalent total drag coefficient $C_{D_{t_{min}}}$ (including equivalent suction drag) and the corresponding optimum suction coefficient at minimum equivalent total drag $C_{Q_{opt}}$ with length Reynolds number R_L at angle of attack $\alpha = 0°$. The values of $C_{D_{t_{min}}}$ and $C_{Q_{opt}}$ were determined from Figures 7 through 52. Also shown in Figure 53 are the coefficients $C_{D_{t_{min}}}$ and $C_{Q_{opt}}$ as determined in the Norair 7- by 10-foot wind tunnel and given in reference 1.

The lengthwise distributions of the nondimensional suction velocity v_o^* for equivalent area suction are shown in Figure 54 for several selected test numbers at 2 and 5 atmospheres wind tunnel pressure. At their respective Reynolds numbers, the chosen test point was that one closest to minimum equivalent total drag. For comparison, a suction distribution measured during the Norair test and the design suction distribution are also shown. The measured boundary layer velocity profiles corresponding to the suction velocity distributions of Figure 54 are given in Figures 55 through 61.

The variation of the boundary layer velocity profiles, as measured by the top boundary layer rake, with total suction flow coefficient C_{Q_t} is shown in Figures 62 through 68 for several test runs. The test runs are the same as those for which Figures 55 through 61 illustrate individual test points. Only the boundary layer profiles measured by the top rake are shown since those measured by the other rakes are similar.

THIS PAGE IS BLANK.

III. THEORETICAL STUDY

A. COMPUTATION PROCEDURE

The tests points chosen for a detailed analysis of the boundary layer development are listed in Table IV and were those whose lengthwise distributions of nondimensional equivalent area suction velocity are shown in Figure 54. The test points were chosen to cover the complete range of Reynolds numbers and both of the wind tunnel pressures used. At their respective Reynolds numbers the chosen test points were those closest to minimum equivalent total drag.

Development of the boundary layer for the selected test points was calculated by means of Raetz's method (reference 10) on an IBM 7090 high speed digital computer. The method calculates boundary layer profiles at a large number of chordwise steps by a finite difference method. Numerical data defining the boundary conditions is required at each point. For computational stability, these data must be smooth and consistent, and their derivatives are restricted in magnitude so that the differences between points are not too large. For this reason, the input parameters are usually defined as analytic approximations to the given data.

Figure 69 is a comparison of the measured lengthwise velocity distribution and the approximation used for the calculations. The approximation is by a method developed by Goldsmith and can be used whenever it is not necessary that the approximation pass through the defining points (in this case the measured points). The degree of approximation can be

adjusted but in this case it was felt that the approximation was sufficiently close since it fell within the experimental accuracy of the points and the velocity gradients were properly defined. The nondimensional equivalent area suction velocity distribution, used for a given test point is illustrated, along with the measured test points, with the summary of results for that test point. They are shown in Figures 70, 73, 76, 79, 82, 85, and 88.

B. THEORETICAL RESULTS

The computed development of the laminar boundary layer for each of the test points studied is shown in Figures 70, 73, 76, 79, 82, 85 and 88. Shown is the Reynolds number based on the boundary layer momentum thickness $R_\theta = \frac{U\theta}{\nu}$ and the shape parameter $H = \delta^*/\theta$, which is an indication of the boundary layer stability.

In Figures 71, 74, 77, 80, 83, 86 and 89 the theoretical boundary layer profiles at the boundary layer rake positions are compared with the boundary layer velocities as measured by the rake total pressure and static pressure tubes. Also included are the boundary layer parameters momentum thickness θ, displacement thickness δ^*, shape parameters H, momentum thickness Reynolds number R_θ and wake drag coefficient C_{D_w}, as determined from the calculated and measured velocities. The development of the boundary layer along the surface of the model is also illustrated by the boundary layer velocity profiles calculated at a number of axial stations and given in Figures 72a and b, 75a and b, 78a and b, 81a and b, 84a and b, 87a and b, and 90a and b.

IV DISCUSSION

At an angle of attack $\alpha = 0°$ full length laminar flow was maintained on the Reichardt body of revolution with low drag suction up to a length Reynolds number $R_L = 57.8 \times 10^6$ (see Figure 53). The minimum equivalent total drag coefficient (based on wetted area and including equivalent suction drag) was $C_{D_{t_{min}}} = 2.65 \times 10^{-4}$ and the corresponding total suction coefficient was $C_{Q_{opt}} = 1.77 \times 10^{-4}$.

According to Figure 53, the total suction coefficient for minimum equivalent total drag $C_{Q_{opt}}$ decreases very slowly with increasing Reynolds number from approximately $C_{Q_{opt}} = 2 \times 10^{-4}$ at $R_L = 15 \times 10^6$ to $C_{Q_{opt}} = 1.77 \times 10^{-4}$ at $R_L = 57.8 \times 10^6$. This relatively slow decrease in C_Q with Reynolds number is to be expected because the boundary layer becomes more sensitive to disturbances at increasing Reynolds numbers, requiring increasing values of $C_{Q_{opt}} \sqrt{R_L}$ to maintain full length laminar flow at higher length Reynolds numbers. The total equivalent drag then decreases with increasing Reynolds numbers at a considerably slower rate than the laminar friction drag of a flat plate.

However, the sudden increase of suction requirements, characteristic of tests of laminar suction models, as the disturbance level (due to turbulence and noise) of the wind tunnel increases beyond a certain level did not occur during the tests in the 12-foot pressure wind tunnel. (An example of this sudden increase in suction requirements can be seen in the Norair data of Figure 53.) This implies that the Reynolds number limit of the Ames wind tunnel was probably not reached during these tests.

Limitations were rather caused by the appearance of a critical roughness but insufficient time was available to run the tunnel again after locating and removing the roughness.

At the low end of the Reynolds number range ($R_L \cong 17 \cdot 10^6$, see Figure 53) the equivalent total drag measured at Ames was higher, at the same Reynolds number, than that measured in the Norair wind tunnel. In Figure 54 are compared the lengthwise distributions of nondimensional equivalent area suction velocity v_o^* as measured in the two wind tunnels at approximately the same Reynolds number R_L. It can be seen that less suction aft of 85% of the body length was used in the Ames tests than in the Norair tests. According to reference 1 the equivalent total drag of the Reichardt body of revolution is very sensitive to the amount of suction in this area. On the basis of these results it appears that the total equivalent drags of the two cases would match more closely if, in the Ames tests, more suction had been used aft of 85% of the body length at the lower Reynolds numbers.

The calculated boundary layer velocity profiles at the aft end of the model show good agreement with the velocity profiles measured by the boundary layer rakes (Figure 71, 74, 77, 80, 83, 86 and 89). The agreement is especially good between the calculated profile and rakes numbered 1, 2, 3 and 4 which were located at radial angles (measured from the top of the model) $\varphi = 0°$, 30°, 60° and 270° respectively. Rakes 5 and 6, which were located at $\varphi = 225°$ and 180°, have velocity profiles characteristic of the presence of turbulent bursts. This discrepancy suggests the possibility that the rear of the model may have been at a slight angle

of attack such that the bottom of the model was on the leeward side of the wind tunnel flow; although it was known from pressure measurements around the circumference at an axial station near the nose that the model was aligned with the flow in this region. The apparent angle of attack at the rear of the model may have been due to slight angularities of flow already present in the wind tunnel or induced by the mounting system. The slightly increased drag over the bottom of the model also may have been due to subcritical roughness or surface imperfections, but, since the drag increase was present to the same extent over a wide range of Reynolds numbers, roughness effects would not appear to be the reason.

The boundary layer development, as determined from the theoretical computations and presented in Figures 70, 73, 76, 82, 85 and 88, shows similar behavior in the seven cases studied. The momentum thickness Reynolds number increased gradually with length, while the shape parameter H was maintained at a value ranging from 2.4 to 2.3 until 81% of the body length had been traversed. Aft of 81% length the region of the rear pressure rise was starting and increased suction was required sufficient to restrain the growth of R_θ to approximately its previous rate while H was dropping in value. The essentially constant rate of growth of R_θ was maintained up to 90% length, at which time R_θ had achieved a value that increased as length Reynolds number R_L increased and varied from $R_\theta = 2300$ at $R_L = 17.14 \times 10^6$ to $R_\theta = 3600$ at $R_L = 56.74 \times 10^6$.

In the region of the strong pressure rise from 90% length to the rear of the model, the momentum thickness Reynolds number R_θ grew rapidly. The ultimate value of R_θ again depended on length Reynolds number and varied from $R_\theta = 4500$ at $R_L = 17.14 \times 10^6$ to $R_\theta = 5500$ at $R_L = 56.74 \times 10^6$.

REFERENCES

1. Gross, L. W. "Investigation of a Reichardt Body of Revolution with Low Drag Suction in the Norair 7- by 10-Foot Wind Tunnel", Northrop Norair Report NOR-62-126 (BLC-143), September 1962.

2. Lang, T. G. and Brooks, J. D., "Control of Torpedo Boundary Layers by Suction," NOTS TP 2231 (NAVORD Report 6536), April 1959.

3. Pfenninger, W., "Development of a Laminar Flow Torpedo," Northrop Norair Report NA1-58-795 (BLC-113), October 1958, revised April 1960.

4. Lang, T. G., "Investigations of Torpedo Drag Reduction at the Naval Ordnance Test Station," NOTS TP 2651 (NAVWEPS Report 7638), March 1961, (Confidential).

5. Bascom, J. D., "A Feasibility Study of Torpedoes with Boundary Layer Control," NOTS TP 2715 (NAVWEPS Report 7748), June 1961, (Confidential).

6. Boltz, F. W., Kenyon, G. C. and Allen, C. C.; "The Boundary Layer Transition Characteristics of Two Bodies of Revolution, A Flat Plate and an Unswept Wing in a Low Turbulence Wind Tunnel", NASA TN D-309.

7. Pfenninger, W., Gross, L. W., Bacon, J. W. Jr., and Tucker, V. L.; "Experiments on a 30-Degree Swept, 12%-Thick Symmetrical Laminar Suction Wing in the NASA-Ames 12-Foot Pressure Wind Tunnel", Northrop Norair Report NOR 60-108 (BLC-129), November 1961.

8. Munzner, H and Reichardt, H.; "Axially Symmetric Source-Sink Bodies with Predominantly Constant Pressure Distributions," NOTS Technical Memo 808-43, October 1950 (Translation of German Report ZWB/UM/6616).

9. Smith, A. M. O. and Pierce, J.; "Exact Solution of the Neumann Problem. Calculation of Non-Circulatory Plane and Axially Symmetric Flows About or Within Arbitrary Boundaries", Douglas Aircraft Company, Inc., Report ES 26988, April 1958.

10. Raetz, G. S.; "A Method of Calculating Three Dimensional Laminar Boundary Layers of Steady Compressible Flows," Northrop Norair Report NAI-58-73 (BLC-114), December 1957.

11. Pankhurst, R. C. and Holder, D. W., "Wind Tunnel Technique," Sir Isaac Pitman and Sons Ltd., London, 1952.

LIST OF TABLES AND FIGURES

Table No.	Table Title
I	Model Coordinates
II	Characteristics of Model Slot and Metering Hole Design
III	Static Pressure Orifice and Microphone Locations of Model
IV	Test Points Studied for Theoretical Analaysis of Experiments

Figure No.	Figure Title
1	Model Cross Section with Details of Suction Slots
2	Installation Drawing-- Reichardt Body of Revolution with Low Drag Suction in NASA-Ames 12-Foot Pressure Wind Tunnel
3	Reichardt Body of Revolution with Low Drag Suction In NASA-Ames 12-Foot Pressure Wind Tunnel
4	Coordinate System
5	Comparison of Measured and Theoretical Velocity Distributions
6	Design Suction Velocity Distribution and Boundary Layer Development
7-52	Drag C_D Versus Suction Quantity C_{Q_t} for Various Reynolds Numbers R_L and Angles of Attack
53	Variation of Minimum Total Drag $C_{D_{t_{min}}}$ and Suction Coefficient at Minimum Total Drag $C_{Q_{opt}}$ with Length Reynolds Number R_L
54	Lengthwise Distribution of Equivalent Distributed Suction Velocity v_o^* for Several Reynolds Numbers R_L
55-61	Boundary Layer Velocity Profiles as Measured at the Aft End of the Model
62-68	Variation of Aft End Boundary Layer Velocity Profile with Suction Coefficient C_{Q_t}
69	Comparison of Assumed lengthwise Velocity Distribution used for Theoretical Calculations and Measured Test Points

Figure No.	Figure Title
70	Nondimensional Equivalent Distributed Suction Velocity Distribution and Boundary Layer Development for Test Point No. 2
71	Comparison of Calculated and Measured Boundary Layer Velocity Profiles at Rear End of Body for the Conditions of Test Point No. 2
72a, b	Calculated Boundary Layer Profiles at Various Lengthwise Positions s/L for the Conditions of Test Point No. 2
73	Nondimensional Equivalent Distributed Suction Velocity Distribution and Boundary Layer Development for Test Point No. 102
74	Comparison of Calculated and Measured Boundary Layer Velocity Profiles at Rea End of Body for the Conditions of Test Point No. 102
75a, b	Calculated Boundary Layer Profiles at Various Lengthwise Positions s/L for the Conditions of Test Point No. 102
76	Nondimensional Equivalent Distributed Suction Velocity Distribution and Boundary Layer Development for Test Point No. 47
77	Comparison of Calculated and Measured Boundary Layer Velocity Profiles at Rear End of Body for the Conditions of Test Point 47
78a, b	Calculated Boundary Layer Profiles at Various Lengthwise Positions s/L for the Conditions of Test Point No. 47
79	Nondimensional Equivalent Distributed Suction Velocity Distribution and Boundary Layer Development for Test Point No. 117
80	Comparison of Calculated and Measured Boundary Layer Velocity Profiles at Rear End of Body for the Conditions of Test Point No. 117
81a, b	Calculated Boundary Layer Profiles at Various Lengthwise Positions s/L for the Conditions of Test Point No. 117
82	Nondimensional Equivalent Distributed Suction Velocity Distribution and Boundary Layer Development for Test Point No. 262

Figure No.	Figure Title
83	Comparison of Calculated and Measured Boundary Layer Velocity Profiles at Rear End of Body for the Conditions of Test Point No. 262
84a, b	Calculated Boundary Layer Profiles at Various Lengthwise Positions s/L for the Conditions of Test Point No. 262
85	Nondimensional Equivalent Distributed Suction Velocity Distribution and Boundary Layer Development for Test Point No. 268
86	Comparison of Calculated and Measured Boundary Layer Velocity Profiles at Rear End of Body for the Conditions of Test Point No. 268
87a, b	Calculated Boundary Layer Profiles at Various Lengthwise Positions s/L for the Conditions of Test Point No. 268
88	Nondimensional Equivalent Distributed Suction Velocity Distribution and Boundary Layer Development for Test Point No. 287
89	Comparison of Calculated and Measured Boundary Layer Velocity Profiles at Rear End of Body for the Conditions of Test Point No. 287
90a, b	Calculated Boundary Layer Profiles at Various Lengthwise Positions s/L for the Conditions of Test Point No. 287

TABLE I

MODEL COORDINATES

x/L	r/L
0	0
.01	.0163
.03	.0255
.05	.0313
.07	.0357
.10	.0408
.15	.0472
.20	.0519
.25	.0554
.30	.0581
.35	.0601
.40	.0614
.45	.0622
.50	.0625
.55	.0622
.60	.0614
.65	.0601
.70	.0581
.75	.0554
.80	.0519
.85	.0472
.90	.0408
.95	.0313
1.00	.0231
1.03	.0226

TABLE II

CHARACTERISTICS OF MODEL SLOT AND METERING HOLE DESIGN

All slot widths = 0.003 inch

Chamber Number	Slot Number	Slot Position (% length)	Hole Diameter (inch)	Number of Holes (per inch)	Chamber Number	Slot Number	Slot Position (% length)	Hole Diameter (inch)	Number of Holes (per inch)
1	1	2.778	0.0260	11.546	6	29	41.667	0.0465	4.160
	2	4.167	0.0260	12.393		30	43.056	0.0400	4.465
	3	5.556	0.0350	11.277		31	44.444	0.0360	4.861
1	4	6.944	0.0465	8.201		32	45.833	0.0330	5.221
2	5	8.333	0.0465	7.934		33	47.222	0.0300	5.186
	6	9.722	0.0400	8.827		34	48.611	0.0310	5.365
	7	11.111	0.0350	9.711		35	50.000	0.0292	5.365
	8	12.500	0.0310	10.559	6	36	51.389	0.0292	5.365
2	9	13.889	0.0280	11.378	7	37	52.778	0.0330	4.721
3	10	15.278	0.0465	6.920		38	54.167		4.753
	11	16.667	0.0350	8.673		39	55.556		4.753
	12	18.056	0.0310	9.550		40	56.944		4.691
	13	19.444	0.0280	10.197		41	58.333		4.713
	14	20.833	0.0260	10.597		42	59.722		4.734
3	15	22.222	0.0260	9.338		43	61.111		4.762
4	16	23.611	0.0465	5.810		44	62.500		4.795
	17	25.000	0.0370	6.975	7	45	63.889		4.835
	18	26.389	0.0330	7.705	8	46	65.278		4.868
	19	27.778	0.0292	8.313		47	66.667		4.688
	20	29.167	0.0280	8.540		48	68.056		4.738
4	21	30.556	0.0260	8.873		49	69.444		4.726
5	22	31.944	0.0465	4.968		50	70.833		4.698
	23	33.333	0.0370	5.898		51	72.222		4.763
	24	34.722	0.0330	6.441		52	73.611		4.734
	25	36.111	0.0310	6.694		53	75.000		4.711
	26	37.500	0.0292	7.008		54	76.389		4.792
	27	38.889	0.0280	7.143		55	77.778		4.675
5	28	40.278	0.0260	7.283	8	56	79.167	0.0330	4.738

TABLE II (continued)

Chamber Number	Slot Number	Slot Position (% length)	Hole Diameter (inch)	Number of Holes (per inch)
9	57	80.035	0.0260	3.026
	58	80.382		3.304
	59	80.729		3.674
	60	81.076	0.0260	4.071
	61	81.424	0.0280	3.985
	62	81.771	0.0260	4.099
	63	82.118		4.035
	64	82.465		4.059
	65	82.812		4.085
	66	83.160		3.938
	67	83.507		3.922
	68	83.854		3.811
	69	34.201		3.653
	70	84.549		3.540
	71	84.896		3.520
	72	85.243		3.452
9	73	85.590	0.0260	3.382
10	74	85.937	0.0390	[illegible].007
	75	86.285	0.0350	3.948
	76	86.632	0.0330	3.888
	77	86.979	0.0292	4.330
	78	87.326	0.0280	4.833
	79	87.674	0.0260	5.140
	80	88.021		4.882
	81	88.368		4.724
	82	88.715		4.377
	83	89.062		4.290
10	84	89.410	0.0260	4.120
11	85	89.757	0.0420	3.970
	86	90.104	0.0370	4.589
11	87	90.451	0.0320	5.396
11	88	90.799	0.0292	6.200
	89	91.146	0.0260	7.028
	90	91.493		6.544
	91	91.840		6.197
	92	92.187		5.837
	93	92.535		5.621
11	94	92.882	0.0260	5.399
12	95	93.229	0.0465	4.538
	96	93.576	0.0380	5.633
	97	93.924	0.0320	6.775
	98	94.271	0.0292	7.623
	99	94.618	0.0280	8.336
	100	94.965	0.0260	8.536
	101	95.312		8.042
	102	95.660		7.634
12	103	96.007	0.0260	7.364
13	104	96.354	0.0465	5.446
	105	96.701	0.0400	6.379
	106	94.049	0.0360	7.140
	107	97.396	0.0320	8.147
	108	97.743	0.0310	8.760
	109	98.090	0.0280	9.624
	110	98.437	0.0260	10.526
	111	98.785		9.363
	112	99.132		8.625
13	113	99.479	0.0260	8.096

TABLE III

STATIC PRESSURE ORIFICE AND MICROPHONE LOCATIONS OF LAMINAR SUCTION MODEL

Static Orifice Number	Position (% length)	Microphone Number	Position (% length)
1	2.00	1	12.847
2a, b, c, d	3.00	2	30.903
3	5.00	3	50.694
4	7.50	4	63.194
5	10.00	5	78.125
6	15.00	6	84.375
7	20.00	7	88.542
8	25.50	8	92.361
9	30.00	9	97.222
10	35.00		
11	40.00		
12	45.00		
13	55.00		
14	60.00		
15	65.00		
16	70.00		
17	75.25		
18	80.00		
19	85.00		
20	90.00		
21	95.00		

TABLE IV

TEST POINTS STUDIED FOR THEORETICAL ANALYSIS OF EXPERIMENTS

Run No.	R_L	Wind Tunnel Pressure (Atmospheres)	$C_{Q_t} \times 10^4$	$C_{Q_t}/C_{Q_{opt}}$
2	17.136	1	2.050	
102	22.166	1	1.979	1.041
47	30.228	4	1.696	.974
117	30.449	1	2.007	1.014
262	38.036	4	1.860	.979
268	46.050	4	1.818	.977
287	56.740	4	1.789	.988

L. W. Gross	NORTHROP CORPORATION CHANCE VISION	60 NO: 63-46 (BIC-14
July 1963		

FIGURE 38

DRAG C_D VERSUS SUCTION QUANTITY C_{Q_c} FOR VARIOUS

REYNOLDS NUMBERS R_L AND ANGLES OF ATTACK

$R_L = 50.14 \times 10^6$

$\alpha = 0°$

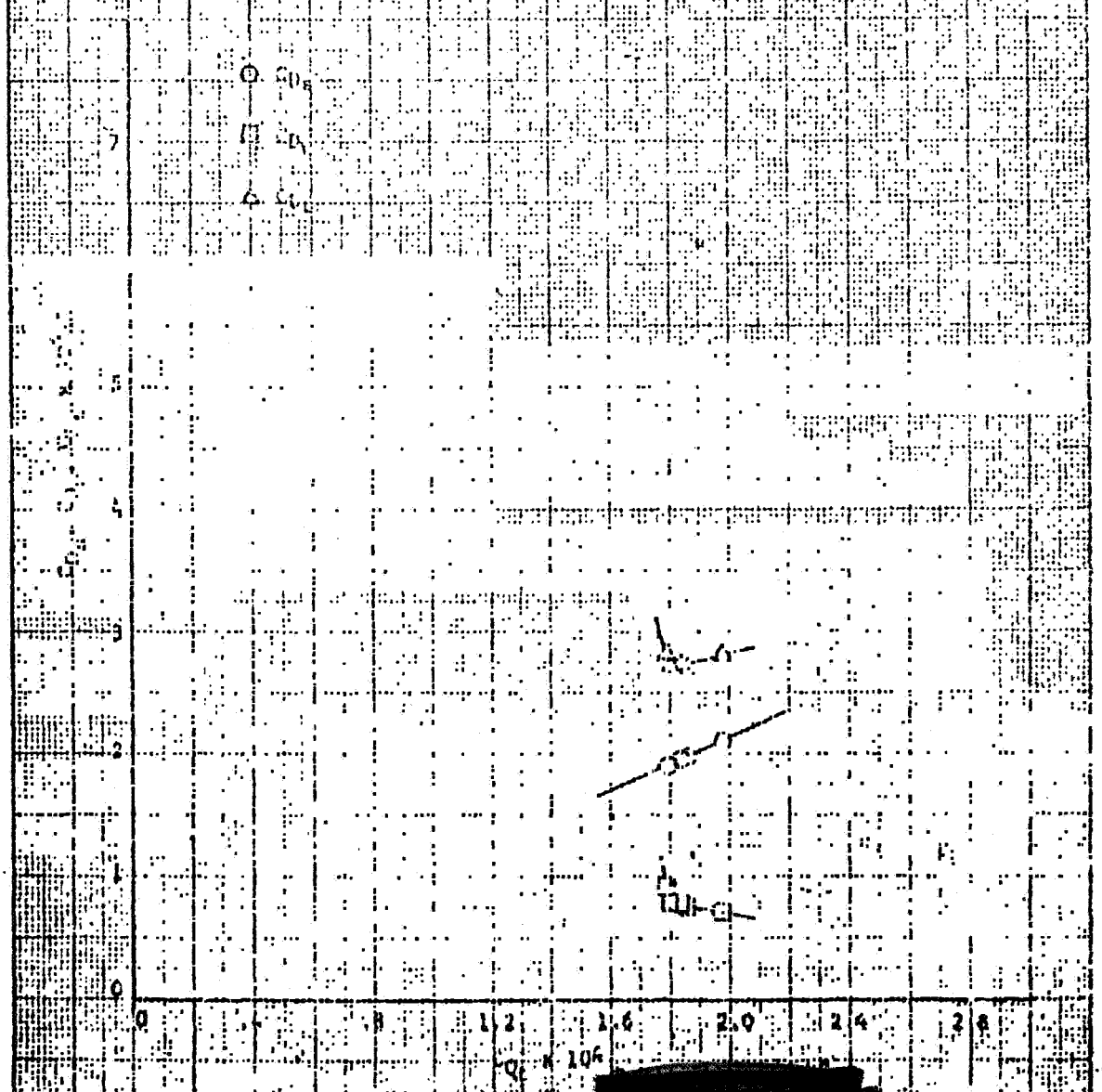

[redacted]

ENGINEER	NORTHROP CORPORATION	PAGE
L. W. Gross	NORAIR DIVISION	51
CHECKED		REPORT NO.
DATE		MODEL
July 1963		

FIGURE 39

DRAG C_D VERSUS SUCTION QUANTITY C_Q FOR VARIOUS REYNOLDS NUMBERS R_L AND ANGLES OF ATTACK

$R_L = 50.68 \times 10^6$

$\alpha = 0°$

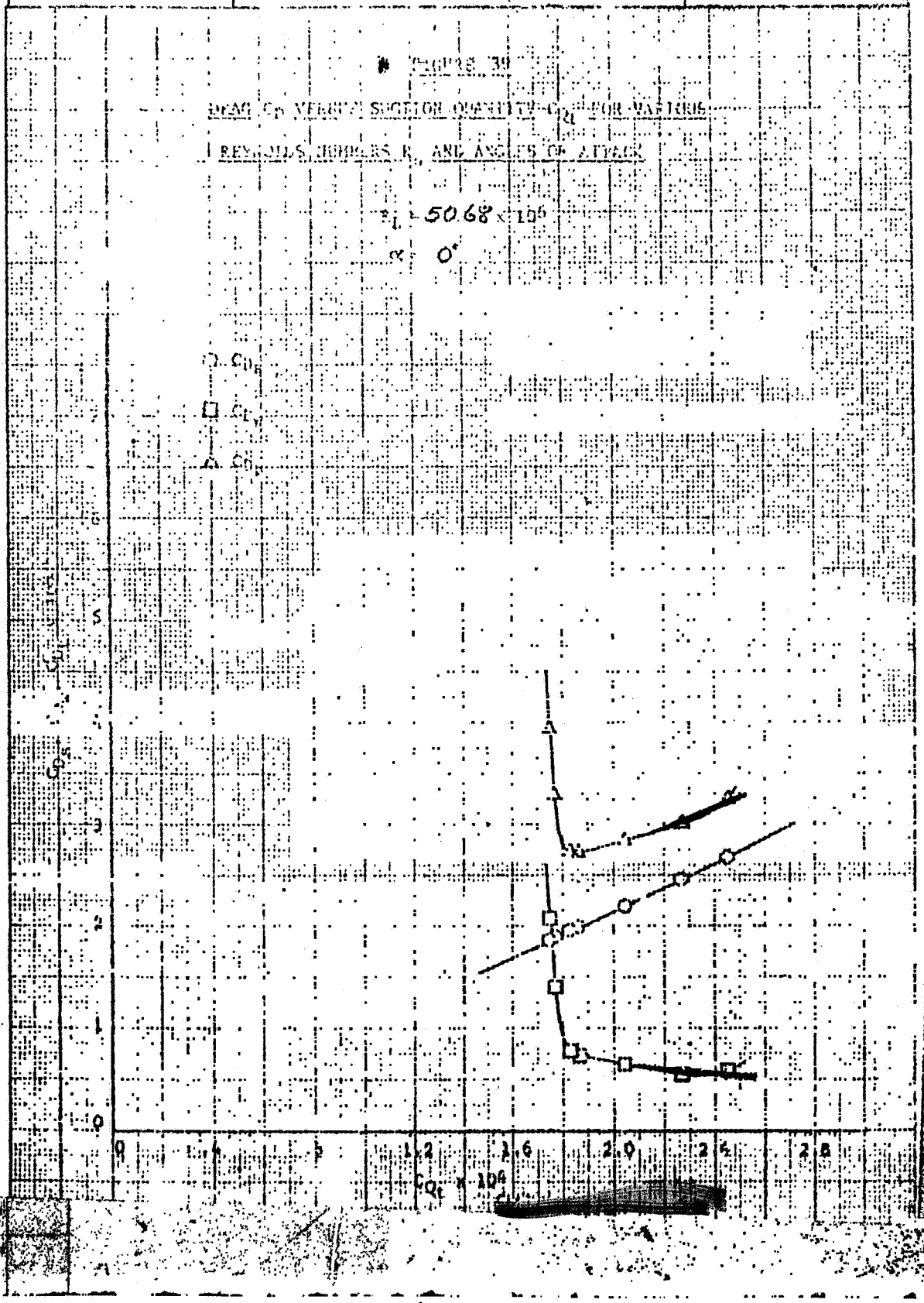

ENGINEER: L. W. Gross	NORTHROP CORPORATION [illegible] DIVISION	PAGE: 62
CHECKED:		REPORT NO.: [illegible] 63-46 (BLC-[illegible])
DATE: July 1963		MODEL:

FIGURE 43

DRAG C_D VERSUS SUCTION QUANTITY C_{Q_t} FOR VARIOUS

REYNOLDS NUMBER ΣP_L AND ANGLES OF ATTACK

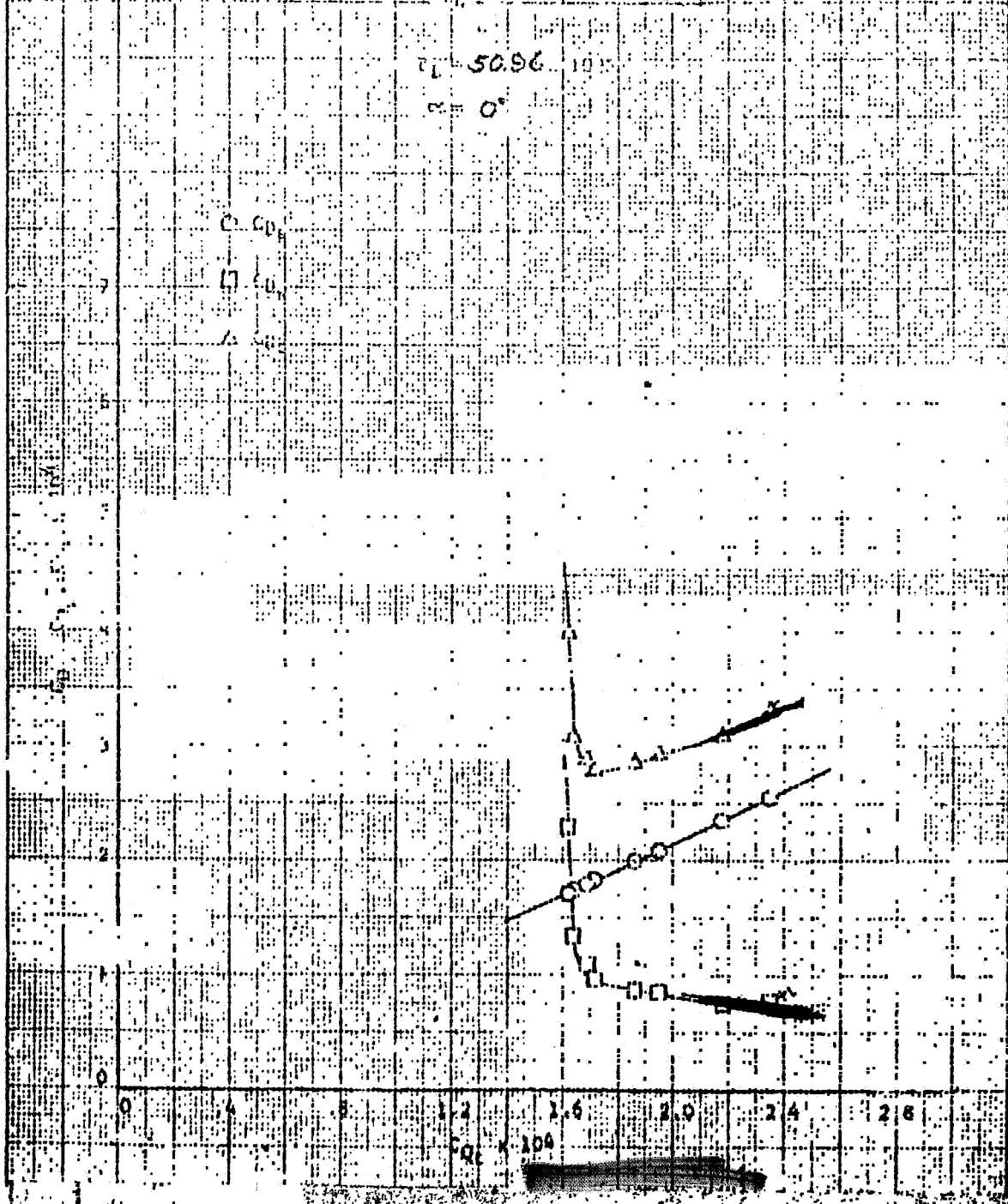

ENGINEER L. W. Gross	NORTHROP CORPORATION NORAIR DIVISION	PAGE 43
CHECKED		REPORT NO. NOR 63-46 (BLC-1[illegible])
DATE July 1963		MODEL

FIGURE 41

DRAG C_D VERSUS SUCTION QUANTITY C_Q FOR VARIOUS COUNTER PRESSURES R_L AND ANGLES OF ATTACK

$R_L = 51.04 \times 10^{[illegible]}$

$\alpha = 0°$

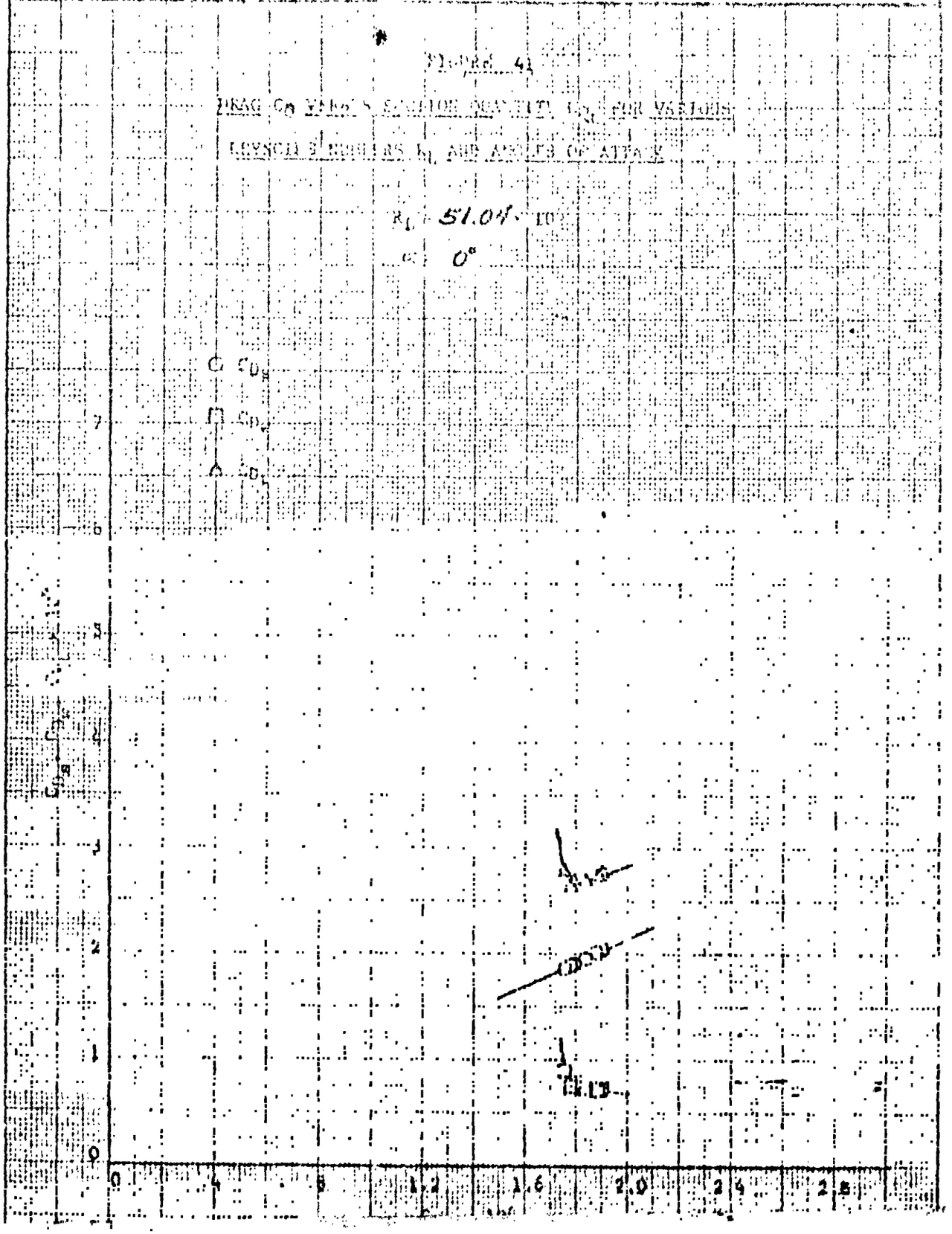

FIGURE 42

DRAG C_D VERSUS SUCTION QUANTITY C_{Q_L} FOR VARIOUS REYNOLDS NUMBERS R_l AND ANGLES OF ATTACK

$R_l = 51.07 \times 10^6$

$\alpha = 0°$

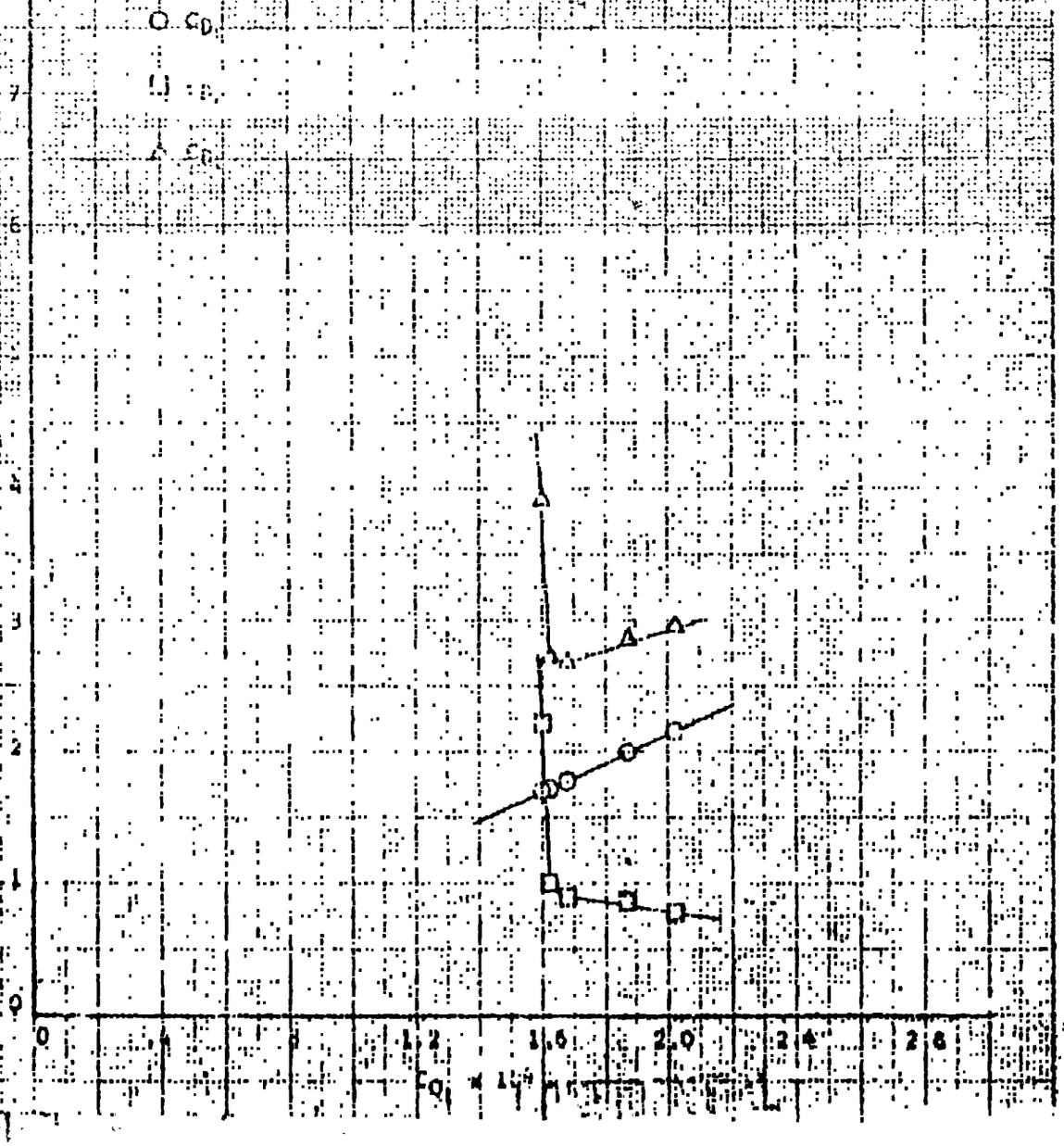

ENGINEER	NORTHROP CORPORATION	PAGE
L. W. Gross	NORAIR DIVISION	65
CHECKER		REPORT NO. NOR 63-46 (LLC-148)
DATE July 1963		MODEL

FIGURE 43

DRAG C_D VERSUS SUCTION QUANTITY C_{Q_L} FOR VARIOUS REYNOLDS NUMBERS R_L AND ANGLES OF ATTACK

$R_L = 51.12 \times 10^5$

$\alpha = 0°$

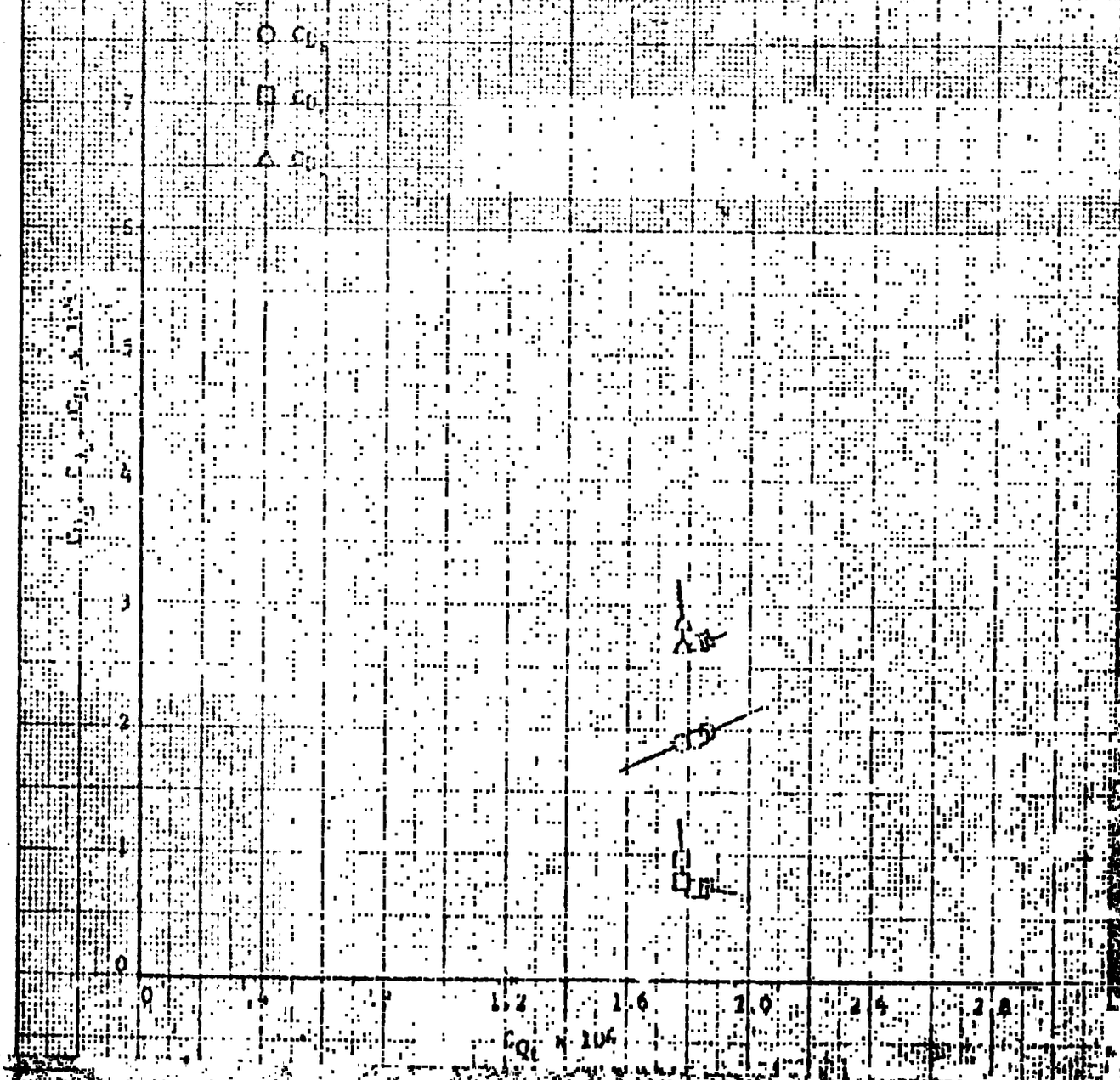

L. W. Gross CHECKER	NORTHROP CORPORATION NORAIR DIVISION	66 REPORT NO. NOR 63-46 (BLC-14
DATE July 1963		MODEL

FIGURE 44

DRAG C_D VERSUS SUCTION QUANTITY C_{Q_L} FOR VARIOUS REYNOLDS NUMBERS R_L AND ANGLES OF ATTACK

$R_L = 51.62 \times 10^6$

$\alpha = 0°$

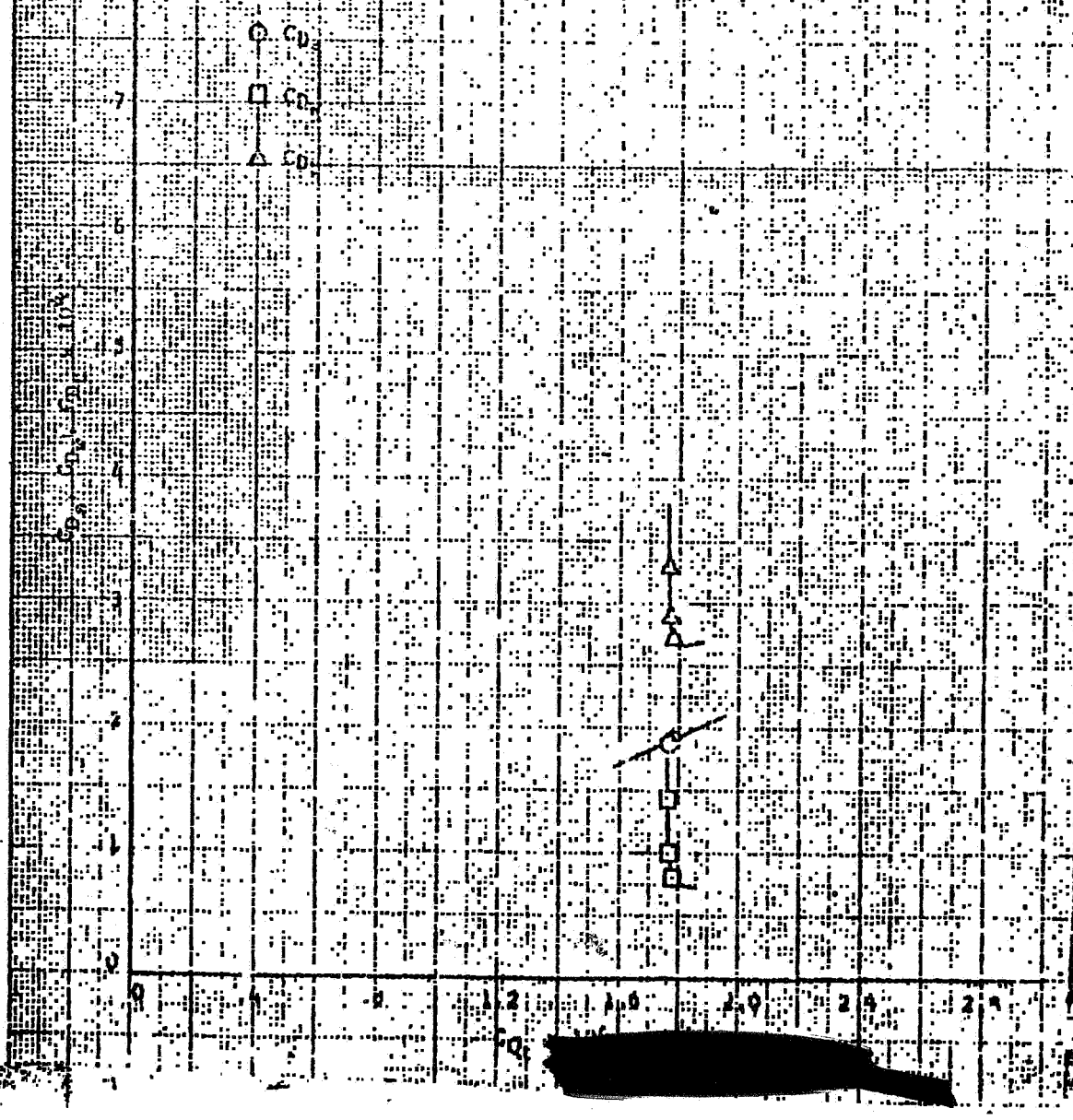

L. W. Gross	NORTHROP CORPORATION NORAIR DIVISION	66
CHECKER		REPORT NO. NOR 63-46 (BLC-14
DATE July 1963		MODEL

FIGURE 44

DRAG C_D VERSUS SUCTION QUANTITY C_{Q_L} FOR VARIOUS REYNOLDS NUMBERS R_L AND ANGLES OF ATTACK

$R_L = 51.62 \times 10^6$

$\alpha = 0°$

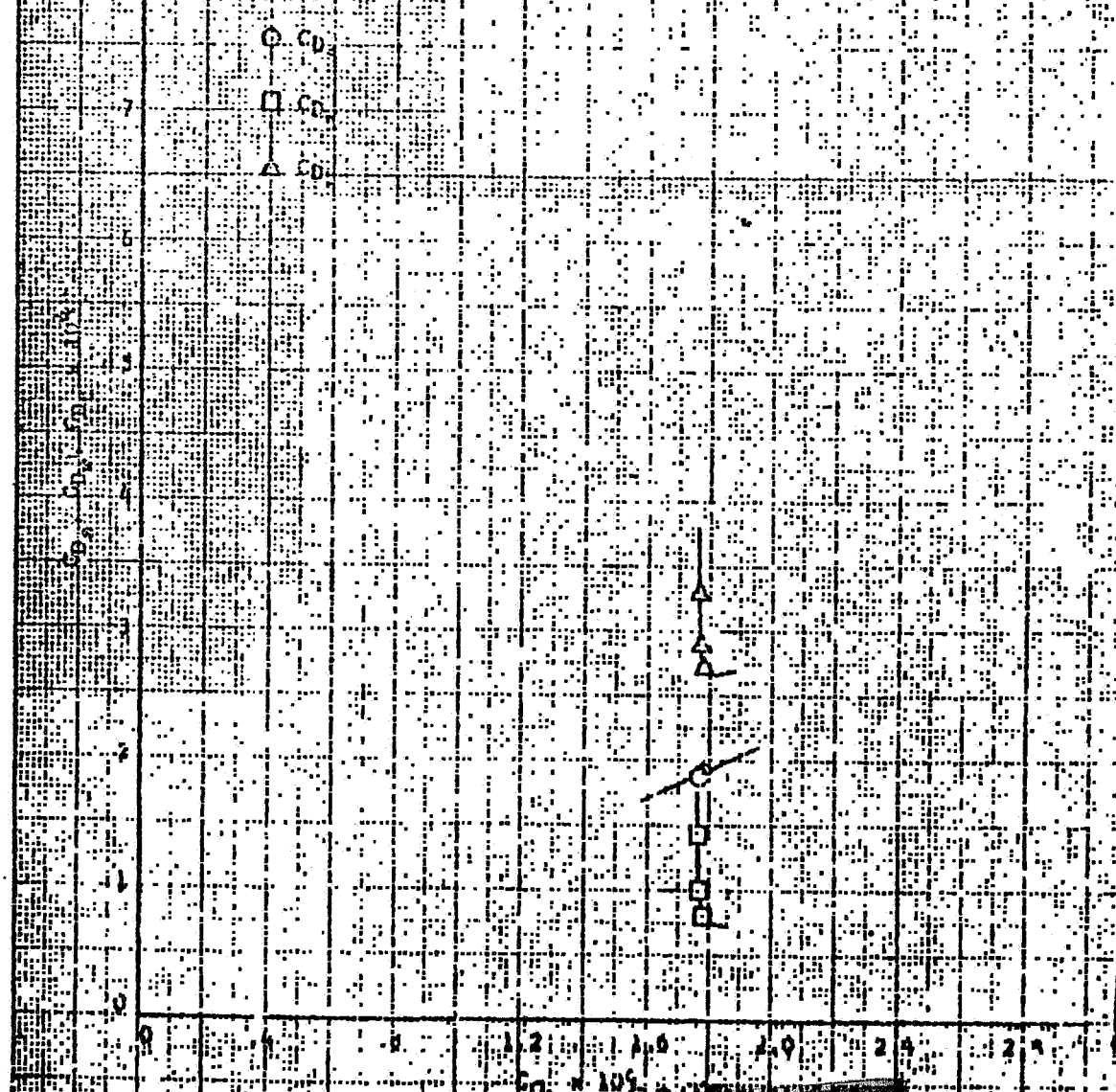

FIGURE [illegible]

DRAG C_D VERSUS SUCTION QUANTITY C_{Q_L} FOR VARIOUS REYNOLDS NUMBERS R_L AND ANGLES OF ATTACK

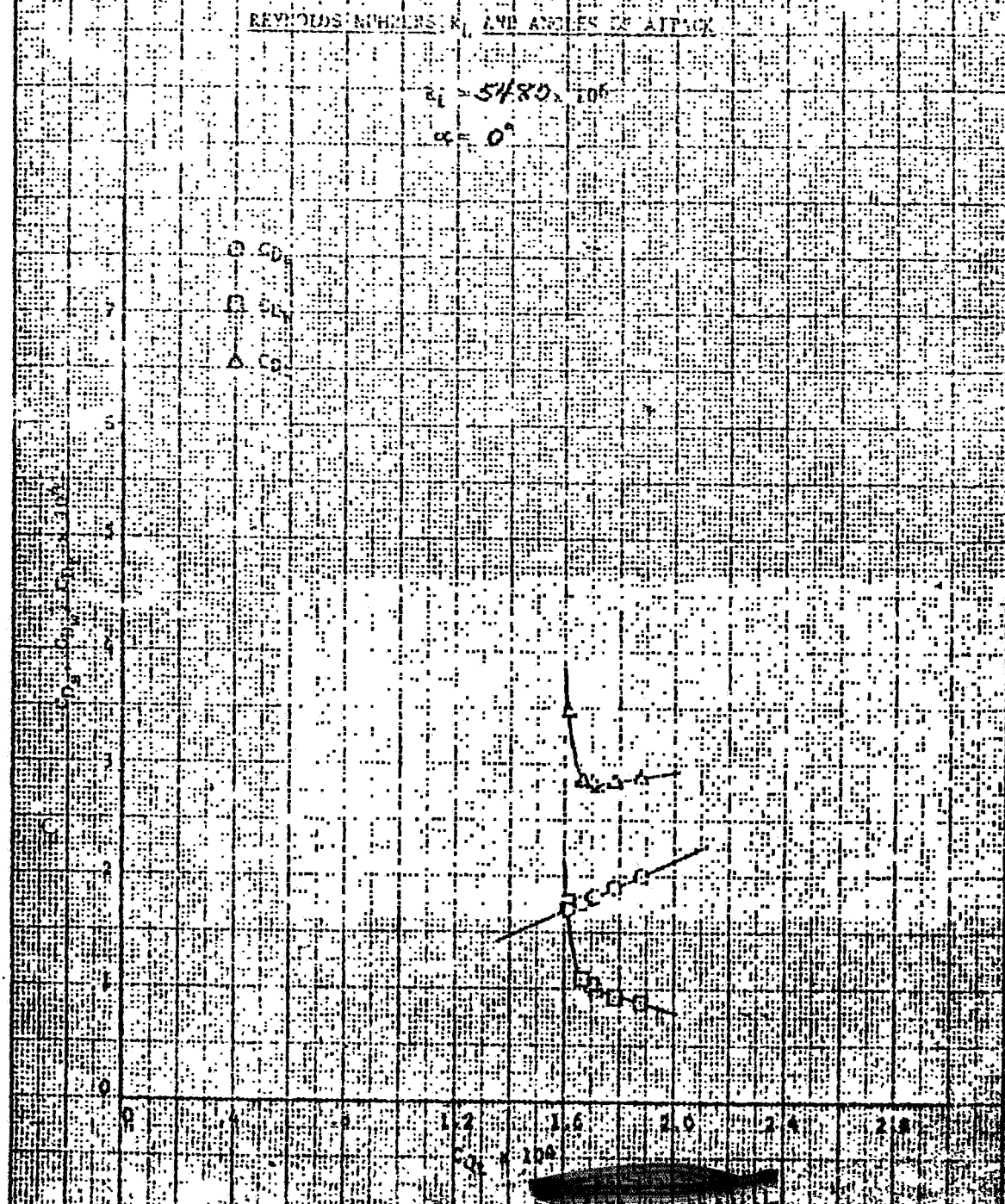

ENGINEER	NORTHROP CORPORATION	PAGE
L. W. Gross	[illegible] DIVISION	69
CHECKER		REPORT NO.
		[illegible] 63-46 ([illegible])
DATE		MODEL
July 1963		

FIGURE 47

DRAG C_D VERSUS SUCTION QUANTITY C_{Q_s} FOR VARIOUS REYNOLDS NUMBERS R_L AND ANGLES OF ATTACK

$R_L = 5498 \times 10^6$

$\alpha = 0°$

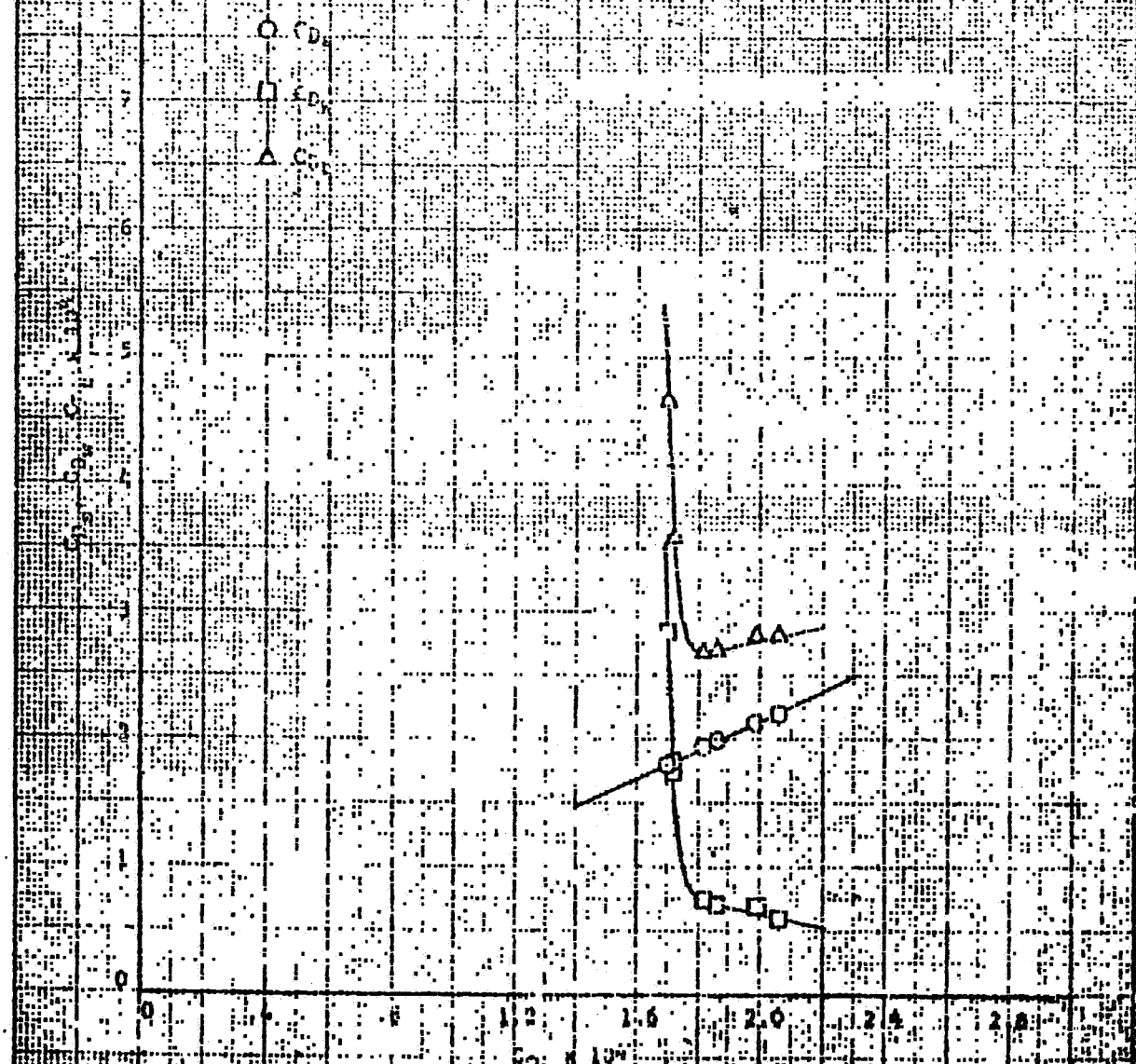

ENGINEER	NORTHROP CORPORATION	PAGE
L. W. Gross	NORAIR DIVISION	72
CHECKER		REPORT NO.
DATE		MODEL
July 1963		

FIGURE 50

DRAG C_D VERSUS SUCTION QUANTITY C_Q FOR VARIOUS REYNOLDS NUMBERS R_L AND ANGLES OF ATTACK

$R_L = 56.80 \times 10^6$

$\alpha = 0°$

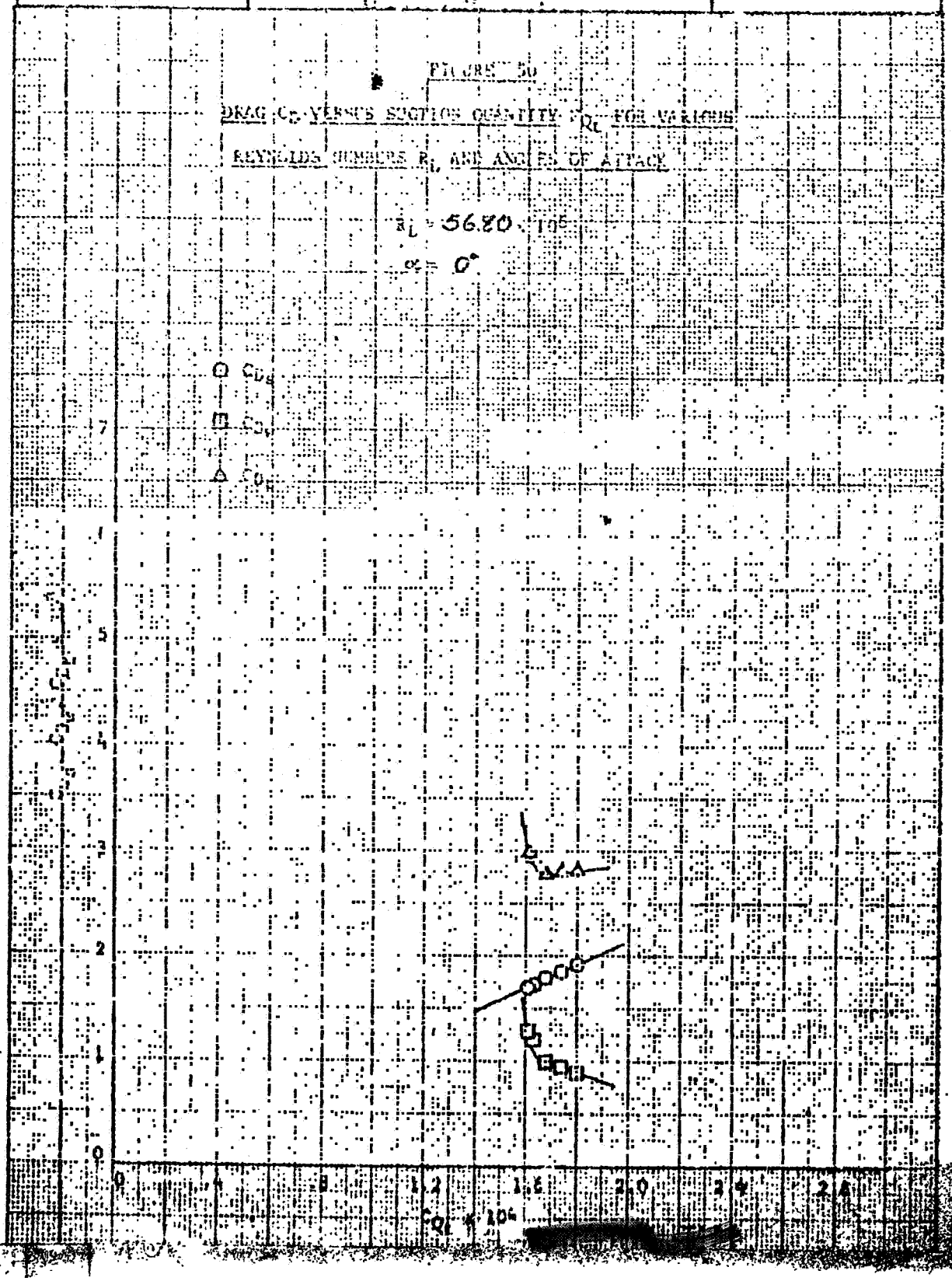

ENGINEER	NORTHROP CORPORATION	PAGE
L. W. Gross	NORAIR DIVISION	73
CHECKER		REPORT NO. NOR 63-46 (BTL-148)
DATE July 1963		MODEL

FIGURE 51

DRAG C_D VERSUS SUCTION QUANTITY C_Q FOR VARIOUS REYNOLDS NUMBERS R_L AND ANGLES OF ATTACK

$R_L = 57.56 \times 10^6$

$\alpha = 0°$

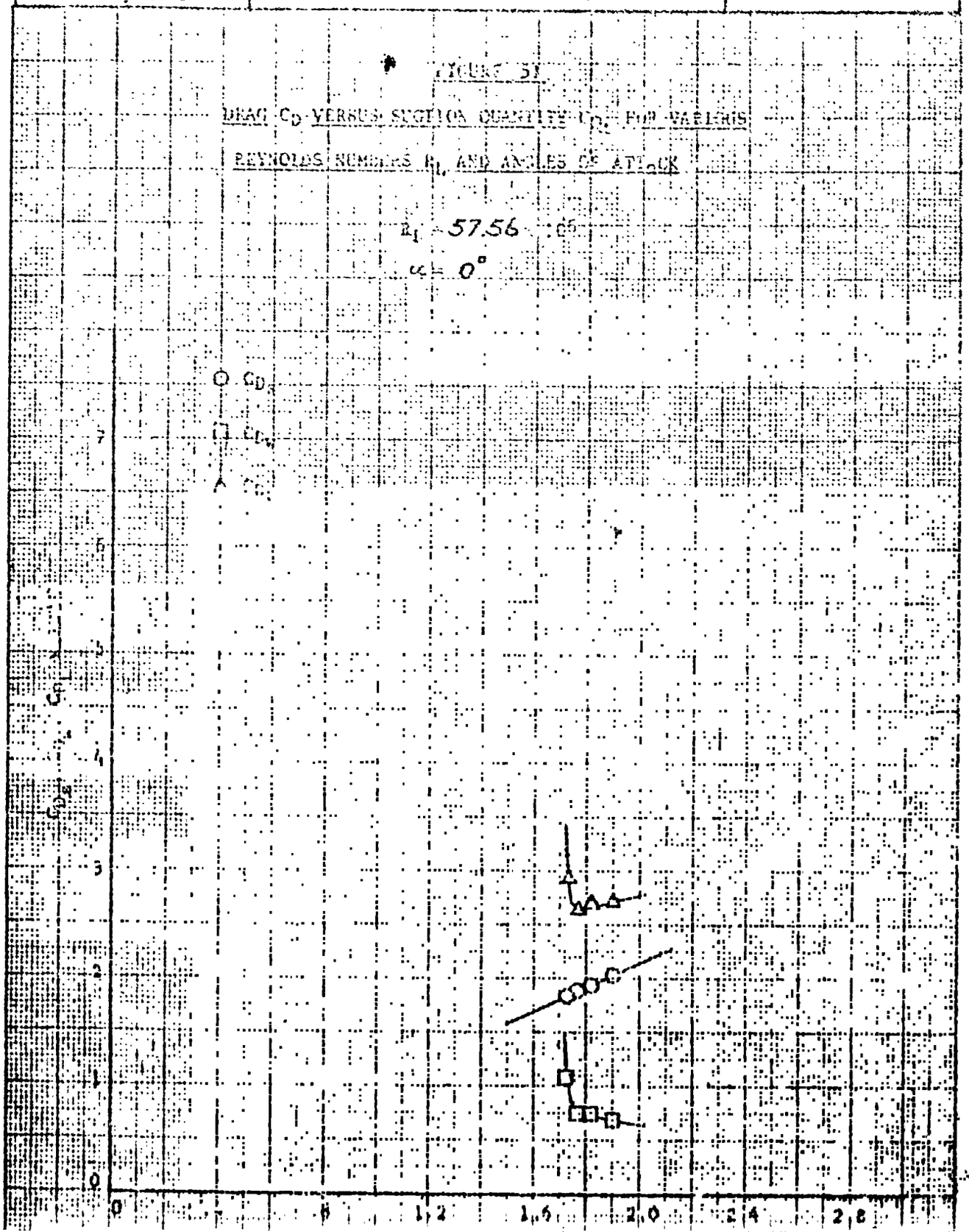

FIGURE 32

DRAG C_D VERSUS FUSTION QUANTITY C_{R_L} FOR VARIOUS REYNOLDS NUMBERS R_L AND ANGLES OF ATTACK

$R_L = 57.76 \times 10^7$

$\alpha = 0°$

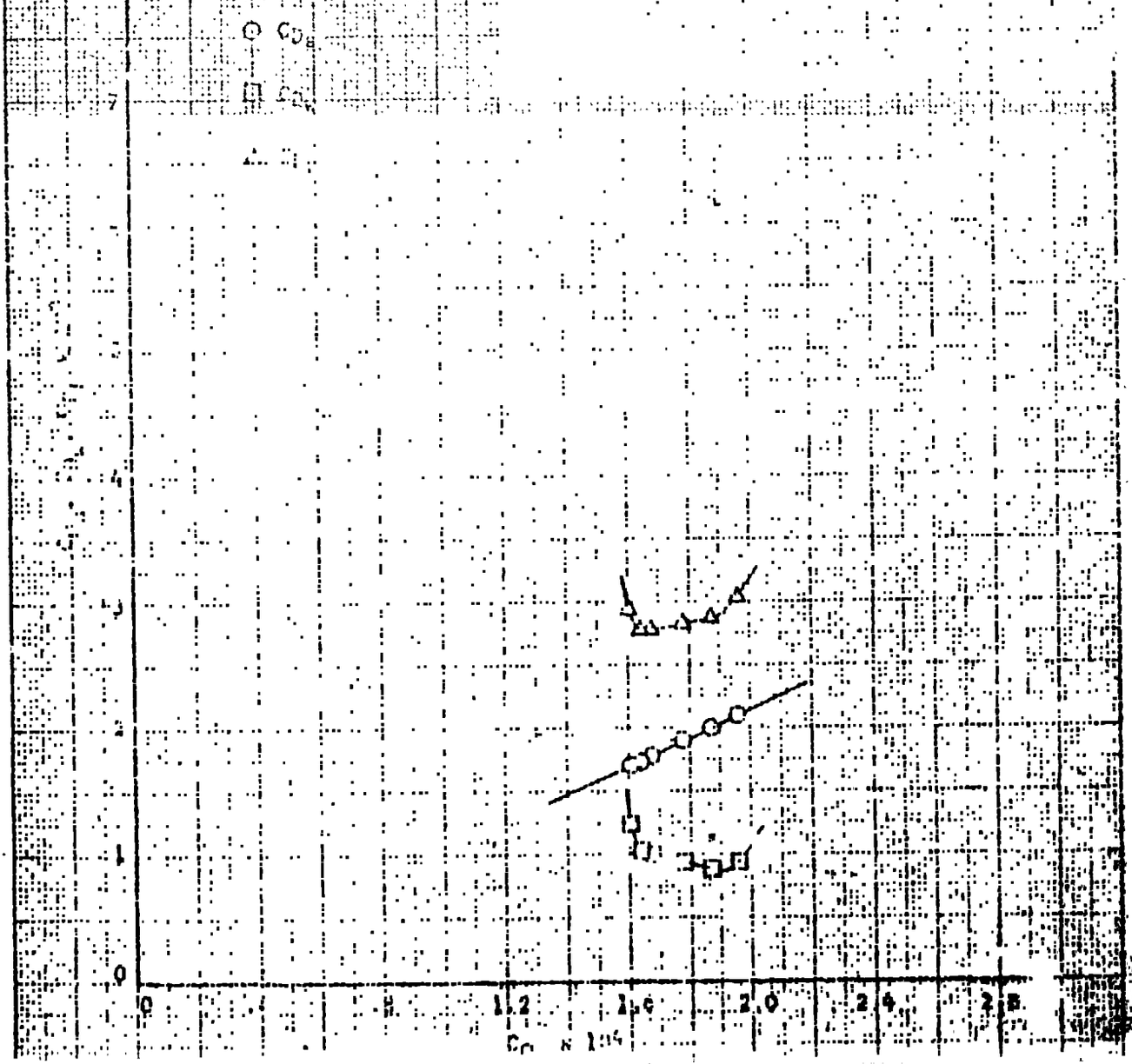

ENGINEER	NORTHROP CORPORATION	75
L. W. Gross	NORAIR DIVISION	REPORT NO.
CHECKER		NOR 63-46 (BLC-148)
DATE	[redacted]	MODEL
July 1963		

FIGURE 53 write

FIG. VARIATION OF MINIMUM TOTAL DRAG $C_{D_{t_{min}}}$ AND SUCTION COEFFICIENT AT MINIMUM TOTAL DRAG $C_{Q_{opt}}$ WITH LENGTH REYNOLDS NUMBER R_L, $\alpha = 0°$

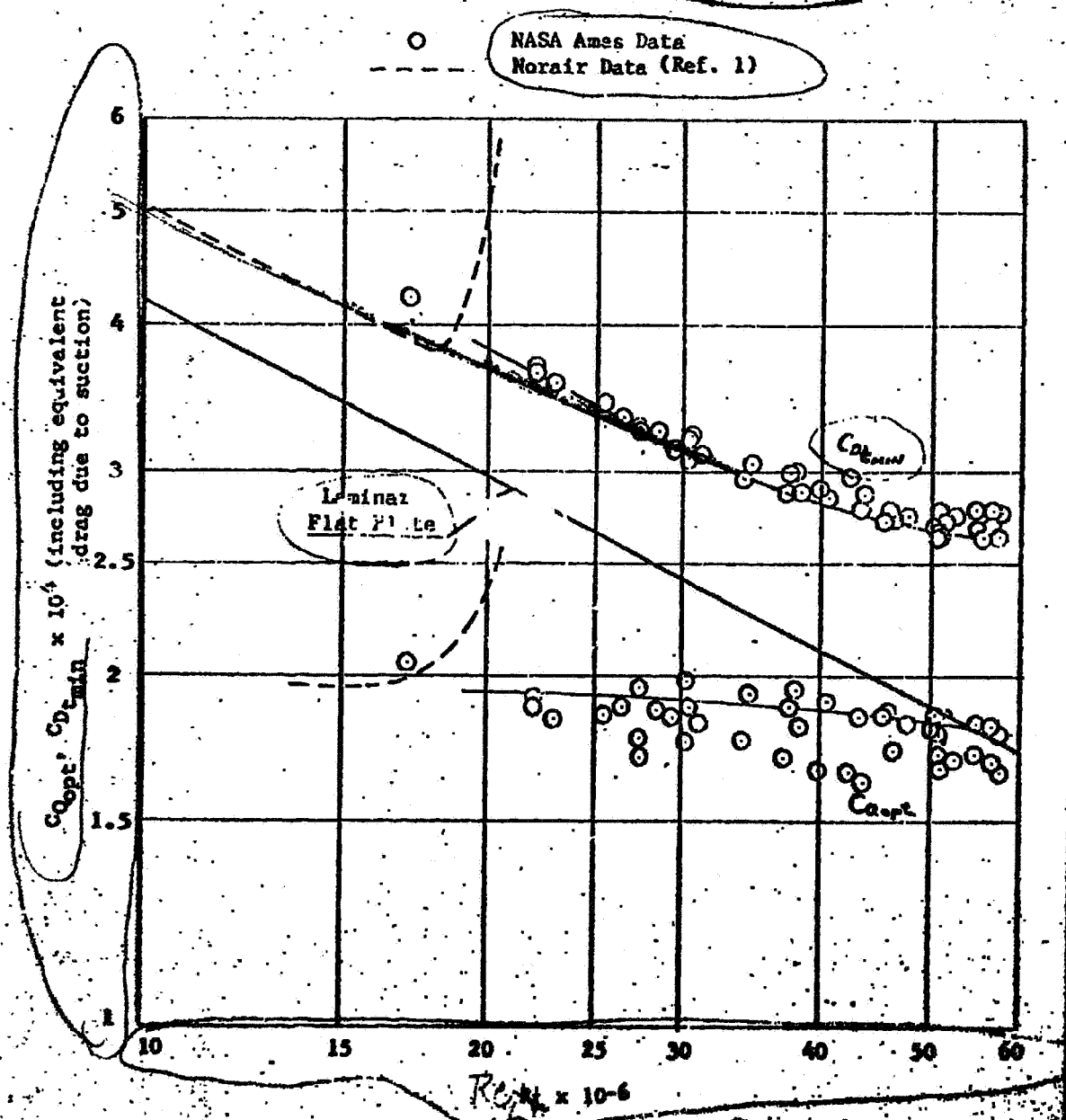

[redacted]

ENGINEER	NORTHROP CORPORATION	11
L. W. Gross	NORAIR DIVISION	REPORT NO. NOR 63-46 (BLC-143)
CHECKER		
DATE July 1963	[redacted]	MODEL

FIGURE 55

BOUNDARY LAYER VELOCITY PROFILES AS MEASURED

AT THE AFT END OF THE MODEL

Run No. 2
$R_L = 17.136 \times 10^6$
$C_{Q_t} = 2.050 \times 10^{-4}$

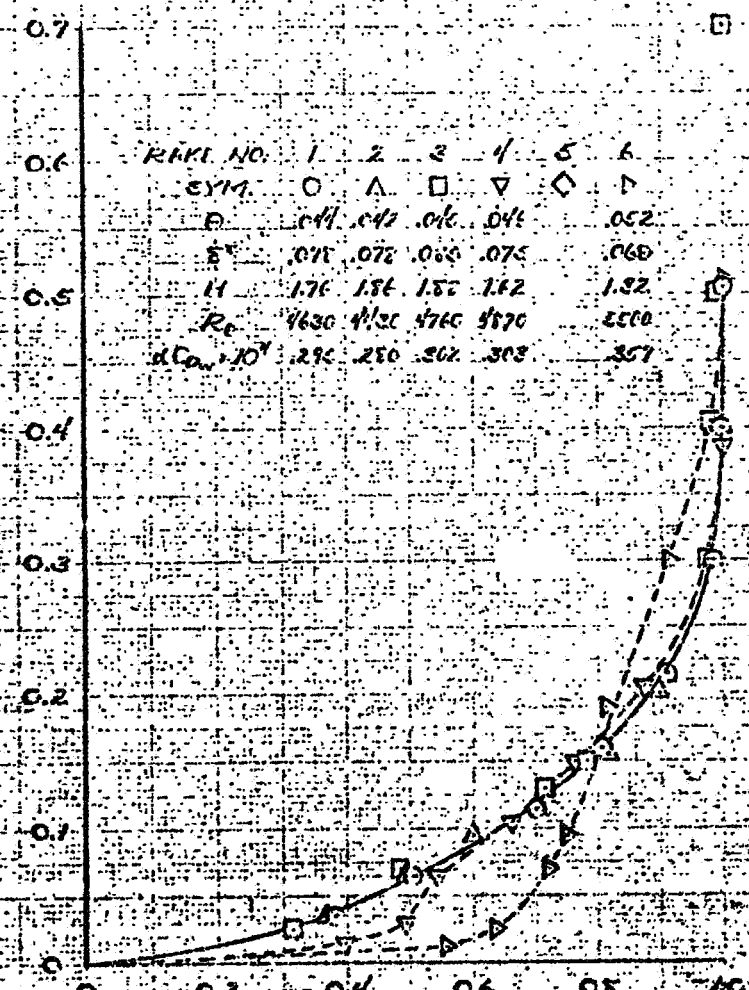

[redacted]

CHECKER	NORAIR DIVISION	REPORT NO. NOR 63-46 (BLC-148)
DATE July 1963	[redacted]	MODEL

FIGURE 56

BOUNDARY LAYER VELOCITY PROFILES AS MEASURED AT THE AFT END OF THE MODEL

Run No. 102
$R_L = 22.166 \times 10^6$
$C_{Q_t} = 1.979 \times 10^{-4}$

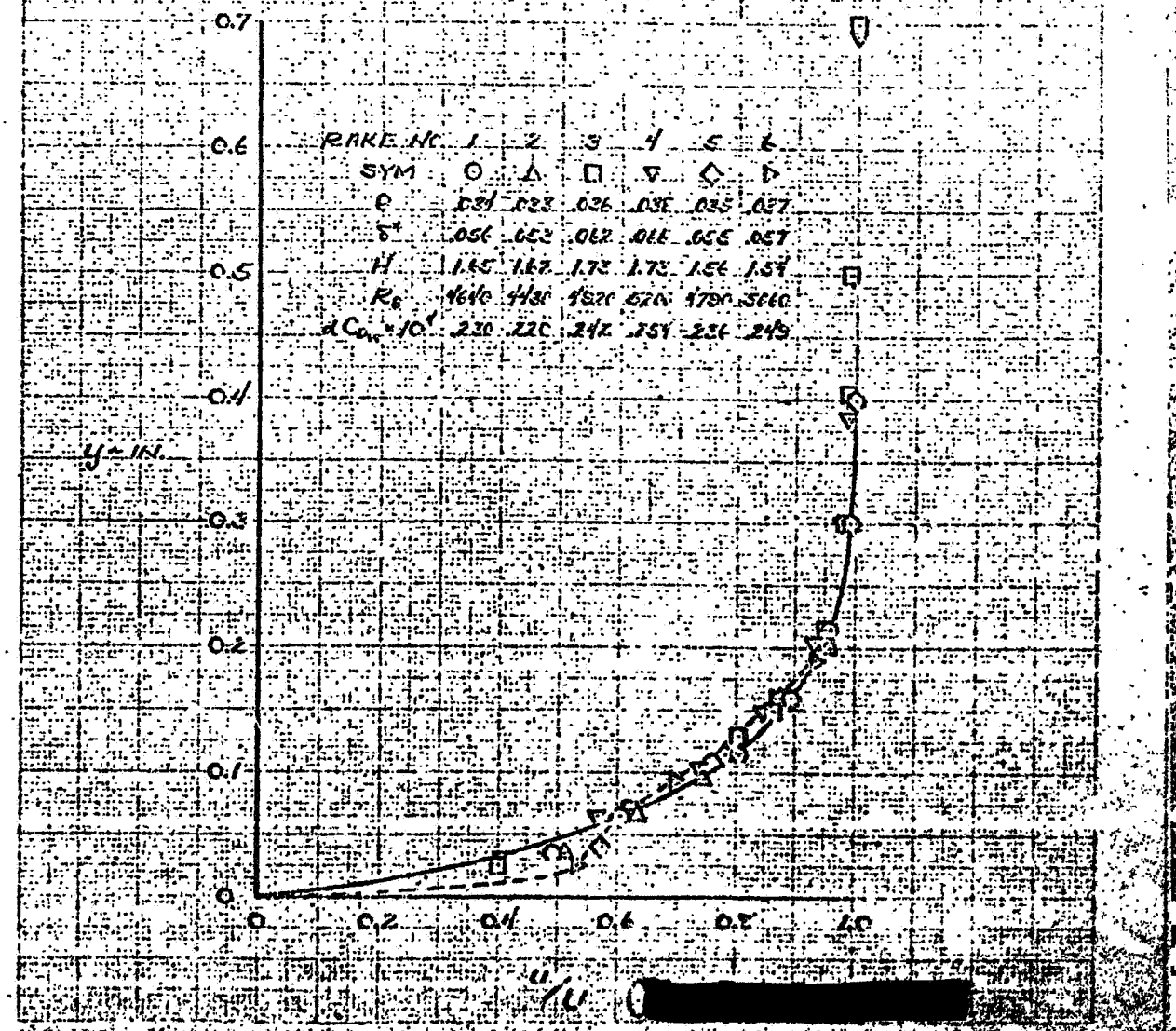

[redacted]

FIGURE 57

BOUNDARY LAYER VELOCITY PROFILES AS MEASURED

AT THE AFT END OF THE MODEL

Run No. 47
$R_L = 30.238 \times 10^6$
$C_{Q_t} = 1.696 \times 10^{-4}$

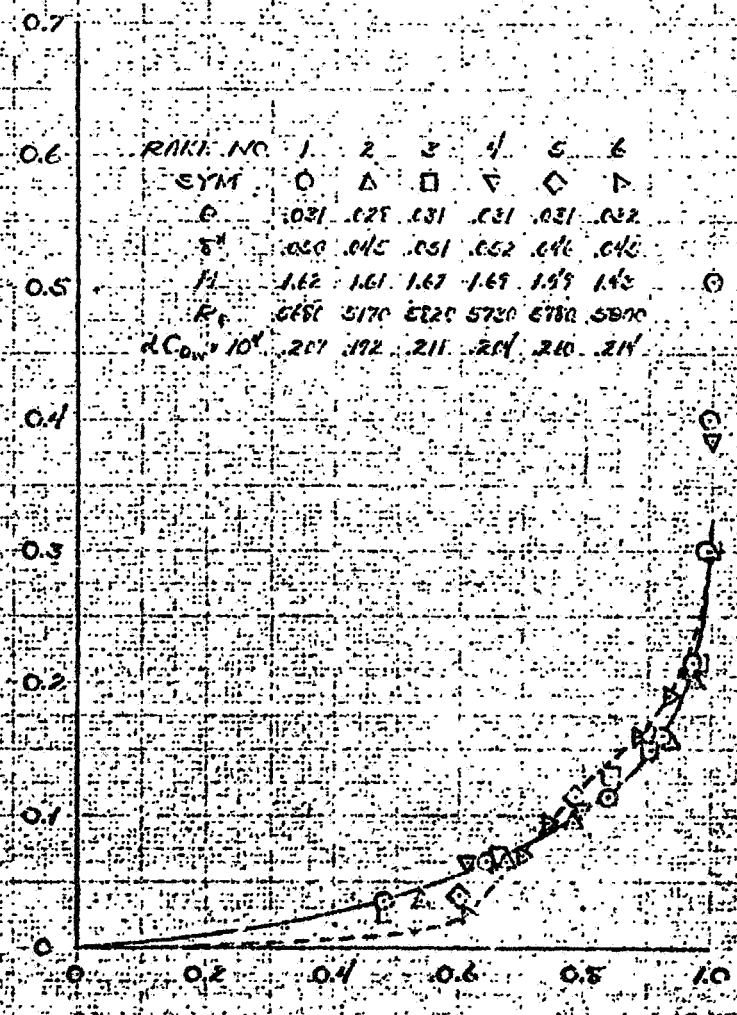

[redacted]

L. W. Gross	NORTHROP CORPORATION NORAIR DIVISION	8C
CHECKER		REPORT NO. NOR 63-46 (BLC-148)
DATE July 1963	[redacted]	MODEL

FIGURE 58

BOUNDARY LAYER VELOCITY PROFILES AS MEASURED

AT THE AFT END OF THE MODEL

Run No. 117
$R_L = 30.449 \times 10^6$
$C_{Q_L} = 2.007 \times 10^{-4}$

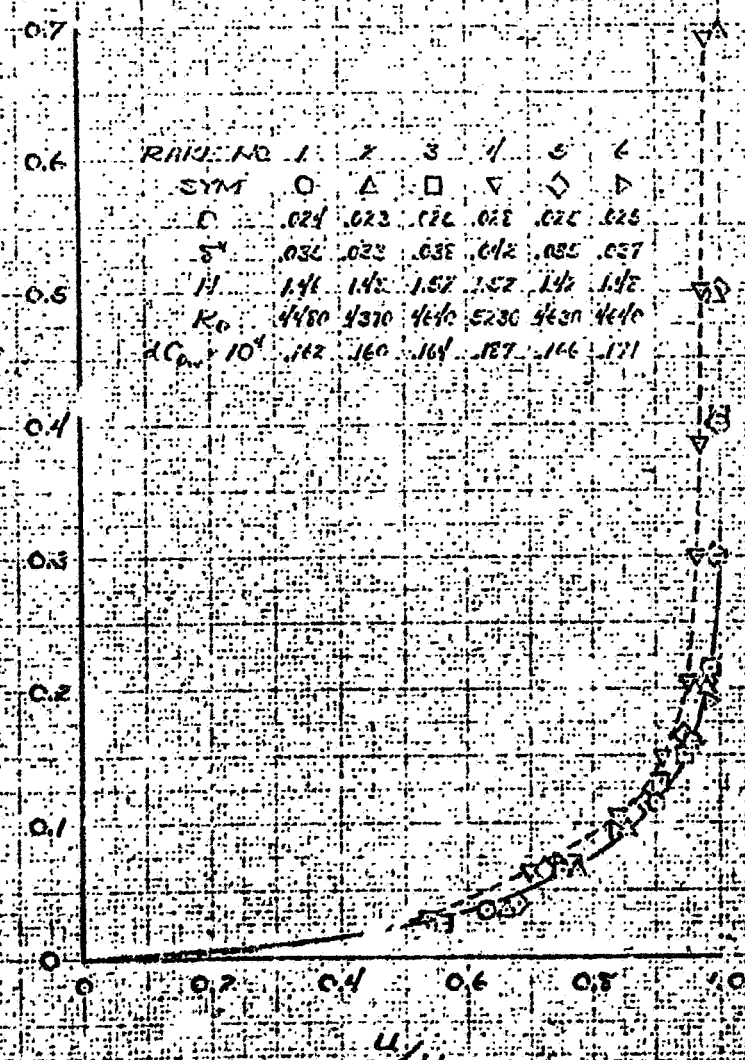

[redacted]

FIGURE 59

BOUNDARY LAYER VELOCITY PROFILES AS MEASURED

AT THE AFT END OF THE MODEL

Run No. 262
$R_L = 38.036 \times 10^6$
$C_{Q_t} = 1.860 \times 10^{-4}$

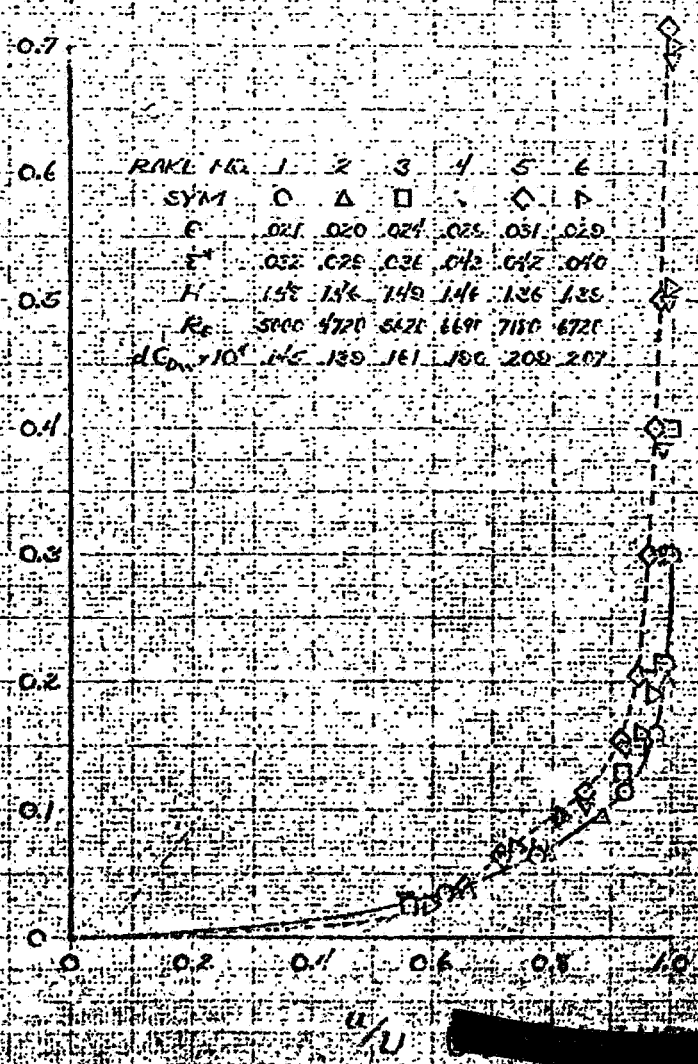

[redacted]

FIGURE 60

BOUNDARY LAYER VELOCITY PROFILES AS MEASURED

AT THE AFT END OF THE MODEL

Run No. 268
$R_L = 46.050 \times 10^6$
$C_{Q_t} = 1.818 \times 10^{-4}$

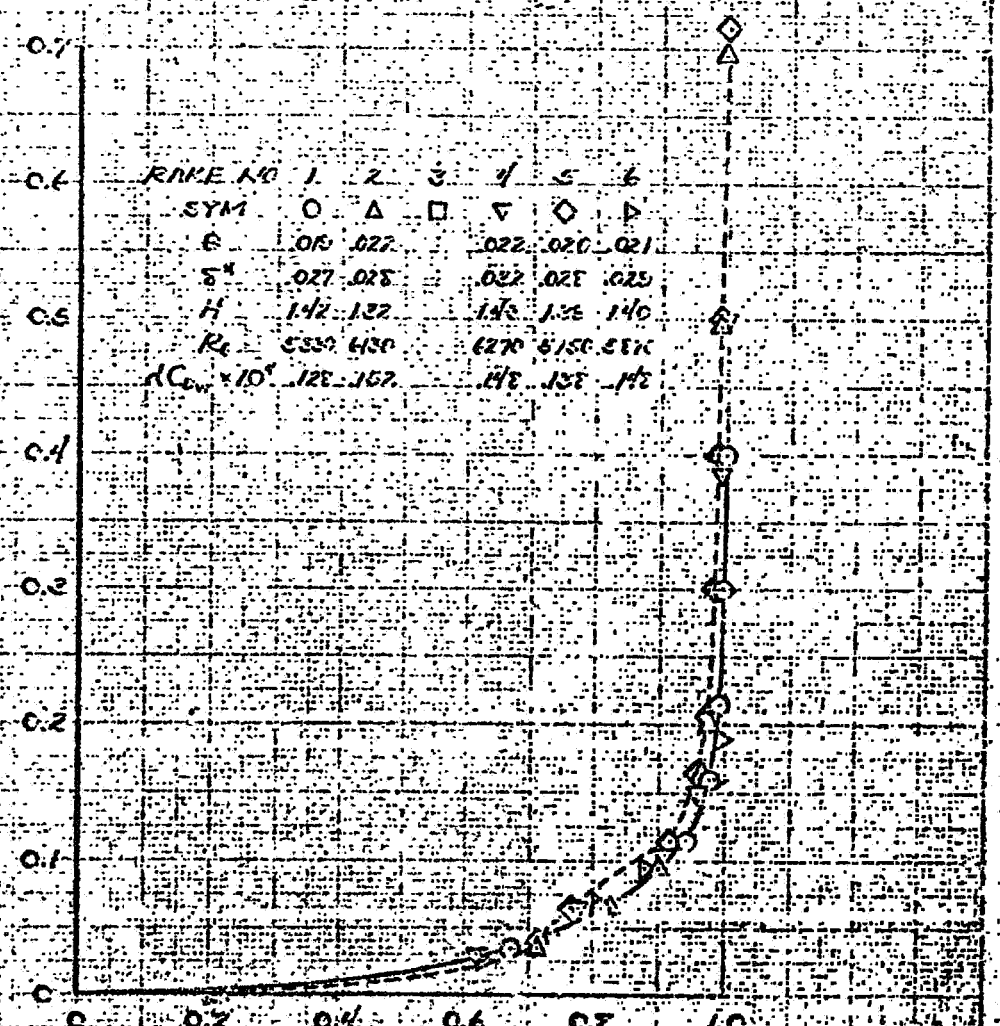

[redacted]

NORTHROP CORPORATION
NORAIR DIVISION

CHECKER

DATE

REPORT NO.

MODEL

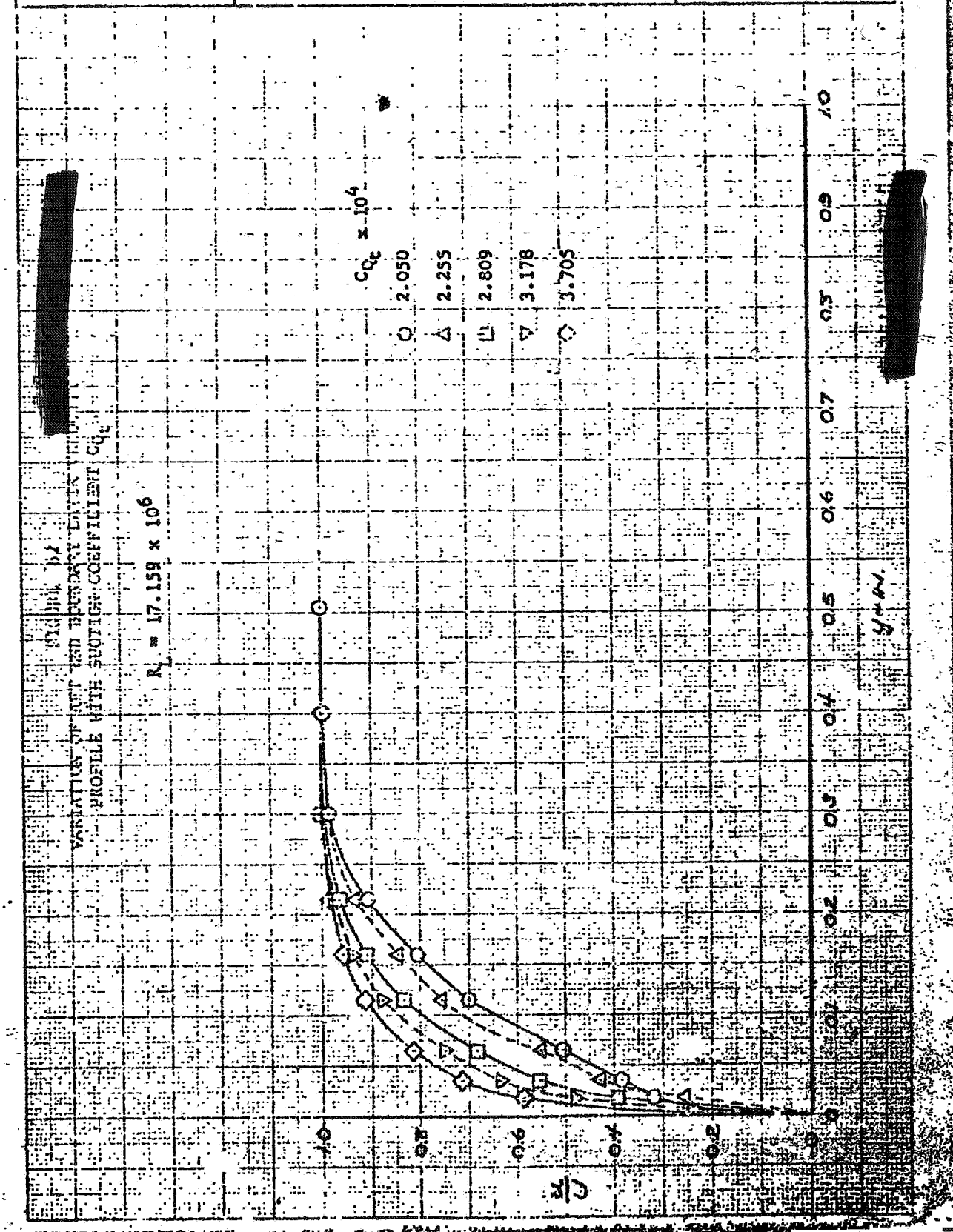

CHECKER	**NORTHROP CORPORATION** **NORAIR DIVISION**	REPORT NO.
DATE		MODEL

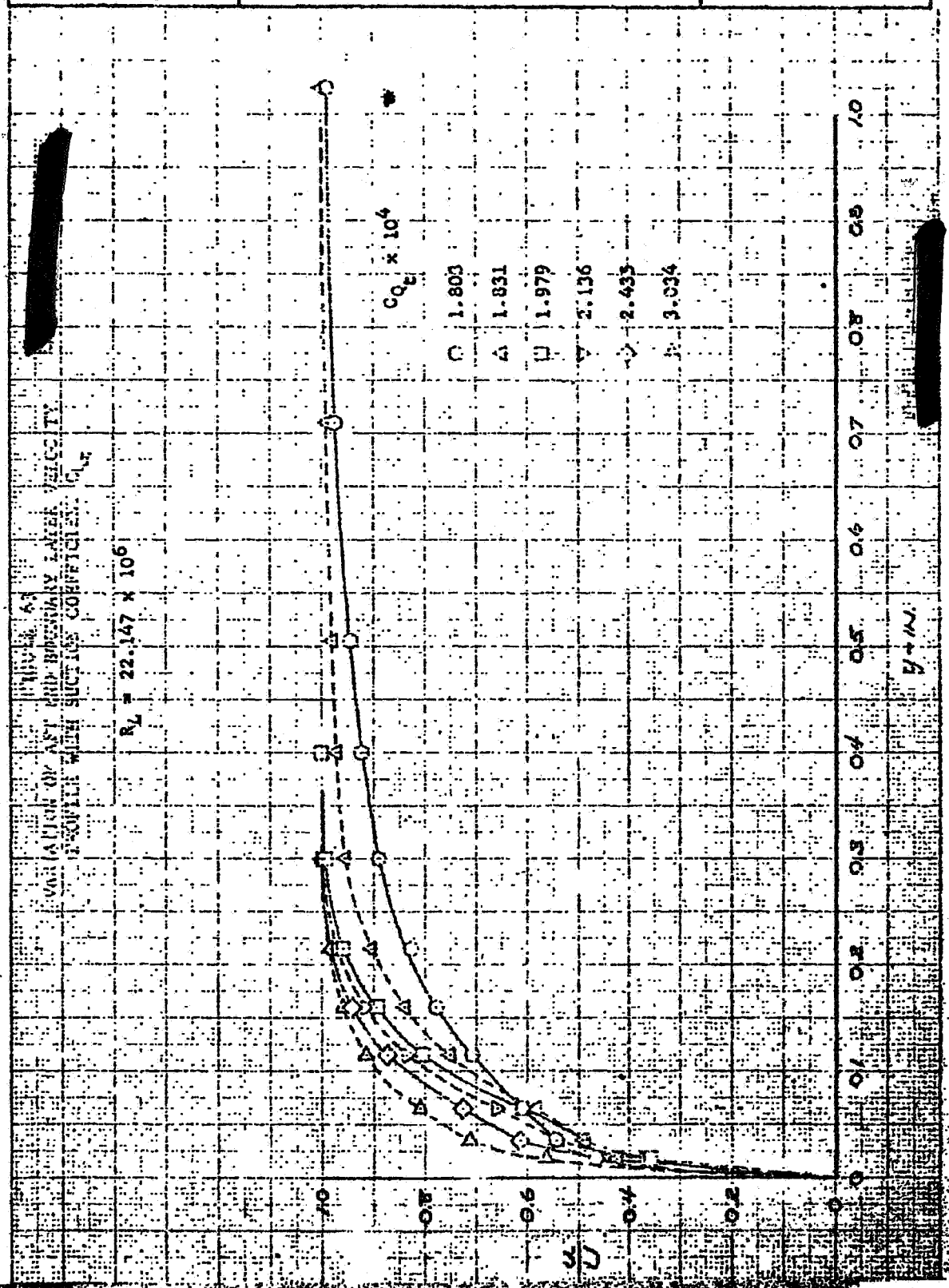

FIGURE 63
VARIATION OF AFT END BOUNDARY LAYER VELOCITY PROFILE WITH SUCTION COEFFICIENT C_{Q_E}

CHECKED	NORTHROP CORPORATION NORAIR DIVISION	REPORT NO.
DATE July 1961		MODEL

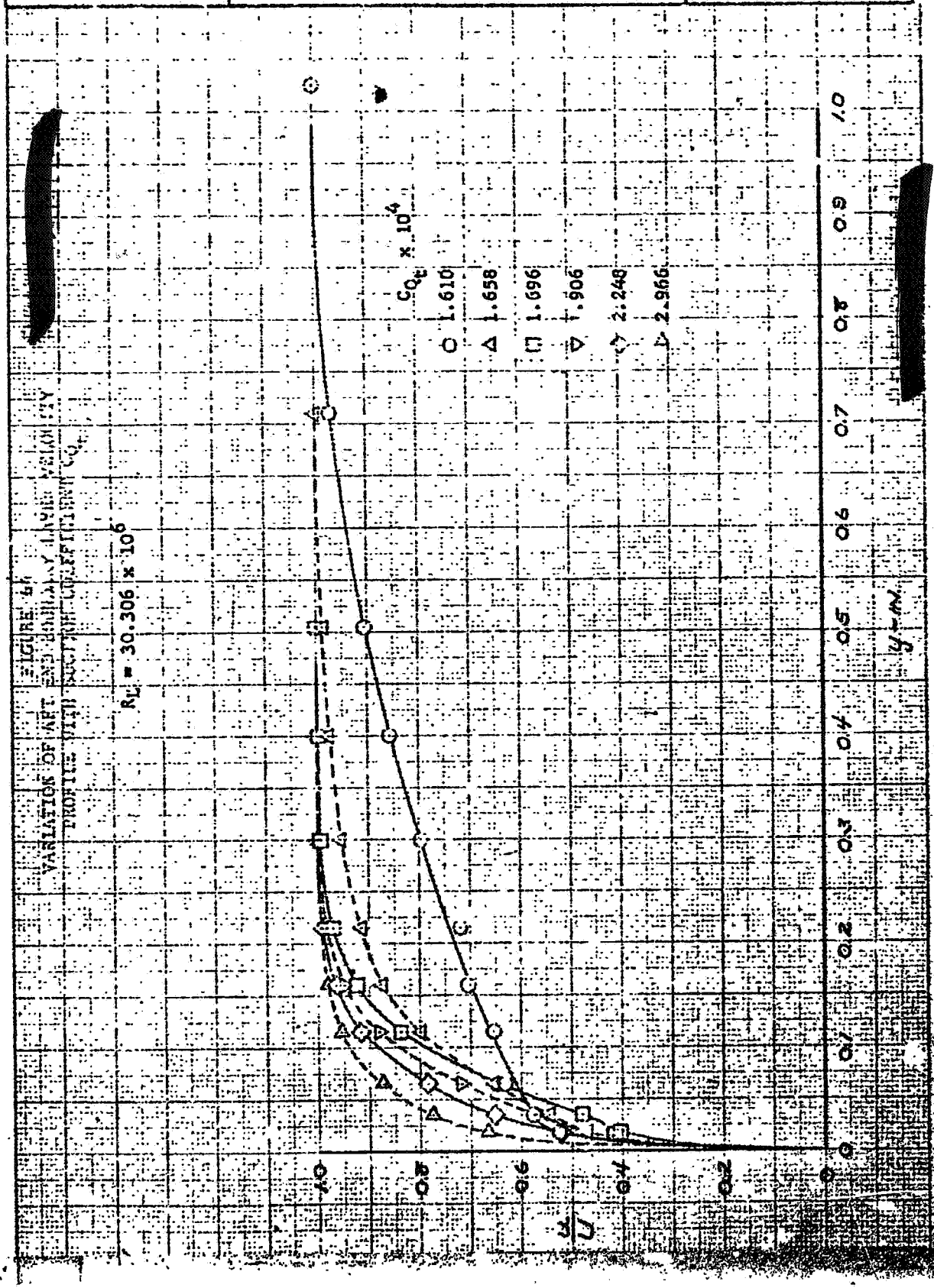

FIGURE 61
VARIATION OF ART. END BOUNDARY LAYER VELOCITY PROFILE WITH SKIN FRICTION COEFFICIENT C_{Q_E}

FIGURE 63
VARIATION OF AFT END BOUNDARY LAYER VELOCITY
PROFILE WITH SUCTION COEFFICIENT C_{Q_t}

[redacted]

$R_L = 30.424 \times 10^6$

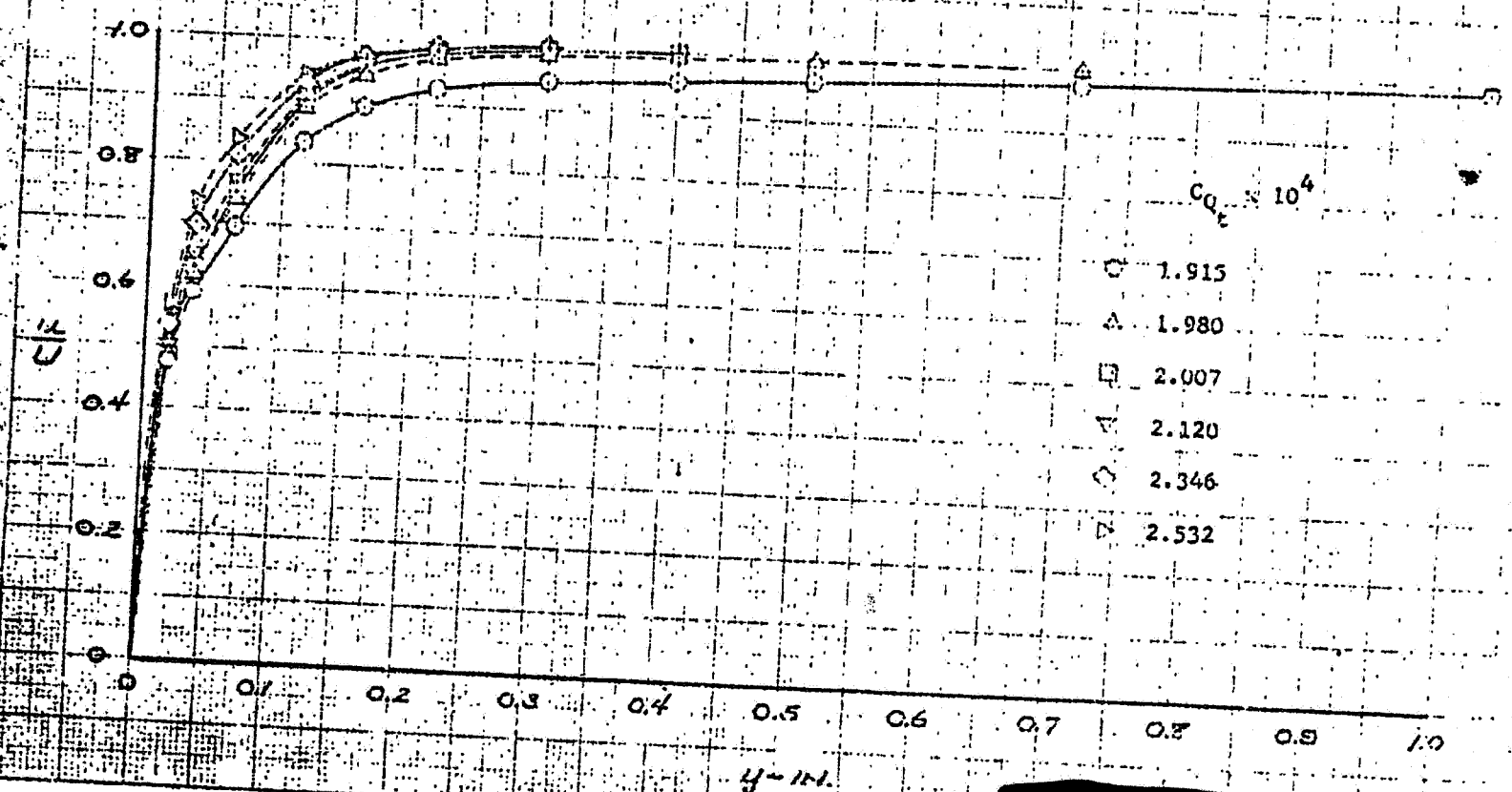

[redacted]

CHECKER

DATE

NORTHROP CORPORATION
NORAIR DIVISION

REPORT NO.

MODEL

NORTHROP CORPORATION
NORAIR DIVISION

CHECKED

REPORT NO.

MODEL

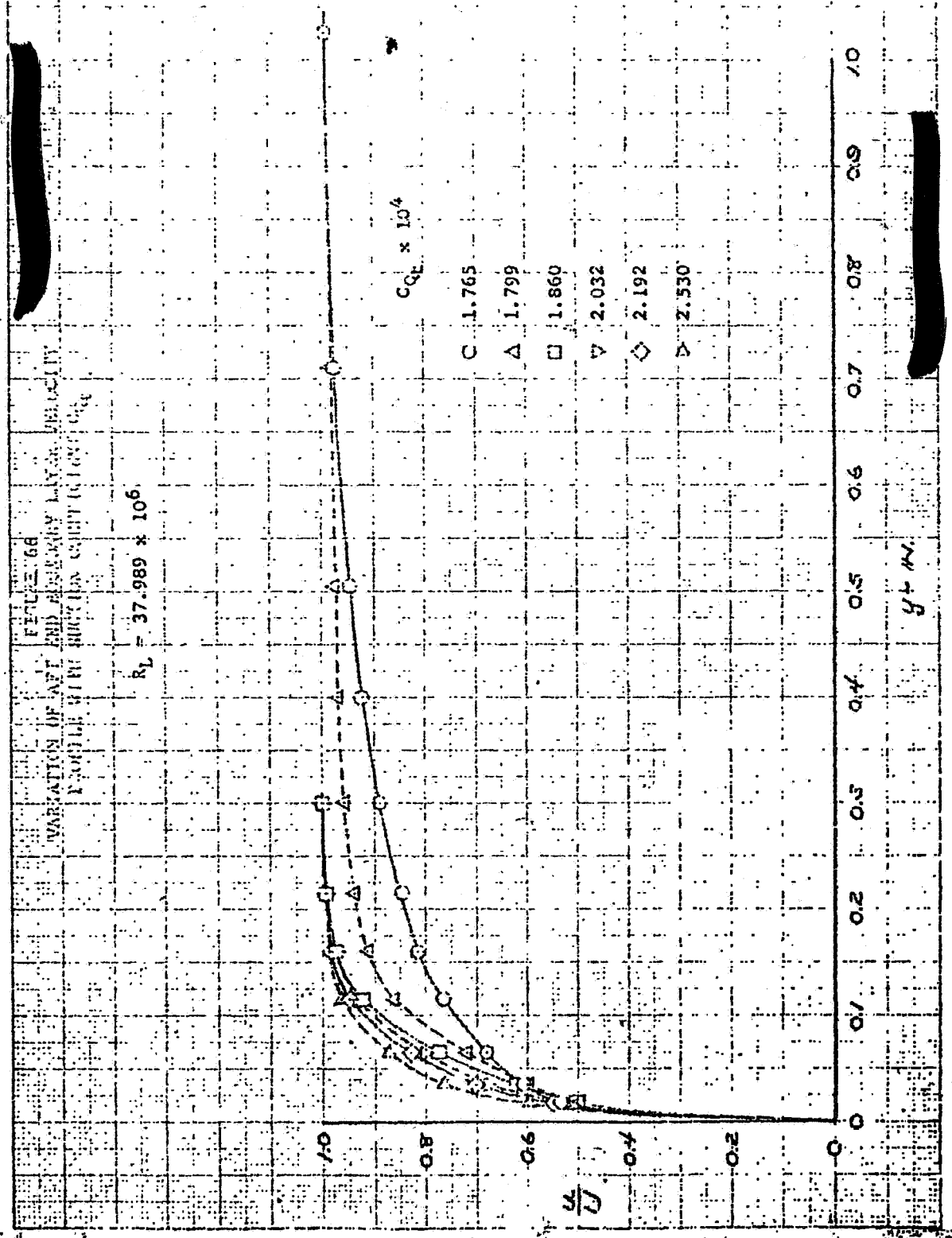

FIGURE 68
VARIATION OF AFT END BOUNDARY LAYER VELOCITY PROFILE WITH SURFACE CURVATURE

NORTHROP CORPORATION
NORAIR DIVISION

CHECKER

DATE

REPORT NO

MODEL

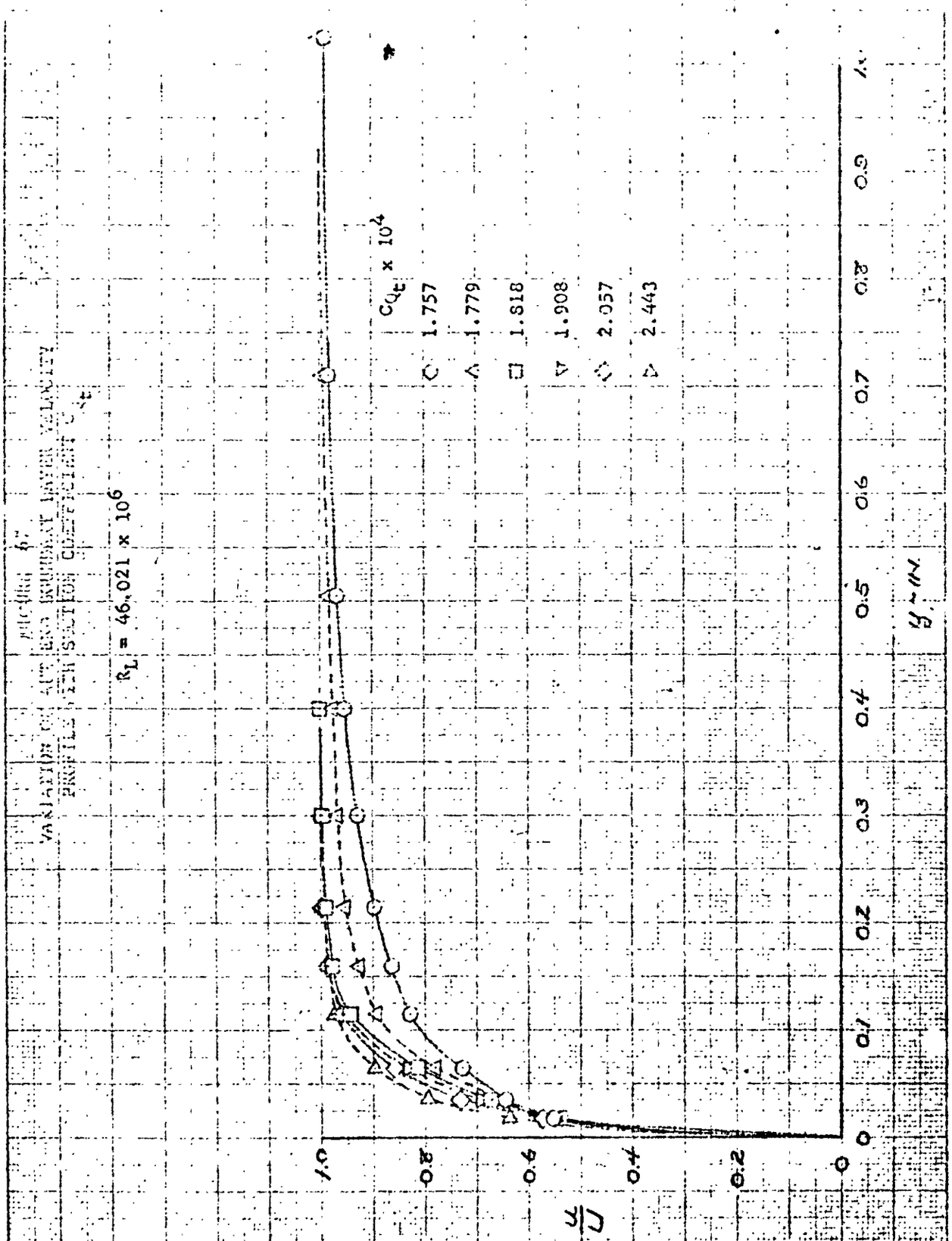

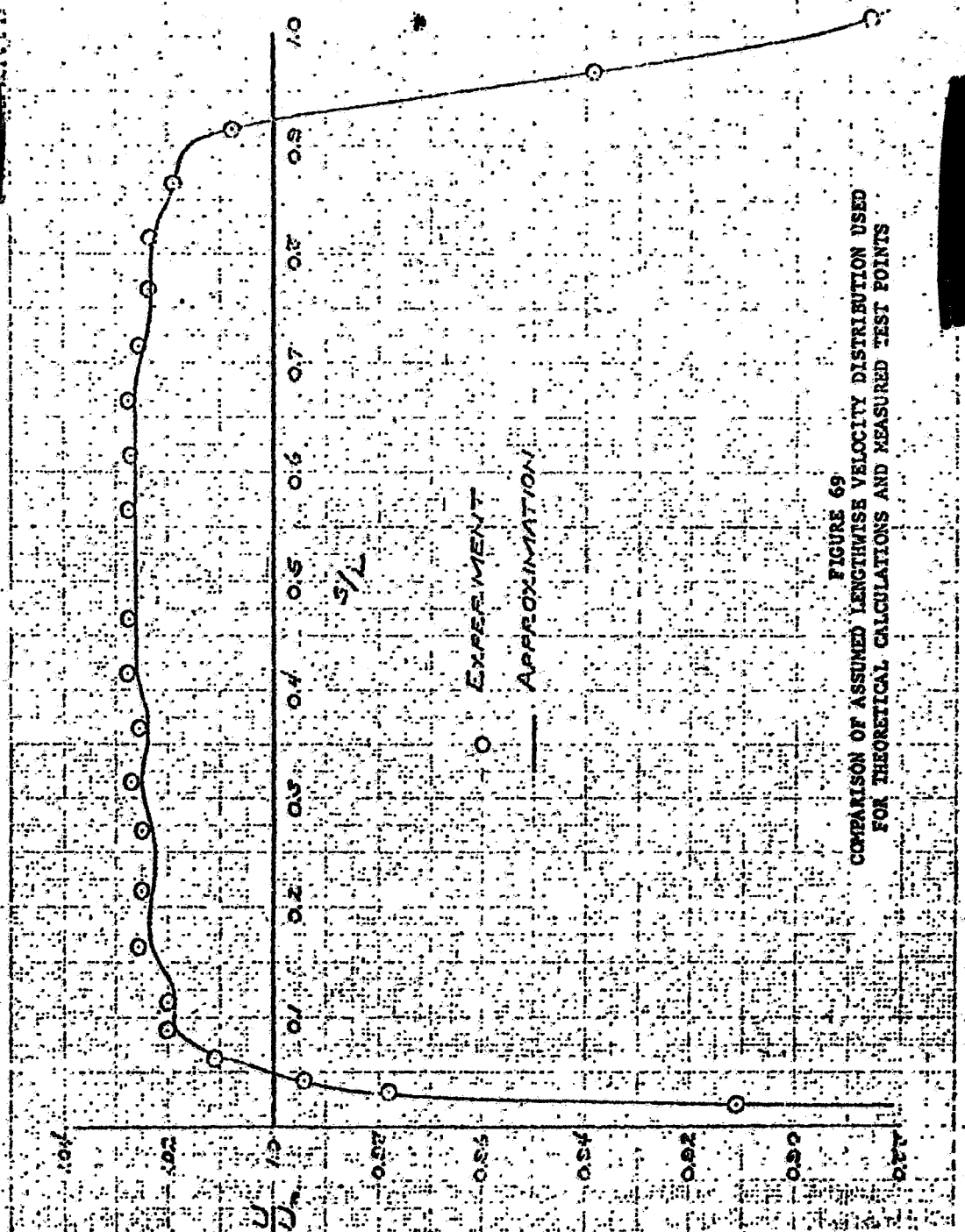

FIGURE 69
COMPARISON OF ASSUMED LENGTHWISE VELOCITY DISTRIBUTION USED FOR THEORETICAL CALCULATIONS AND MEASURED TEST POINTS

[redacted]

FIGURE 70
NONDIMENSIONAL EQUIVALENT DISTRIBUTED SUCTION VELOCITY
DISTRIBUTION AND BOUNDARY LAYER DEVELOPMENT FOR TEST POINT NO. 2

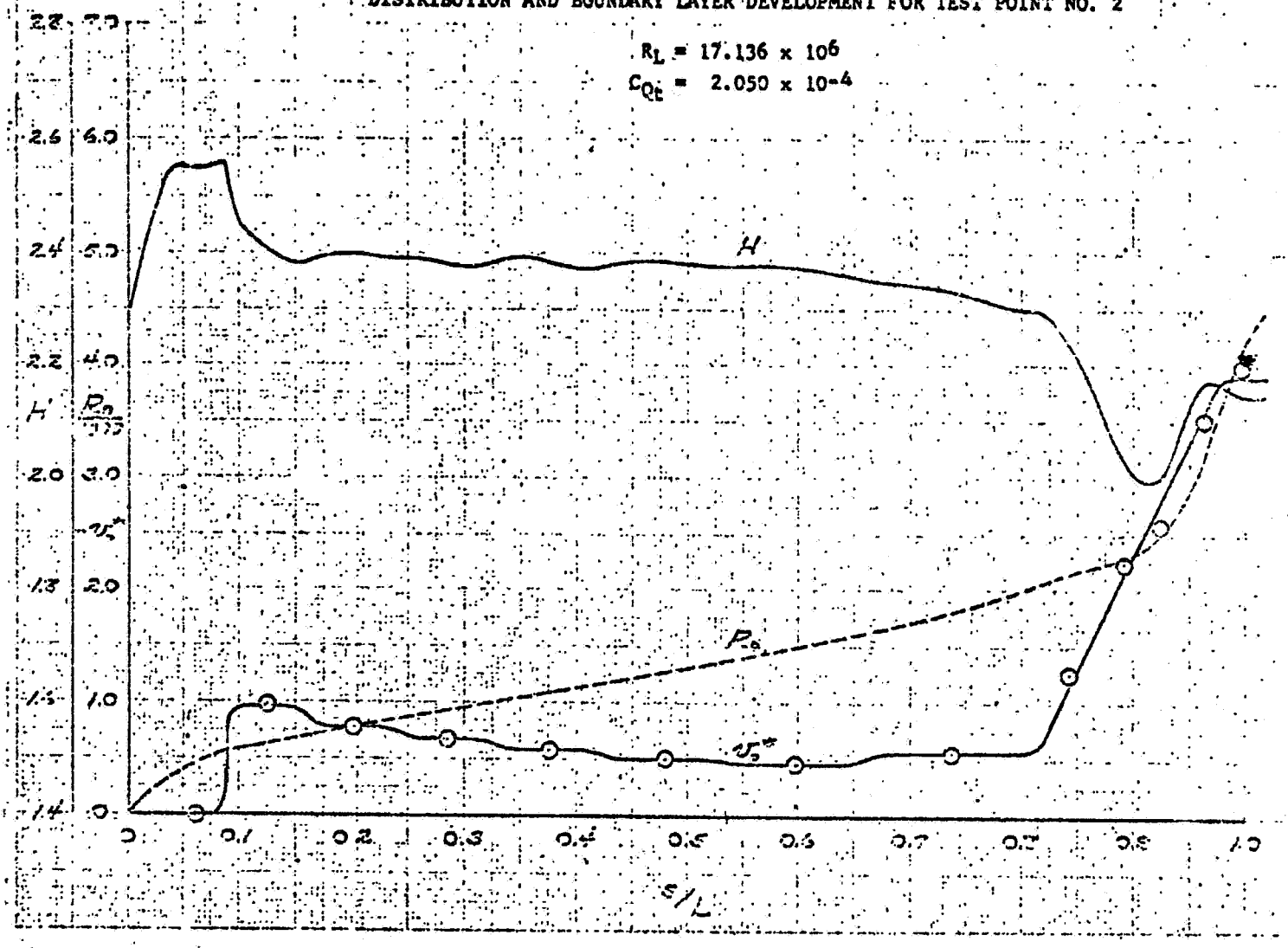

[redacted]

FIGURE 71
COMPARISON OF CALCULATED AND MEASURED BOUNDARY LAYER VELOCITY PROFILES AT REAR END OF BODY FOR THE CONDITIONS OF TEST POINT NO. 2

$R_L = 17.136 \times 10^6$

$C_{Q_t} = 2.050 \times 10^{-4}$

	CALC	MEASURED						
RAKE NO.		1	2	3	4	5	6	
SYM	—	○	△	□	▽	◇	▷	
θ	.0423	.044	.042	.046	.046		.052	(IN.)
δ^*	.0965	.073	.072	.085	.075		.069	(IN.)
H	2.15	1.76	1.86	1.88	1.61		1.37	
R_e	4470	4630	4430	4760	[illegible]		[illegible]	
$C_{D_w} \times 10^4$	1.78			1.93				

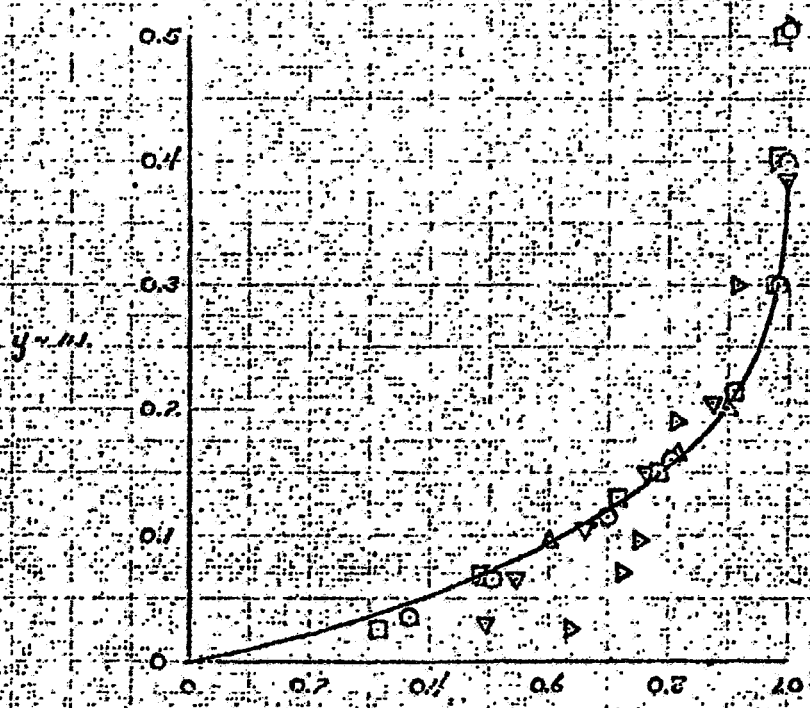

[redacted]

FIGURE 72a
CALCULATED BOUNDARY LAYER PROFILES AT VARIOUS LENGTHWISE POSITIONS s/L FOR THE CONDITIONS OF TEST POINT NO. 2

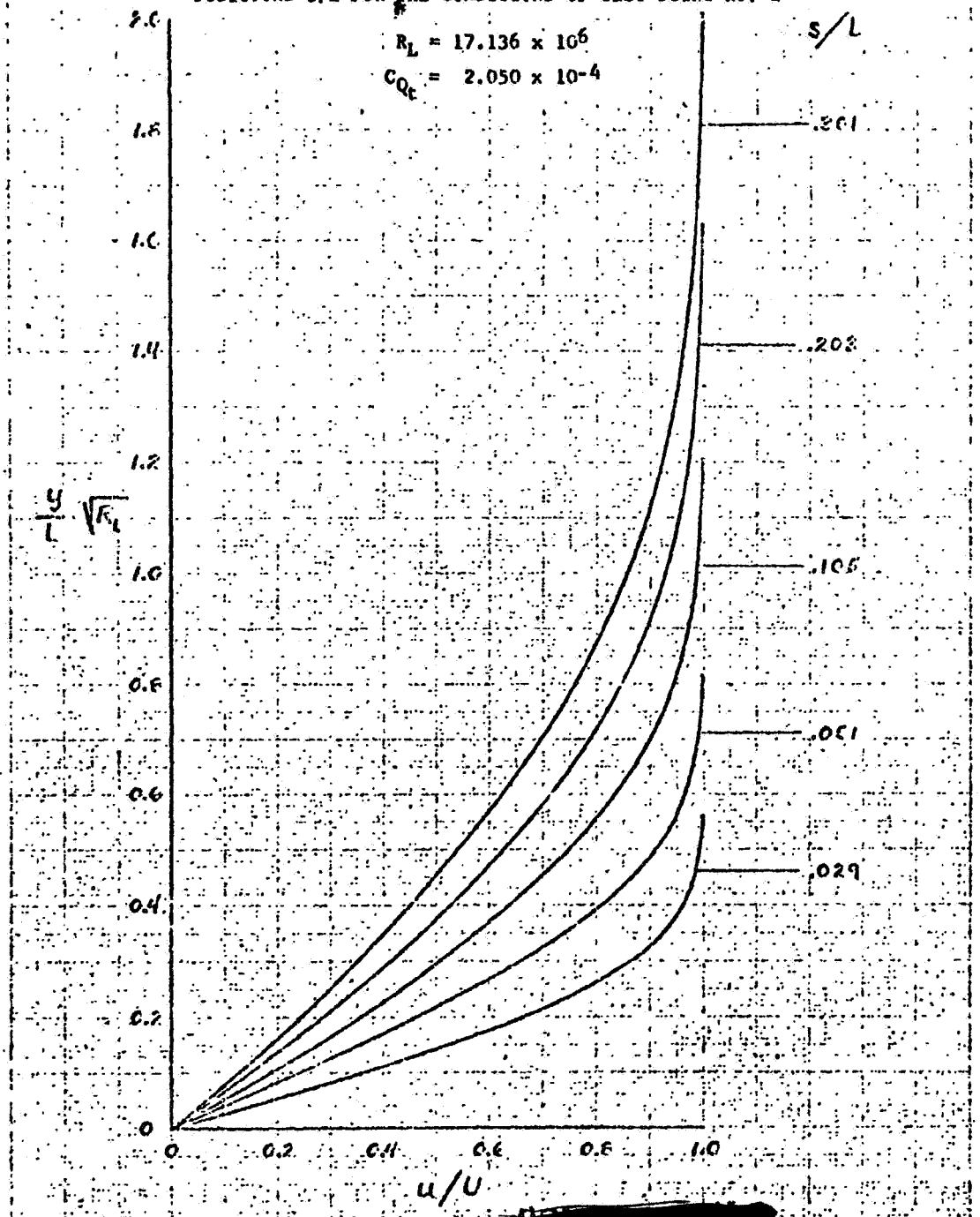

[redacted]

FIGURE 72b
CALCULATED BOUNDARY LAYER PROFILES AT VARIOUS LENGTHWISE POSITIONS s/L FOR THE CONDITIONS OF TEST POINT NO. 2

$R_L = 17.136 \times 10^6$
$C_{Q_t} = 2.050 \times 10^{-4}$

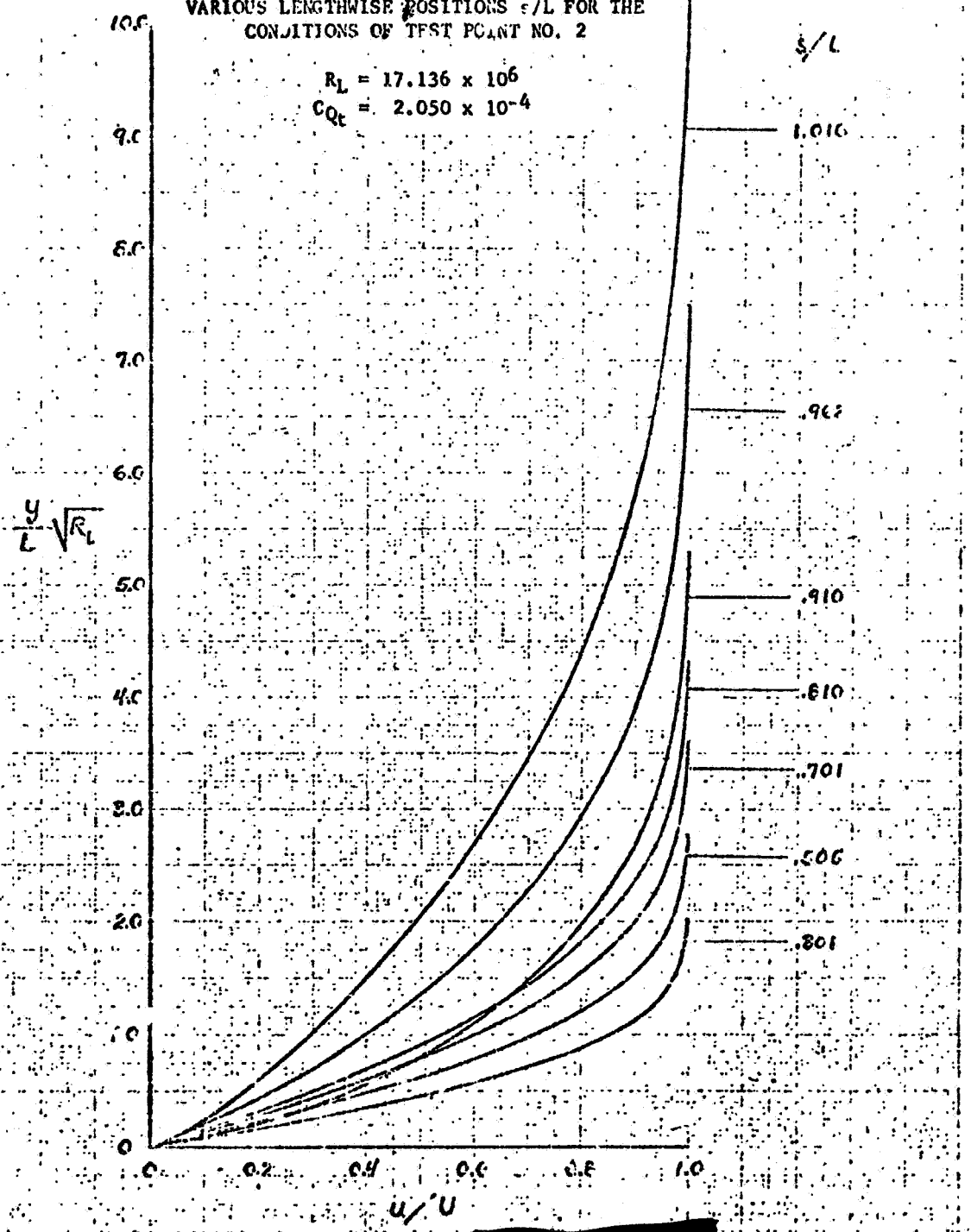

[redacted]

FIGURE 7A
NONDIMENSIONAL EQUIVALENT DISTRIBUTED SUCTION
VELOCITY DISTRIBUTION OVER BOUNDARY LAYER
DEVELOPMENT FOR TEST POINT NO. 102

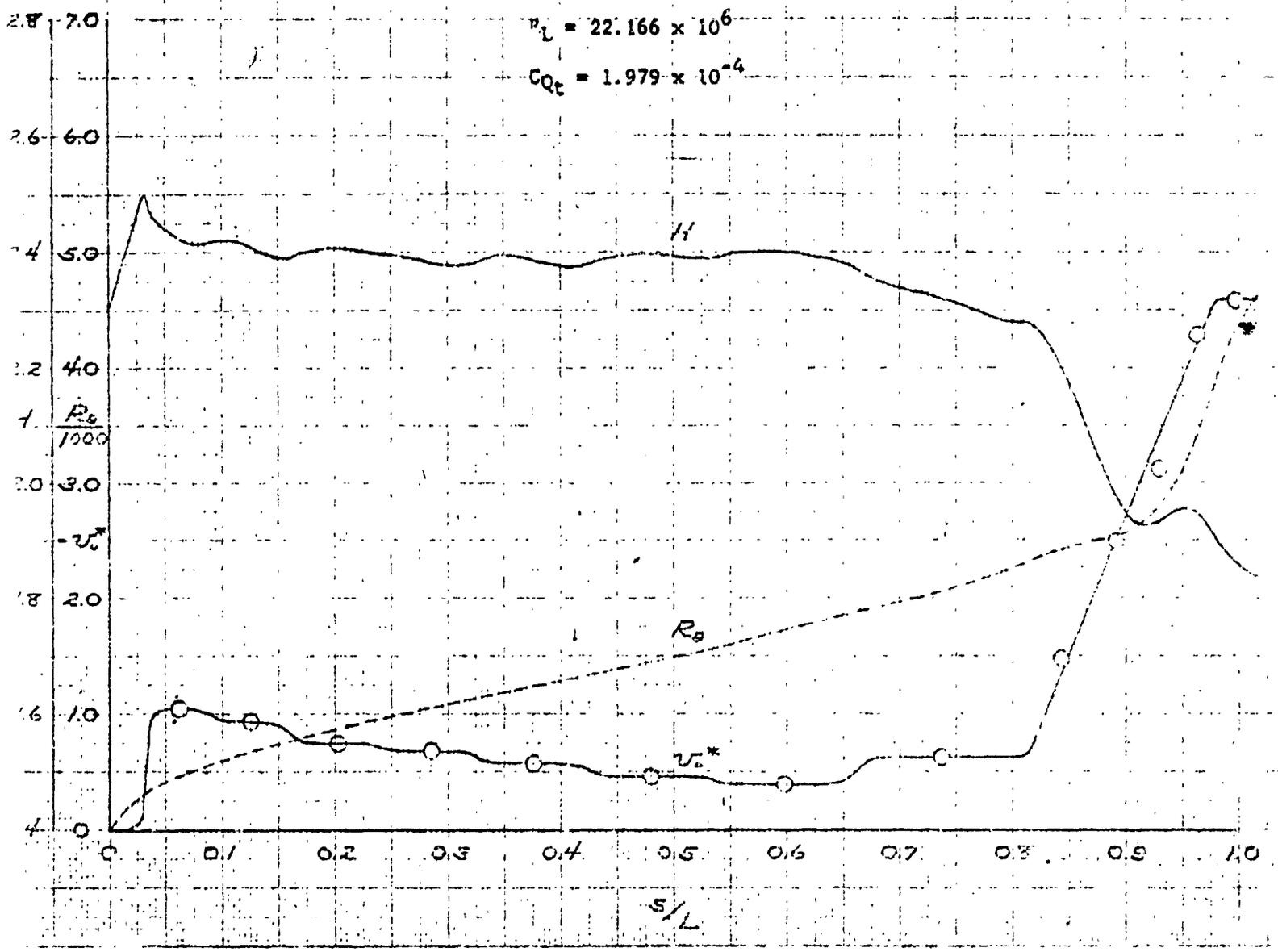

CHECKER	NORTHROP CORPORATION NORAIR DIVISION	REPORT NO.
DATE		MODEL

FIGURE 14

[illegible]

FOR THE CONDITIONS OF TEST POINT NO. 102

$R_L = 22.166 \times 10^6$

$C_{Q_t} = 1.979 \times 10^{-4}$

	CALC.	MEASURED						
RAKE NO.		1	2	3	4	5	6	
SYM.	—	○	△	□	▽	◇	▷	
θ	.0359	.0340	.0325	.0361	.0381	.0352	.0371	(IN.)
ε^*	.0622	.0560	.0522	.0622	.0653	.0550	.0572	(IN.)
H	1.838	1.647	1.624	1.725	1.726	1.564	1.543	
R_θ	4620	4640	4430	4920	5200	4800	5060	
$C_{Q_t} \times 10^4$	1.437			1.459				

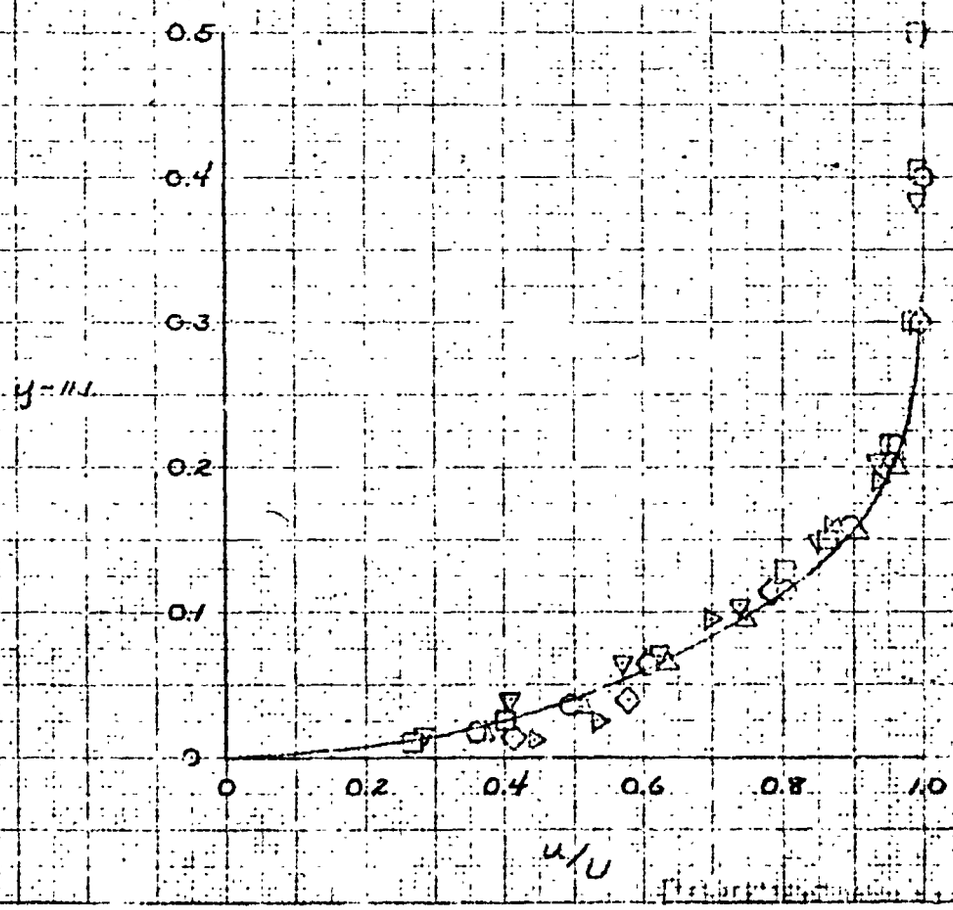

NORTHROP CORPORATION
NORAIR DIVISION

CHECKER

DATE

REPORT NO.

MODEL

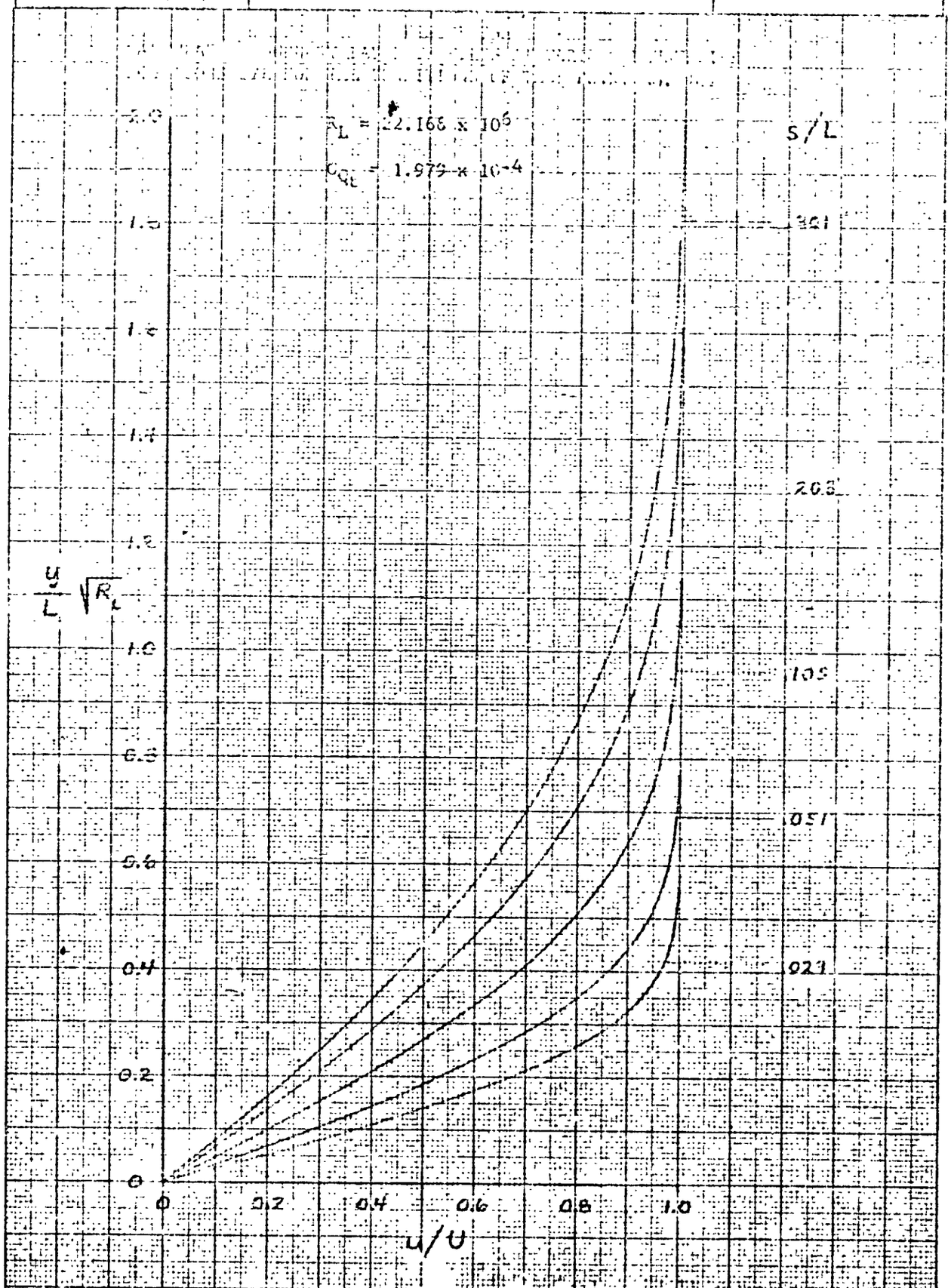

NORTHROP CORPORATION
NORAIR DIVISION

CHECKER

DATE

REPORT NO.

MODEL

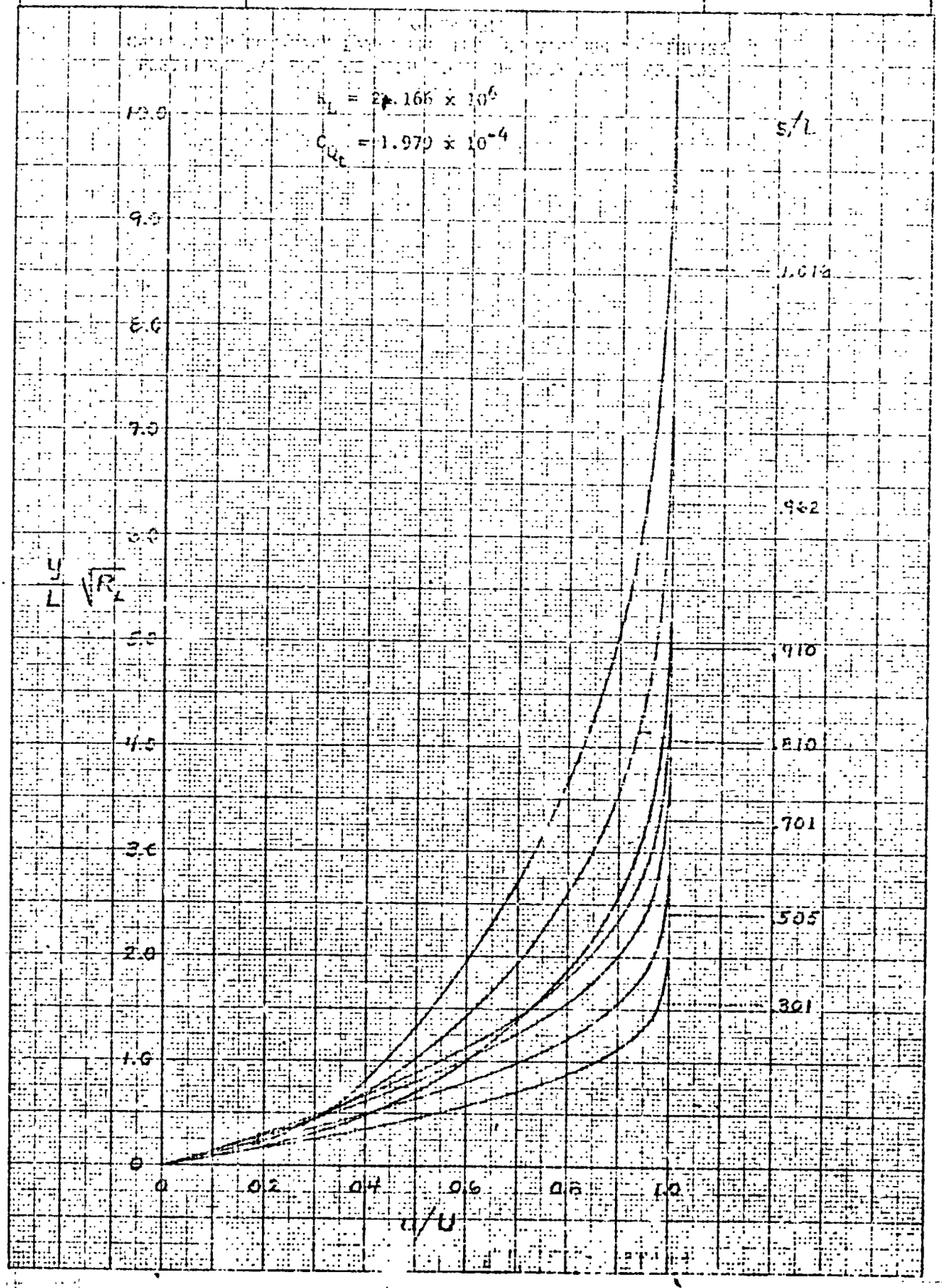

FIGURE 76
NONDIMENSIONAL EQUIVALENT DISTRIBUTED SUCTION
VELOCITY DISTRIBUTION AND BOUNDARY LAYER
DEVELOPMENT FOR TEST POINT NO. 47

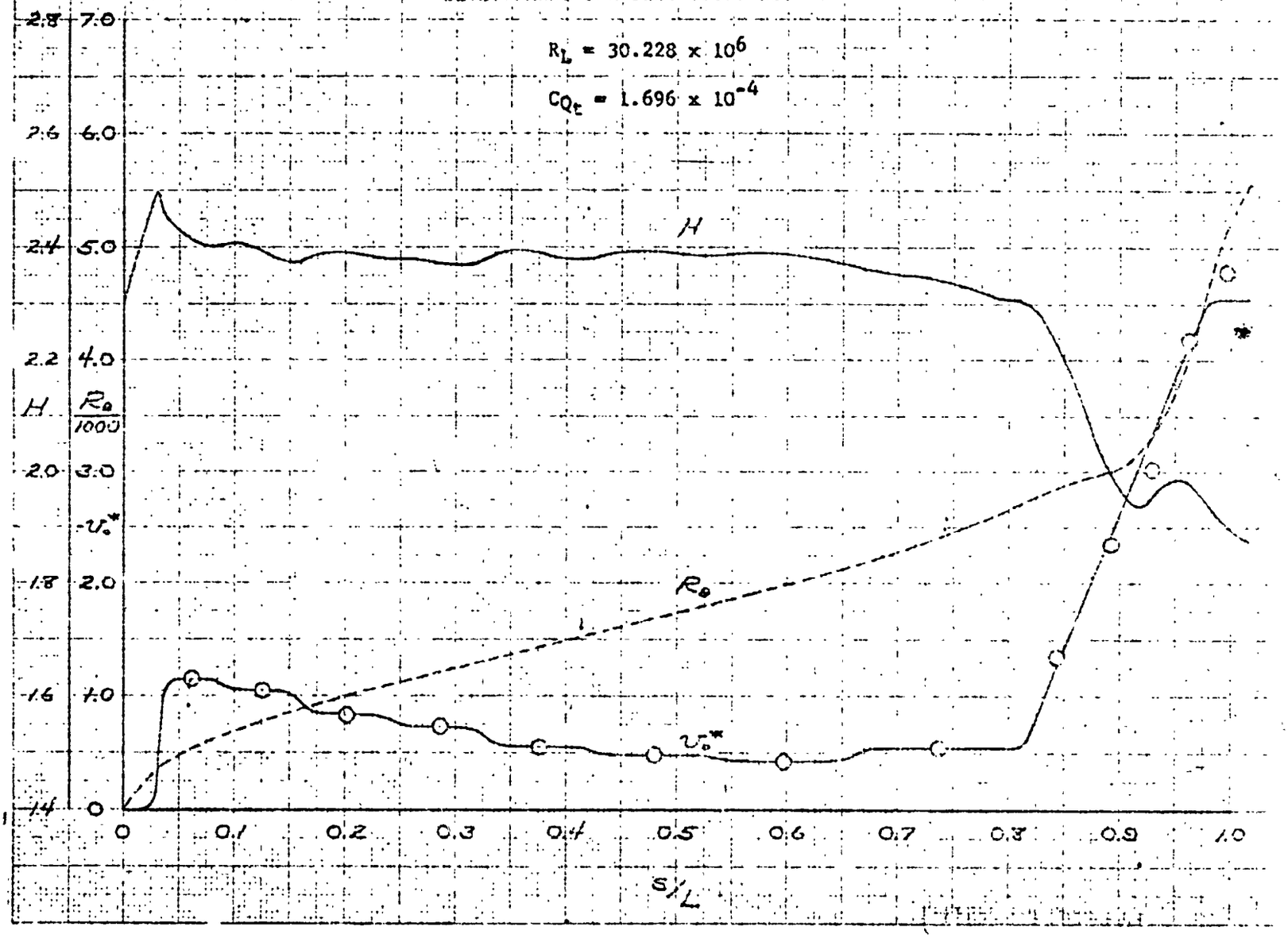

CHECKED	BOEING CORPORATION NORAIR DIVISION	REPORT NO.
DATE		MODEL

$R_L = 30.228 \times 10^6$

$C_{Q_t} = 1.696 \times 10^{-4}$

	CALC.	MEASURED						
RAKE NO.		1	2	3	4	5	6	
SYM.	—	○	△	□	▽	◇	▷	
θ	.0256	.0305	.0278	.0313	.0308	.0311	.0317	(IN.)
δ^*	.0555	.0496	.0447	.0509	.0522	.0463	.0454	(IN.)
H	1.876	1.625	1.605	1.624	1.692	1.455	1.431	
R_θ	5520	5680	5790	5840	5750	5790	5920	
$C_{D_w} \times 10^4$	1.255			1.297				

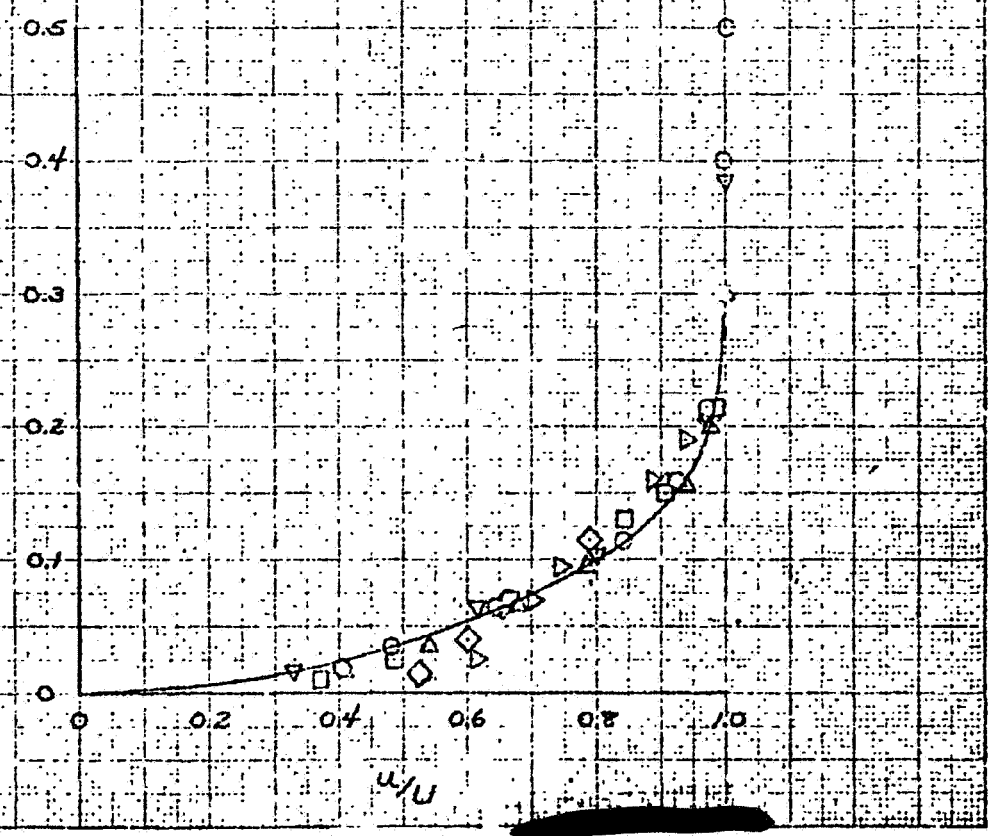

[redacted]

CHECKER	NORTHROP CORPORATION NORAIR DIVISION	REPORT NO.
DATE		MODEL

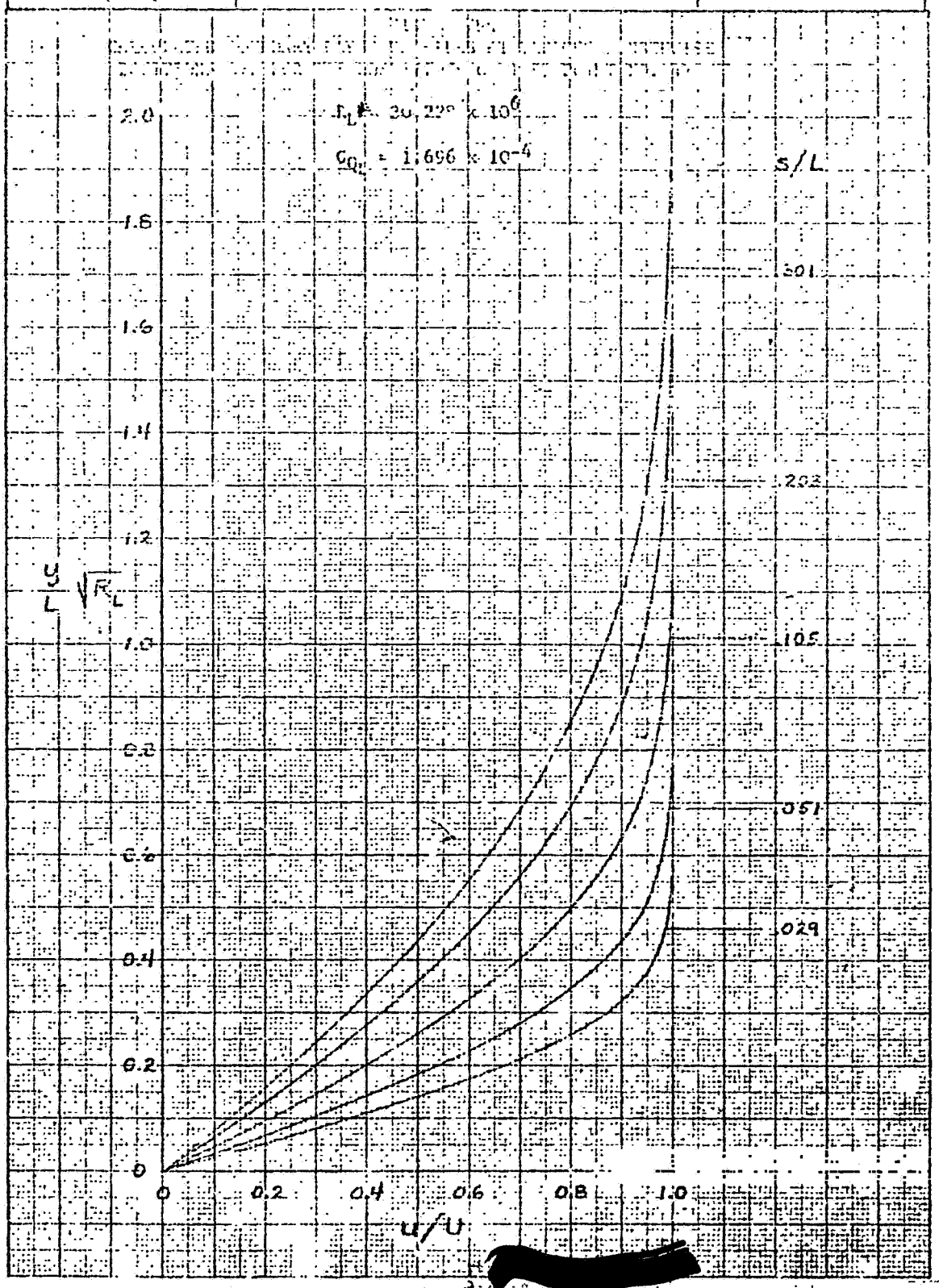

[redacted]

NORTHROP CORPORATION
NORAIR DIVISION

CHECKER

DATE

REPORT NO.

MODEL

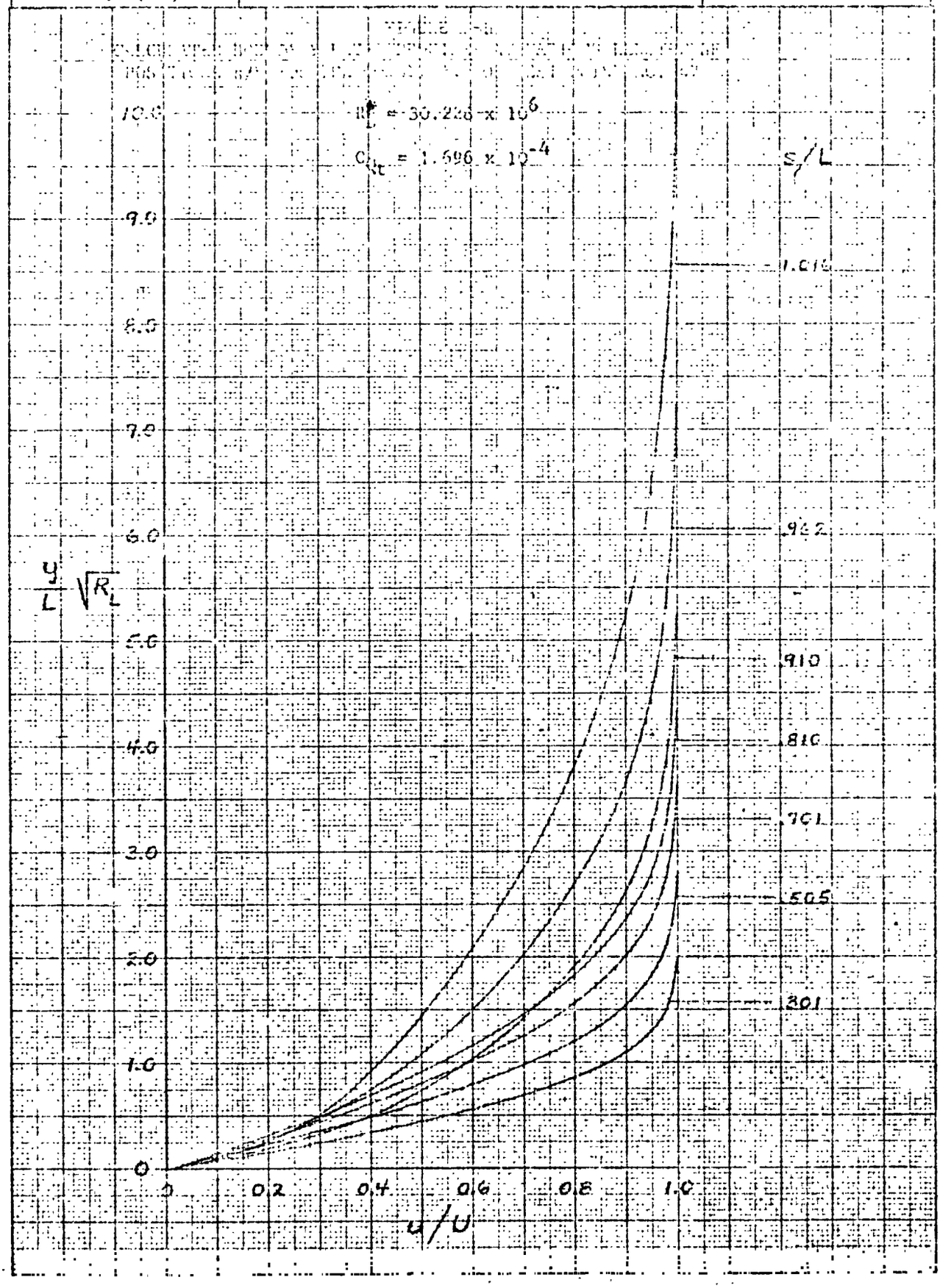

FIGURE 79
NONDIMENSIONAL EQUIVALENT DISTRIBUTED SUCTION
VELOCITY DISTRIBUTION AND BOUNDARY LAYER
DEVELOPMENT FOR TEST POINT NO. 117

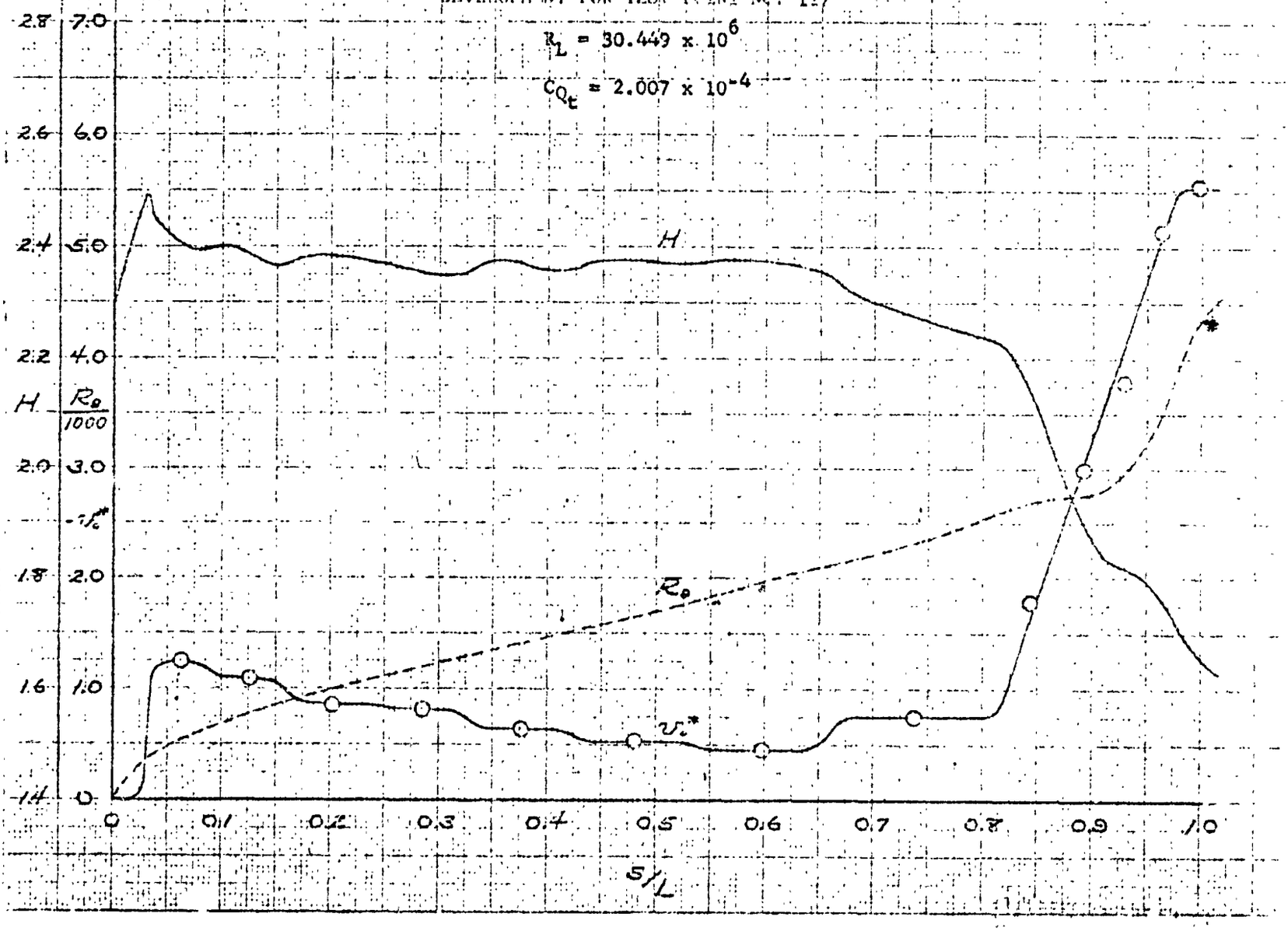

CHECKER	NORTHROP CORPORATION NORAIR DIVISION	REPORT NO.
DATE		MODEL

FIGURE [illegible]

COMPARISON OF CALCULATED AND MEASURED BOUNDARY LAYER

VELOCITY PROFILES [illegible]

FOR THE CONDITIONS OF TEST POINT NO. 117

$R_L = 30.449 \times 10^6$

$C_{Q_t} = 2.007 \times 10^{-4}$

	CALC.	MEASURED						
RAKE NO		1	2	3	4	5	6	
SYM	—	○	△	□	▽	◇	▷	
θ	.0242	.0235	.0233	.0242	.0278	.0247	.0247	(IN.)
δ^*	.0354	.0298	.0334	.0376	.0423	.0350	.0367	(IN.)
H	1.630	1.540	1.425	1.512	1.520	1.417	1.422	
R_θ	4530	4480	4360	4550	5230	4630	4630	
$C_{D_A} \times 10^5$	1.013			1.056				

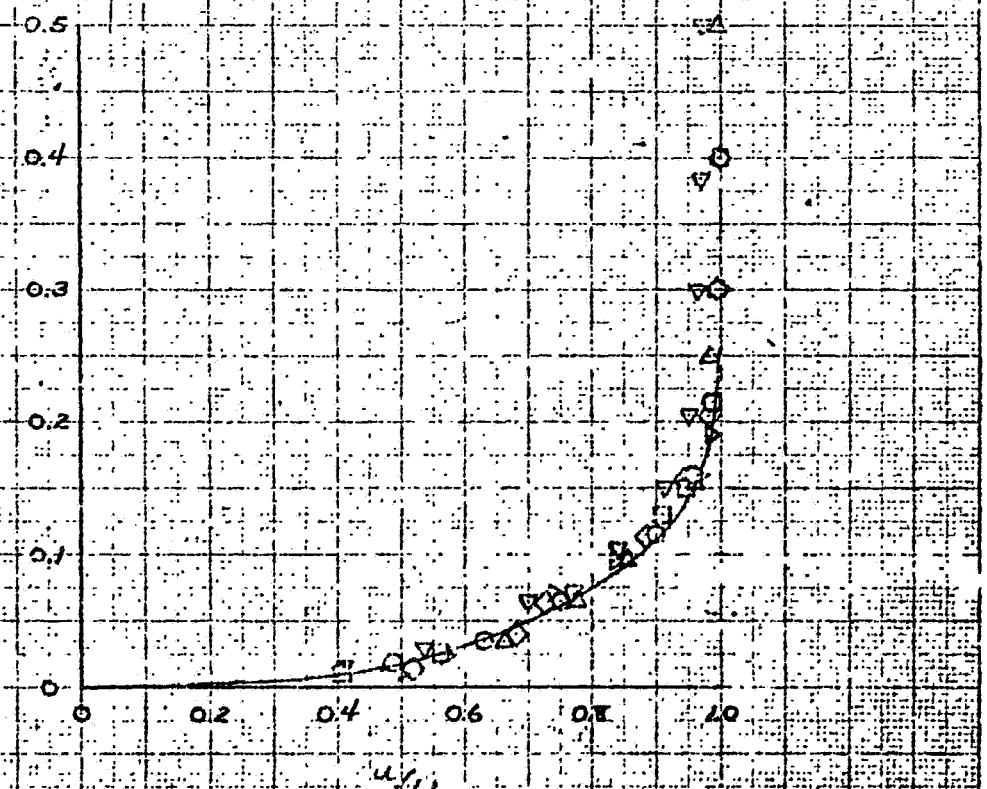

[redacted]

CHECKED	NORTHROP CORPORATION NORAIR DIVISION	REPORT NO.
DATE		MODEL

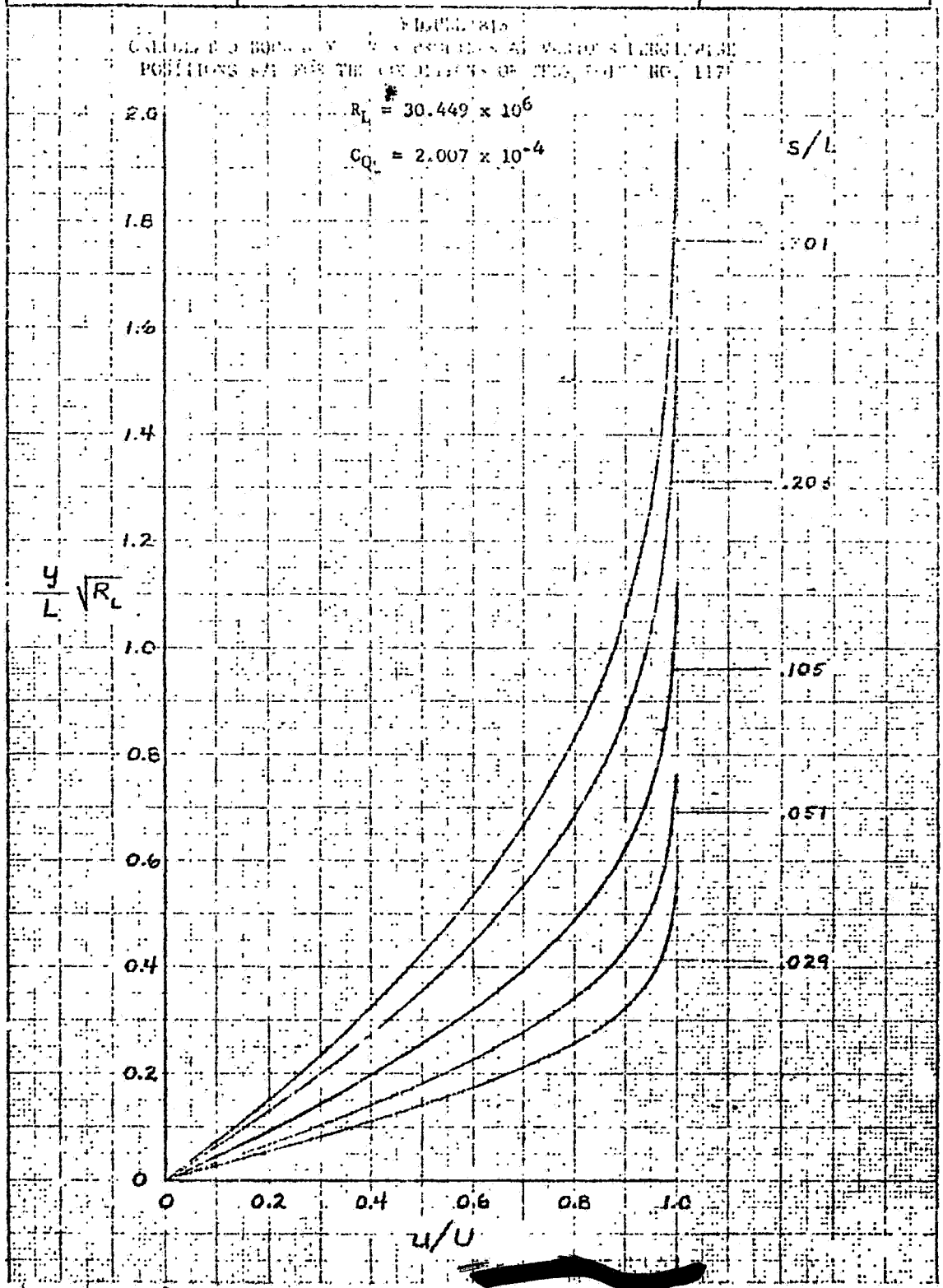

CHECKER	NORTHROP CORPORATION NORAIR DIVISION	REPORT NO.
DATE		MODEL

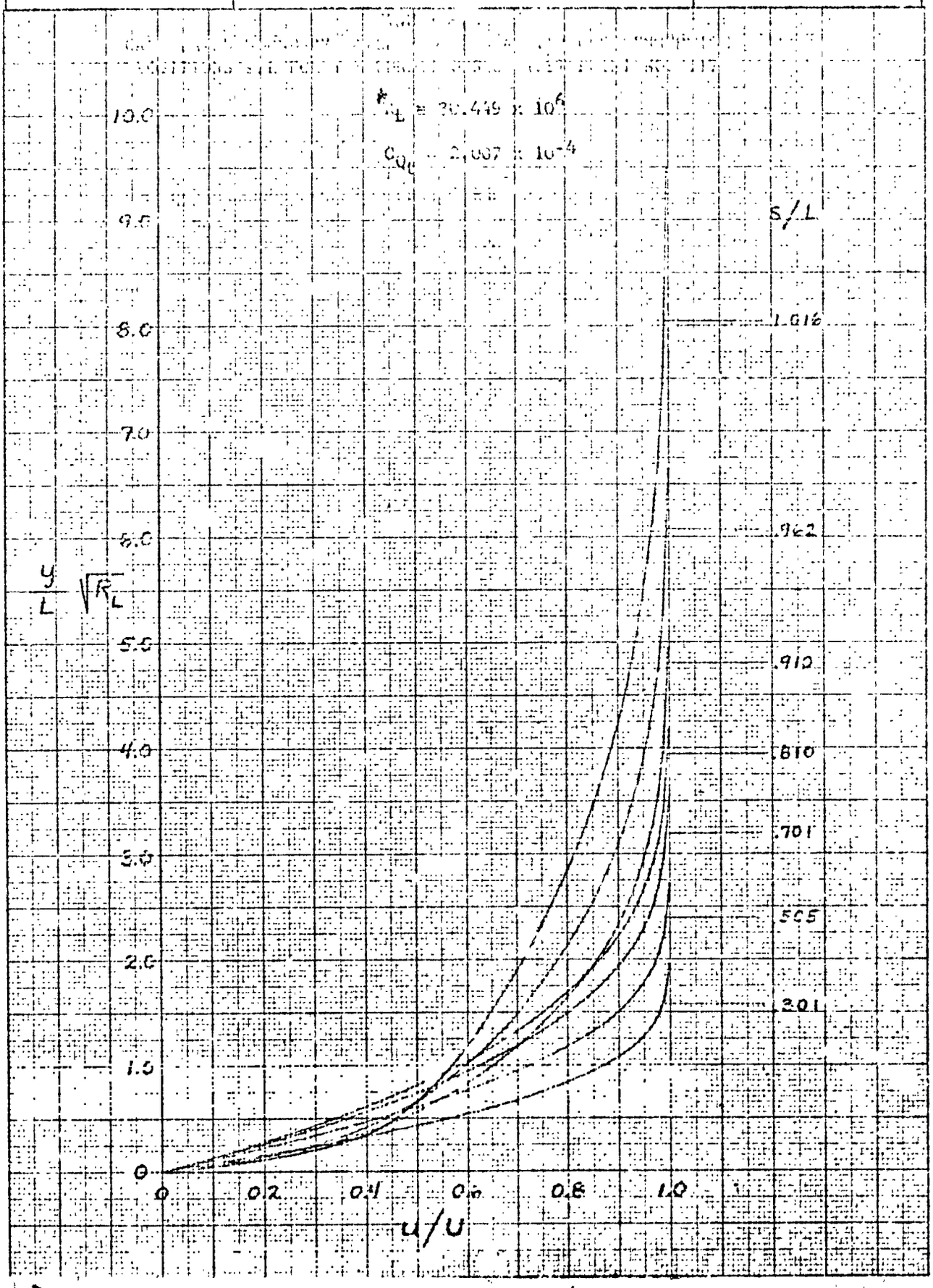

[redacted]

FIGURE 82
NONDIMENSIONAL EQUIVALENT DISTRIBUTED SUCTION VELOCITY
DISTRIBUTION AND BOUNDARY LAYER DEVELOPMENT FOR TEST POINT NO. 262

$R_L = 38.036 \times 10^6$
$C_{Q_t} = 1.860 \times 10^{-4}$

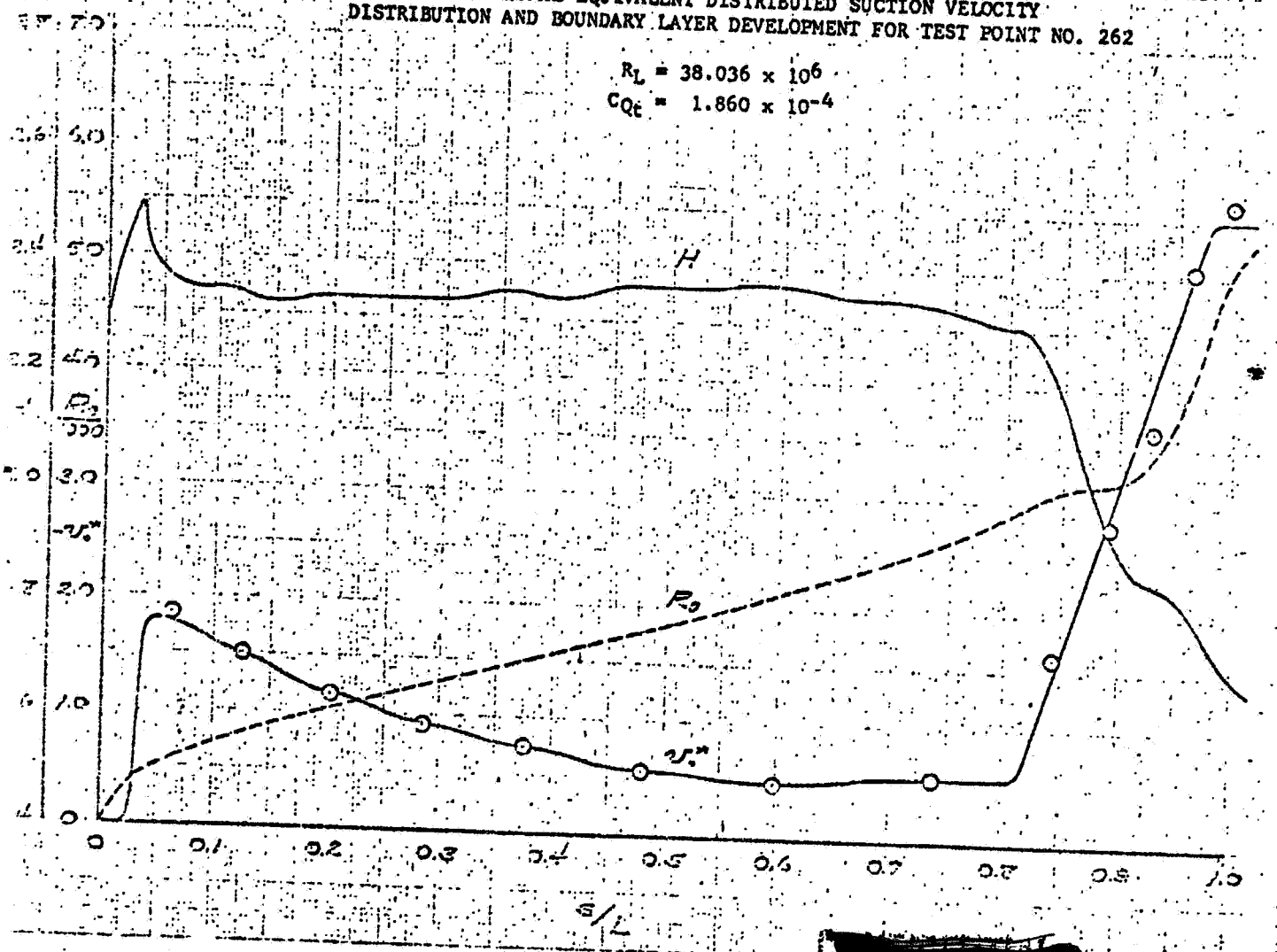

[redacted]

FIGURE 83
COMPARISON OF CALCULATED AND MEASURED BOUNDARY LAYER VELOCITY PROFILES AT REAR END OF BODY FOR THE CONDITIONS OF TEST POINT NO. 262

$R_L = 38.036 \times 10^6$
$C_{Q_L} = 1.860 \times 10^{-4}$

	CALC.	MEASURED					
RAKE NO.		1	2	3	4	5	6
SYM	—	○	△	□	▽	◇	▷
θ	.0225	.021	.020	.021	.023	.021	.025
δ*	.0374	.032	.029	.036	.042	.042	.040
H	1.67	1.45	1.46	1.49	1.46	1.36	1.39
R_θ	5750	5000	4720	5620	6650	7100	6720
$C_D \times 10^4$	1.02			1.10			

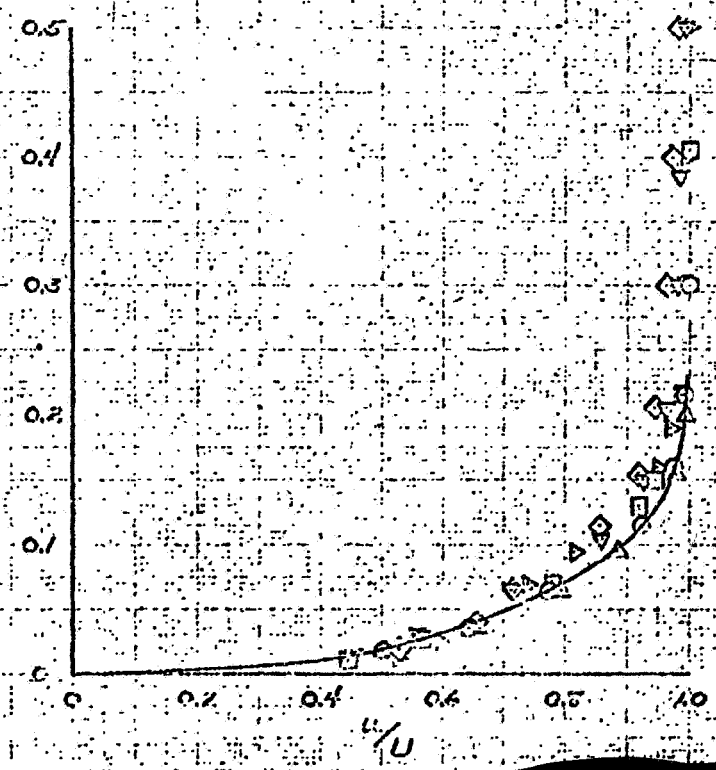

[redacted]

FIGURE 84a
CALCULATED BOUNDARY LAYER PROFILES AT VARIOUS LENGTHWISE POSITIONS s/L FOR THE CONDITIONS OF TEST POINT NO. 262

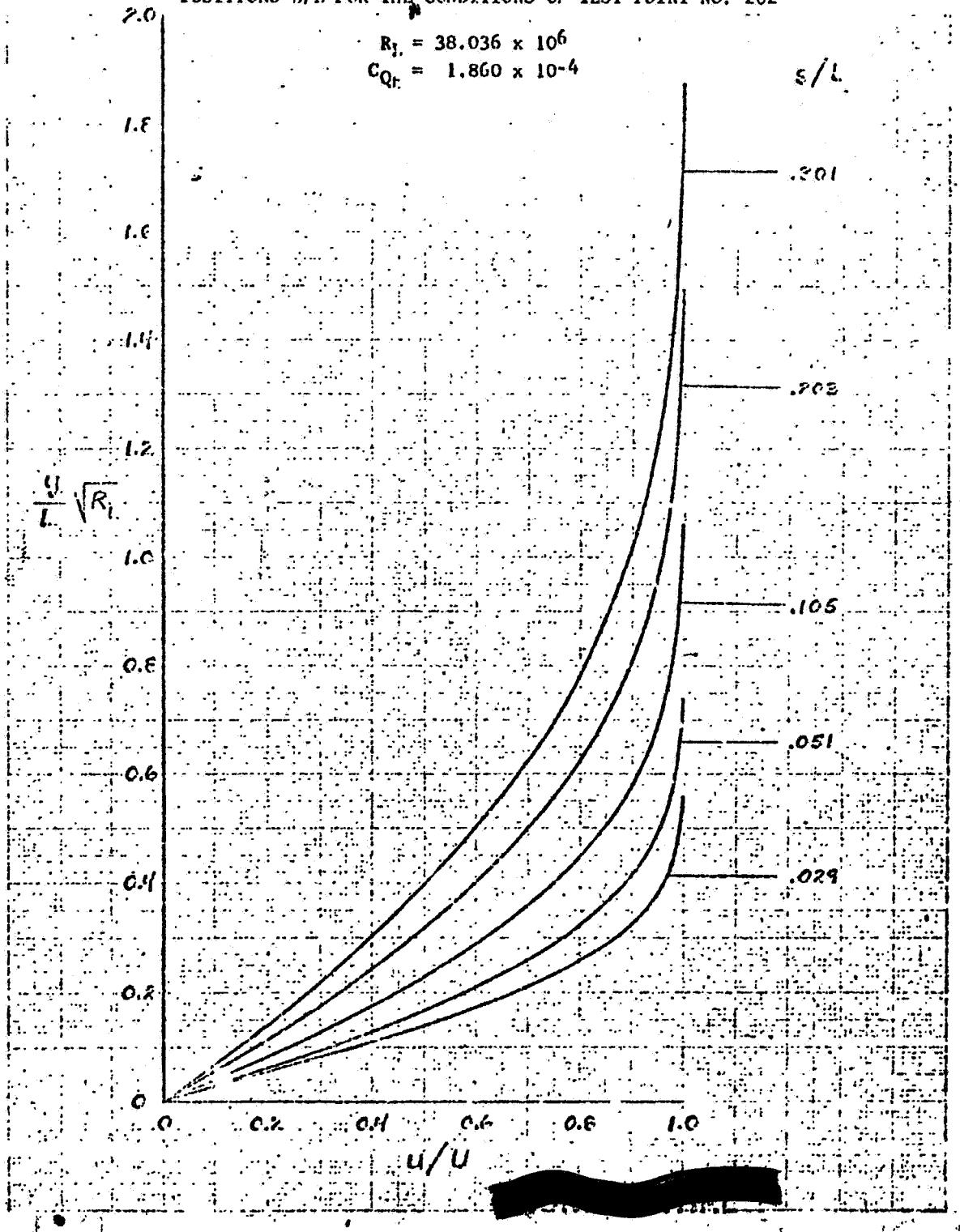

[redacted]

FIGURE 84b
CALCULATED BOUNDARY LAYER PROFILES AT VARIOUS LENGTHWISE POSITIONS s/L FOR THE CONDITIONS OF TEST POINT NO. 262

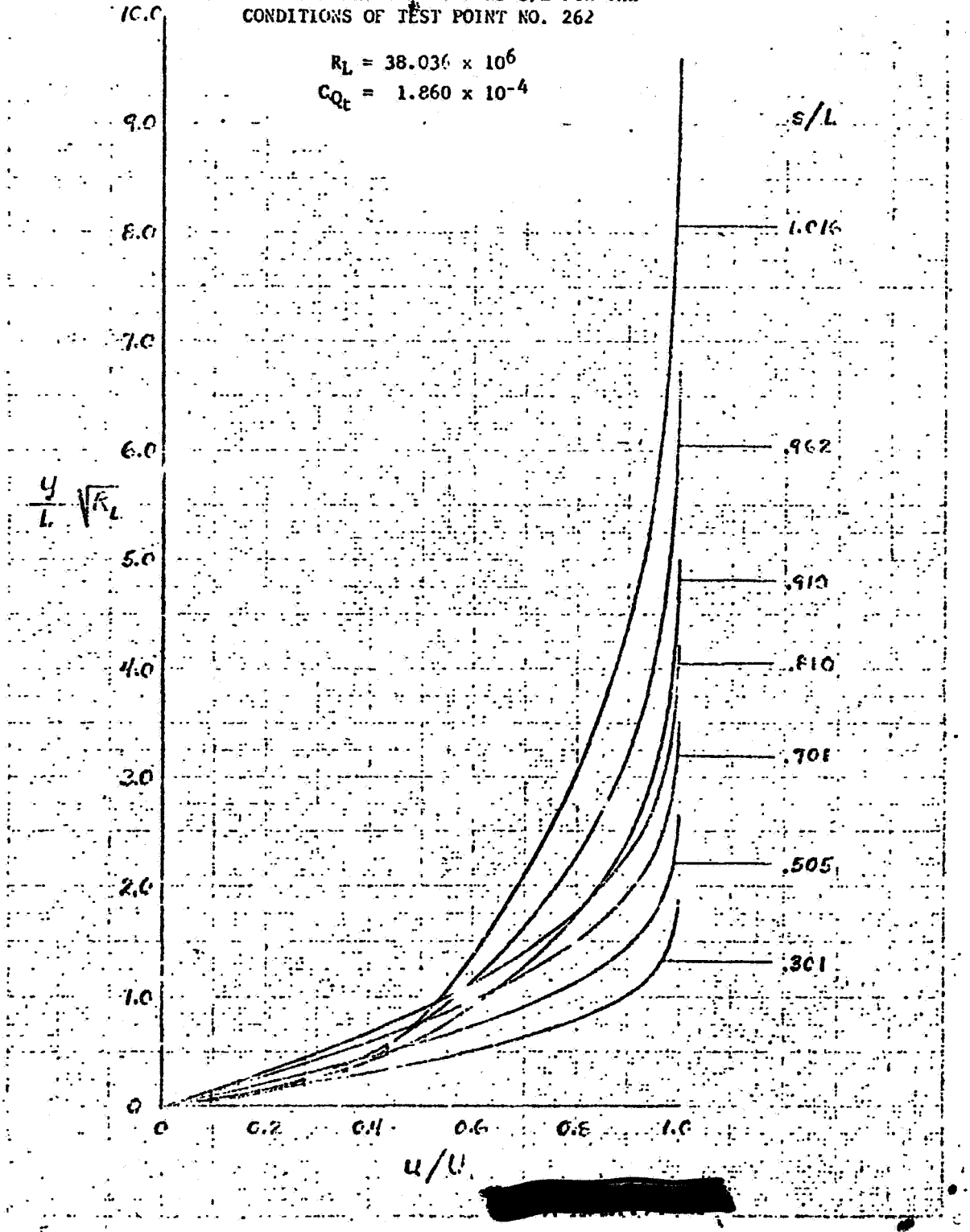

[redacted]

FIGURE 85

NONDIMENSIONAL EQUIVALENT DISTRIBUTED SUCTION VELOCITY DISTRIBUTION AND BOUNDARY LAYER DEVELOPMENT FOR TEST POINT NO. 268

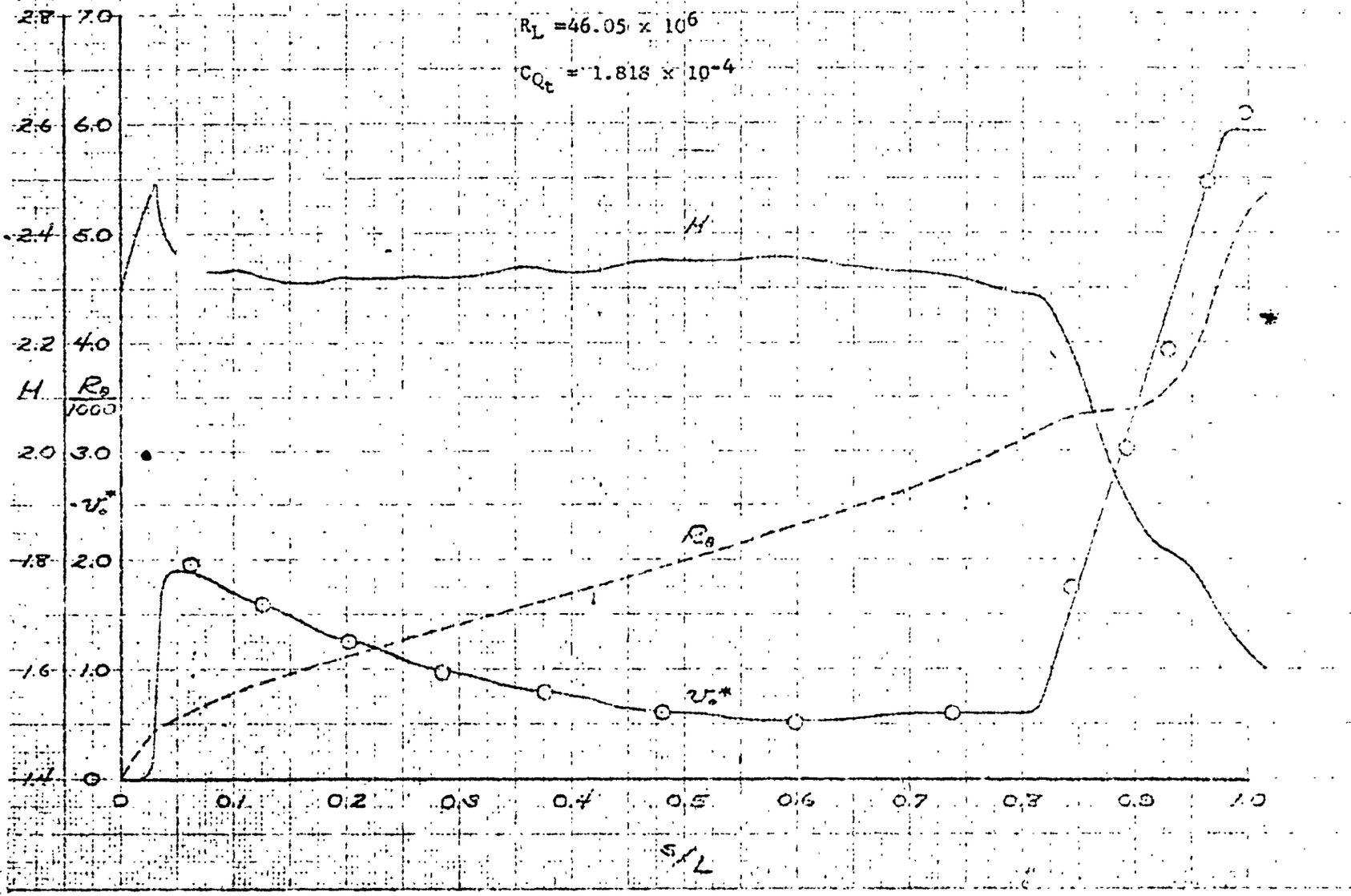

NORTHROP CORPORATION
NORAIR DIVISION

CHECKED
DATE
REPORT NO.
MODEL

CHECKED

DATE

NORTHROP CORPORATION

NORAIR DIVISION

REPORT NO.

MODEL

$R_L^* = 46.05 \times 10^6$

$C_{Q_t} = 1.816 \times 10^{-4}$

	CALC.	MEASURED						
RAKE NO.		1	2	3	4	5	6	
SYM	---	○	△	□	▽	◇	▷	
θ	.0159	.0158	.0217		.0221	.0203	.0208	(IN.)
δ^*	.0303	.0266	.0285		.0317	.0282	.0290	(IN.)
H	1.600	1.418	1.312		1.430	1.388	1.395	
R_θ	5360	5330	6150		6260	5750	5500	
$C_{f_w}/10^4$	0.891			0.886				

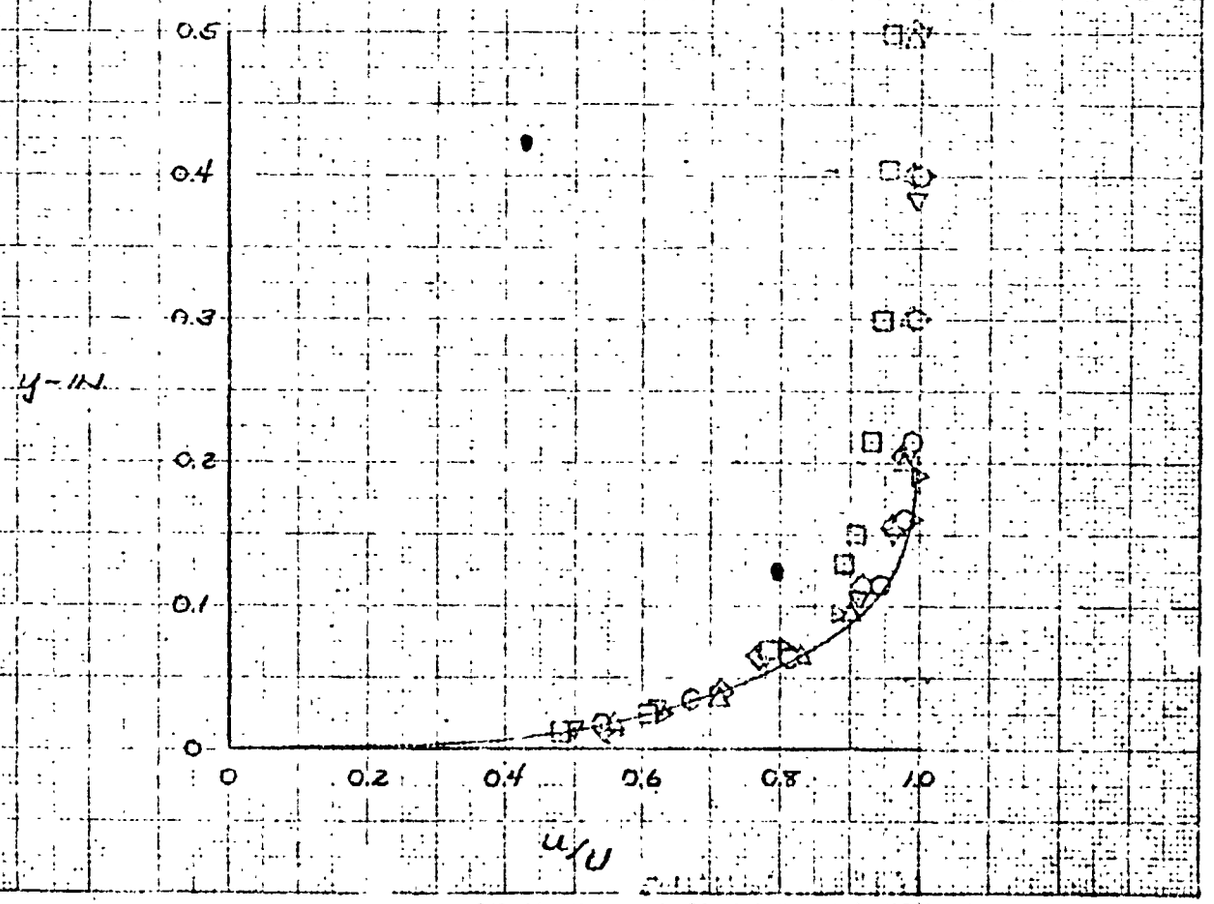

NORTHROP CORPORATION
NORAIR DIVISION

CHECKED | REPORT NO. | DATE | MODEL

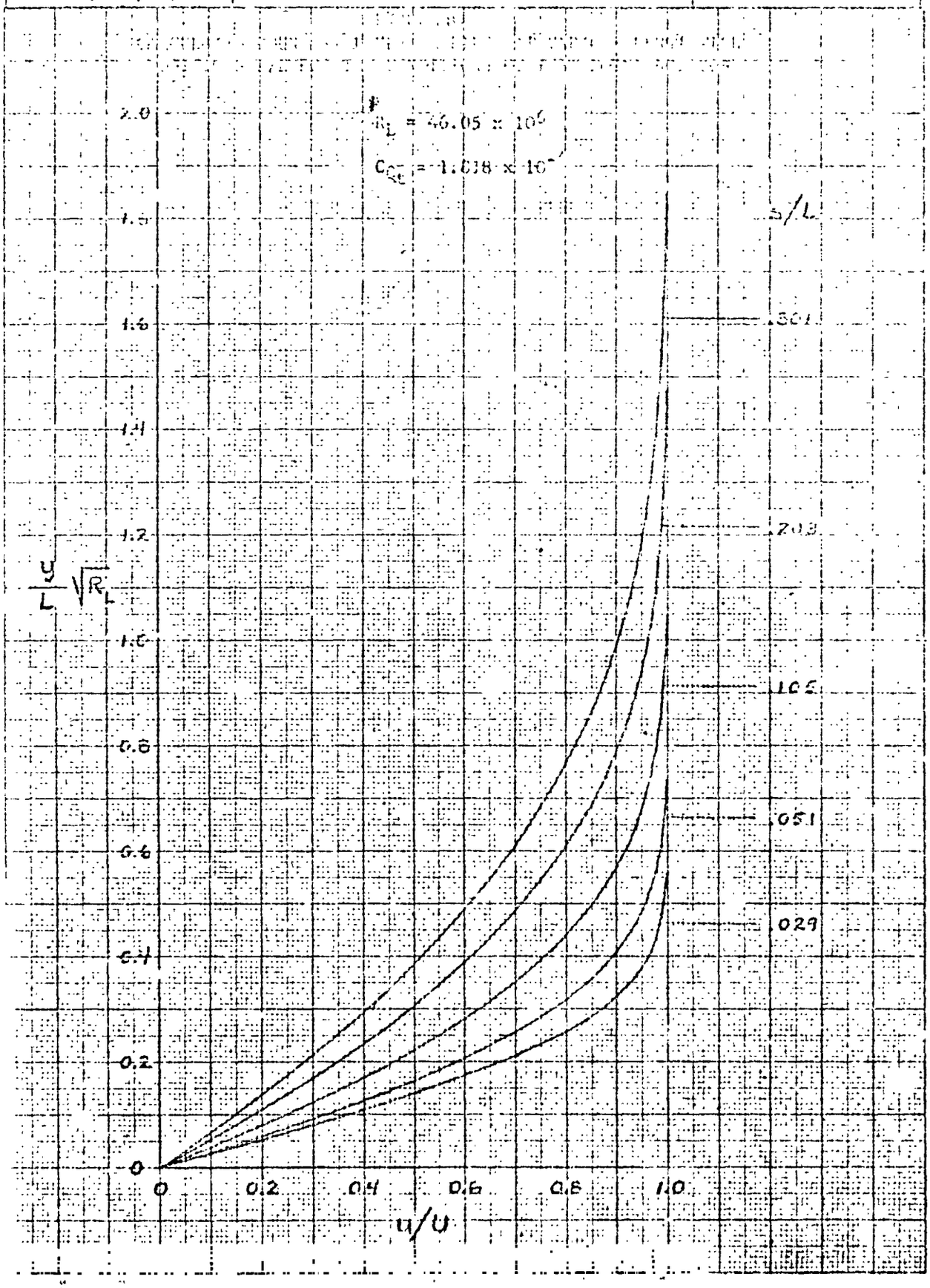

NORTHROP CORPORATION

NORAIR DIVISION

CHECKED

DATE

REPORT NO.

MODEL

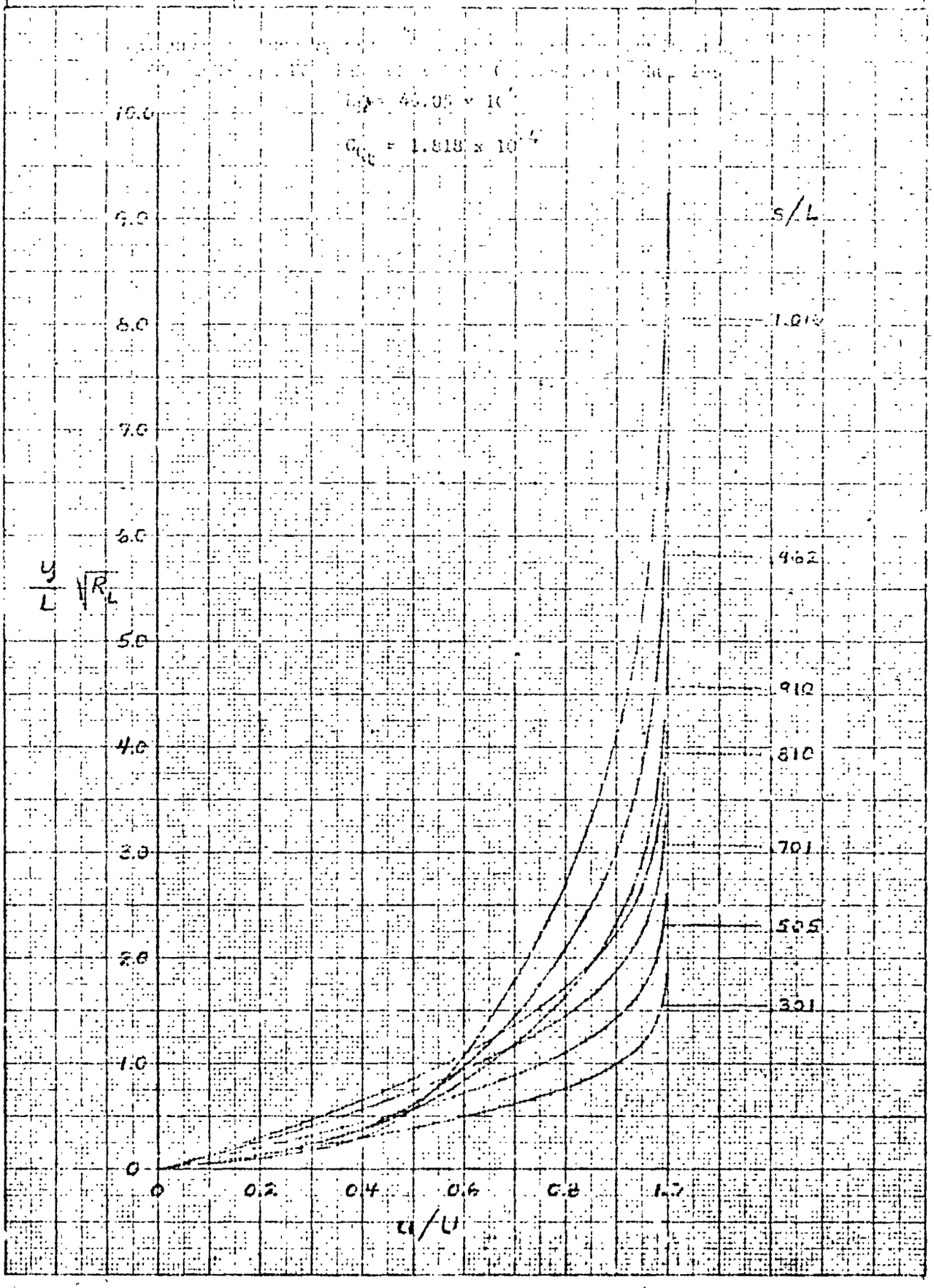

CHECKED

DATE

NORAIR DIVISION

REPORT NO.

MODEL

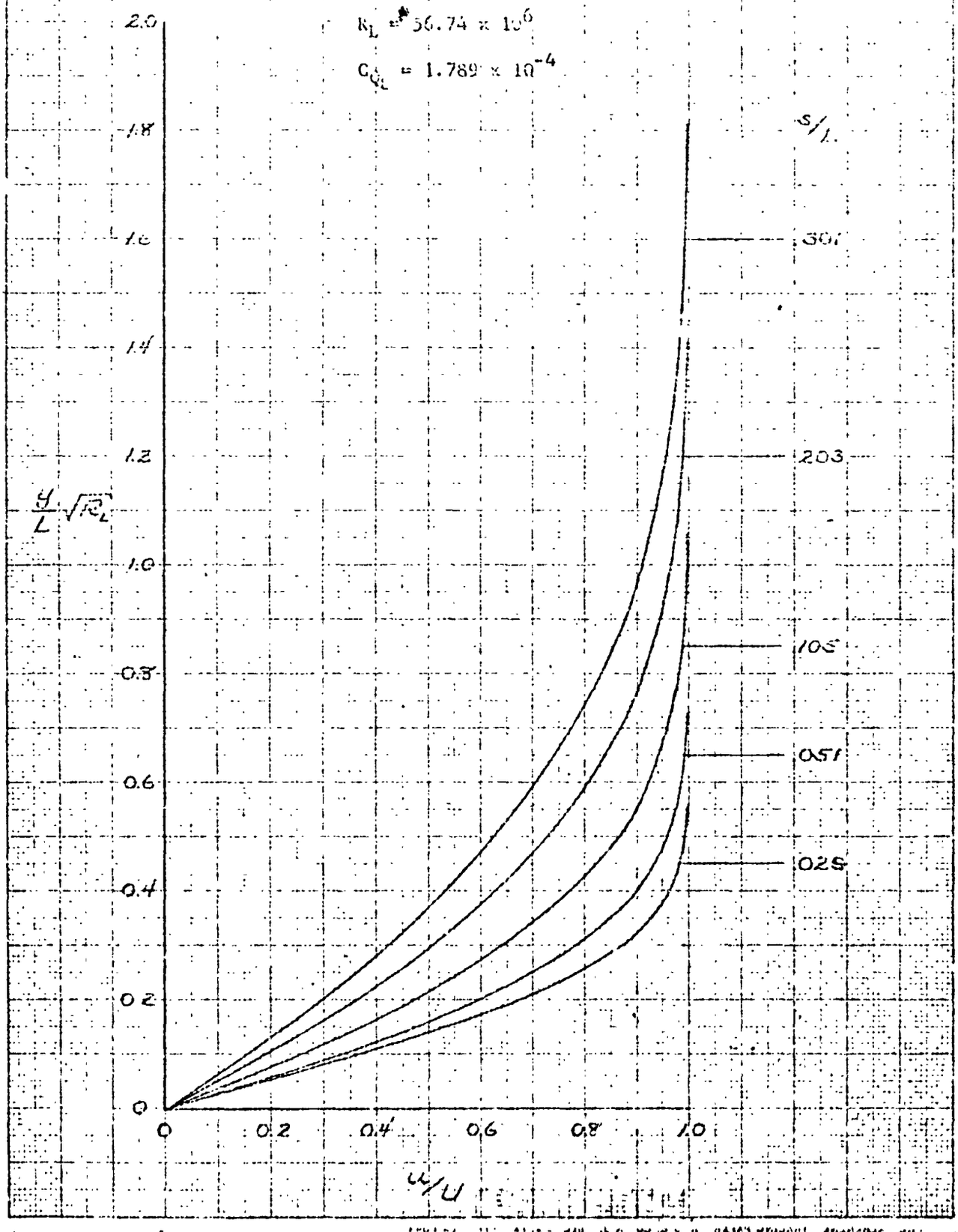

NORTH AMERICAN CORPORATION
NORAIR DIVISION

CHECKED

DATE

Reichardt LFC body (L/D=8)

$Re_L^* = 56.74 \times 10^6$

$C_{Q_t} = 1.759 \times 10^{-4}$

RAKE NO.	CALC	MEASURED 1	2	3	4	5	
SYM.	—	○	△	◁	▽	◇	
θ''	.0156	.0156	.0138		.0196	.0158	(IN.)
δ''	.0240	.0210	.0182		.0272	.0212	(IN.)
H	1.544	1.346	1.320		1.348	1.340	
Re_θ	5440	5450	4820		6850	5520	
$C_{D_W} \cdot 10^4$	0.661			0.713			
$10^4 C_{D_{inst.}}$				1.88			
$10^4 C_{D_{tot.}}$				2.59			

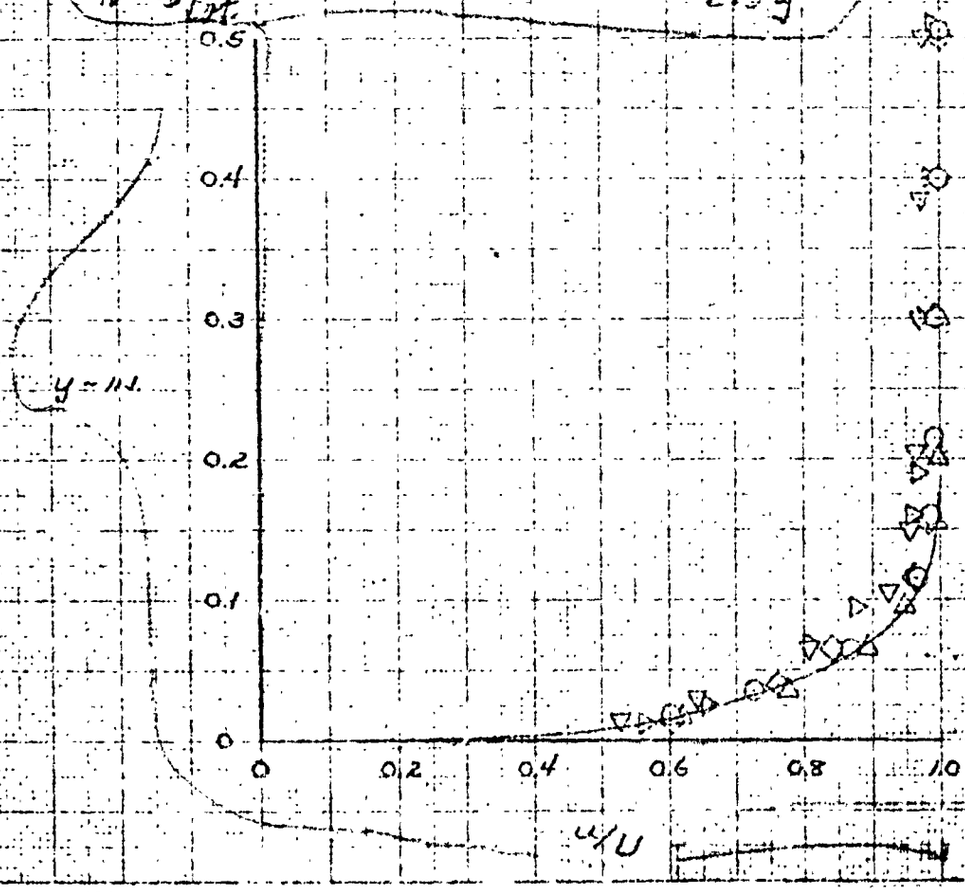

Reichardt LFC body ($L/D = 8$)

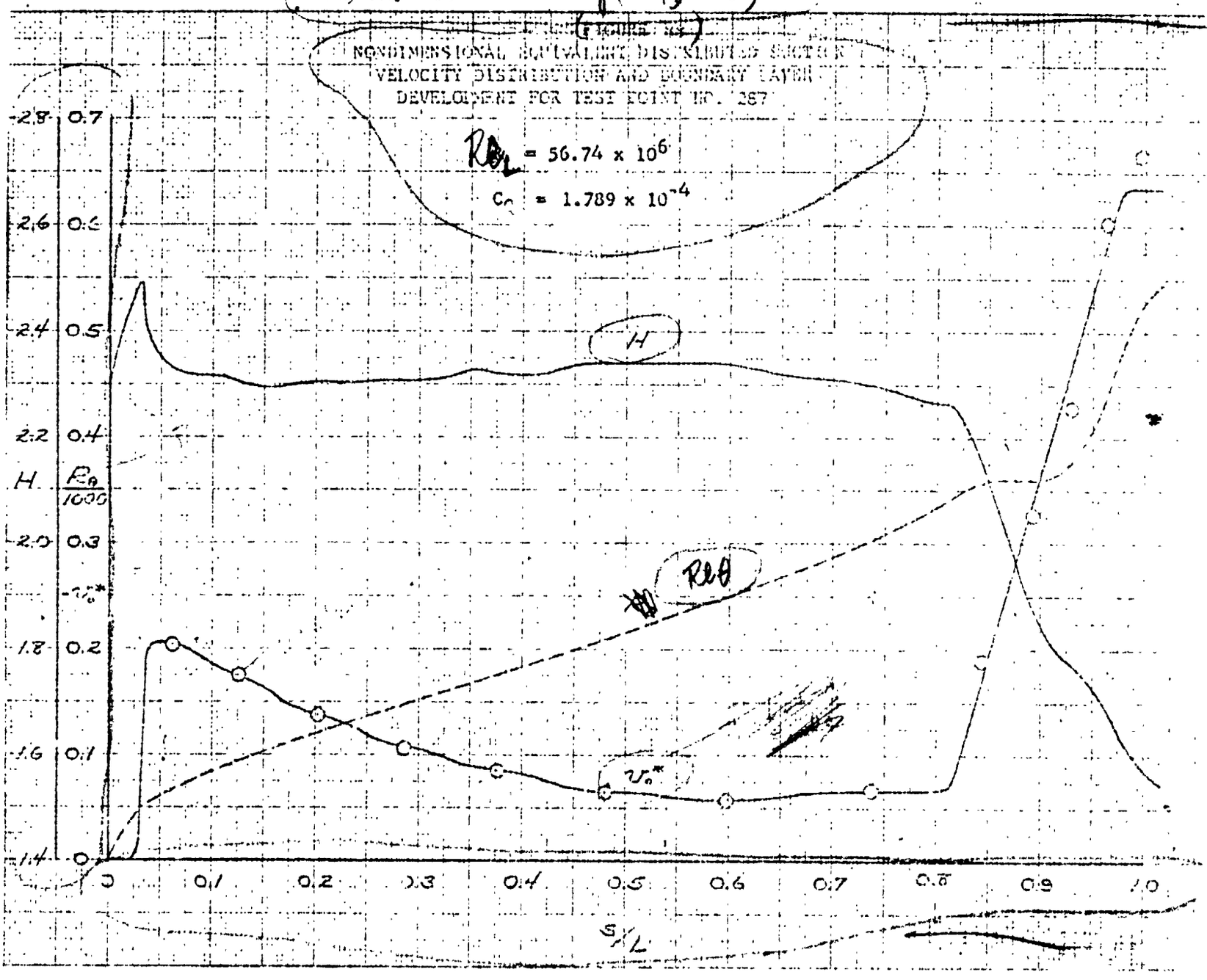

Reichardt LFC body (L/D = 8)

(FIGURE 54)

~~CONFIDENTIAL~~

LENGTHWISE DISTRIBUTION OF EQUIVALENT DISTRIBUTED

SUCTION VELOCITY v_o^* FOR SEVERAL REYNOLDS NUMBERS R_L

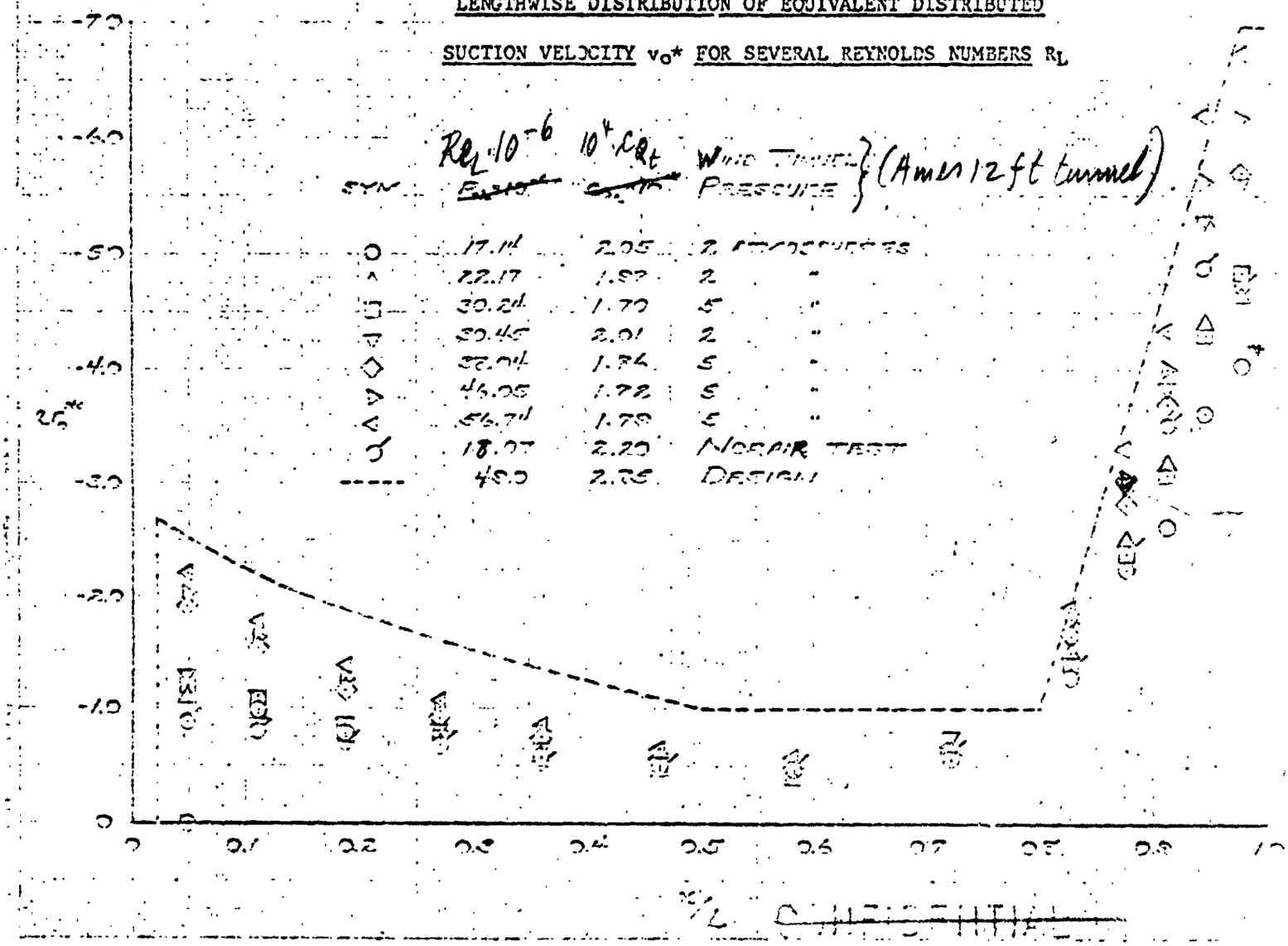

~~CONFIDENTIAL~~

NORTHROP CORPORATION
NORAIR DIVISION

CHECKED

DATE

REPORT NO.

MODEL

Fischardt LFC body (L/D = 8).

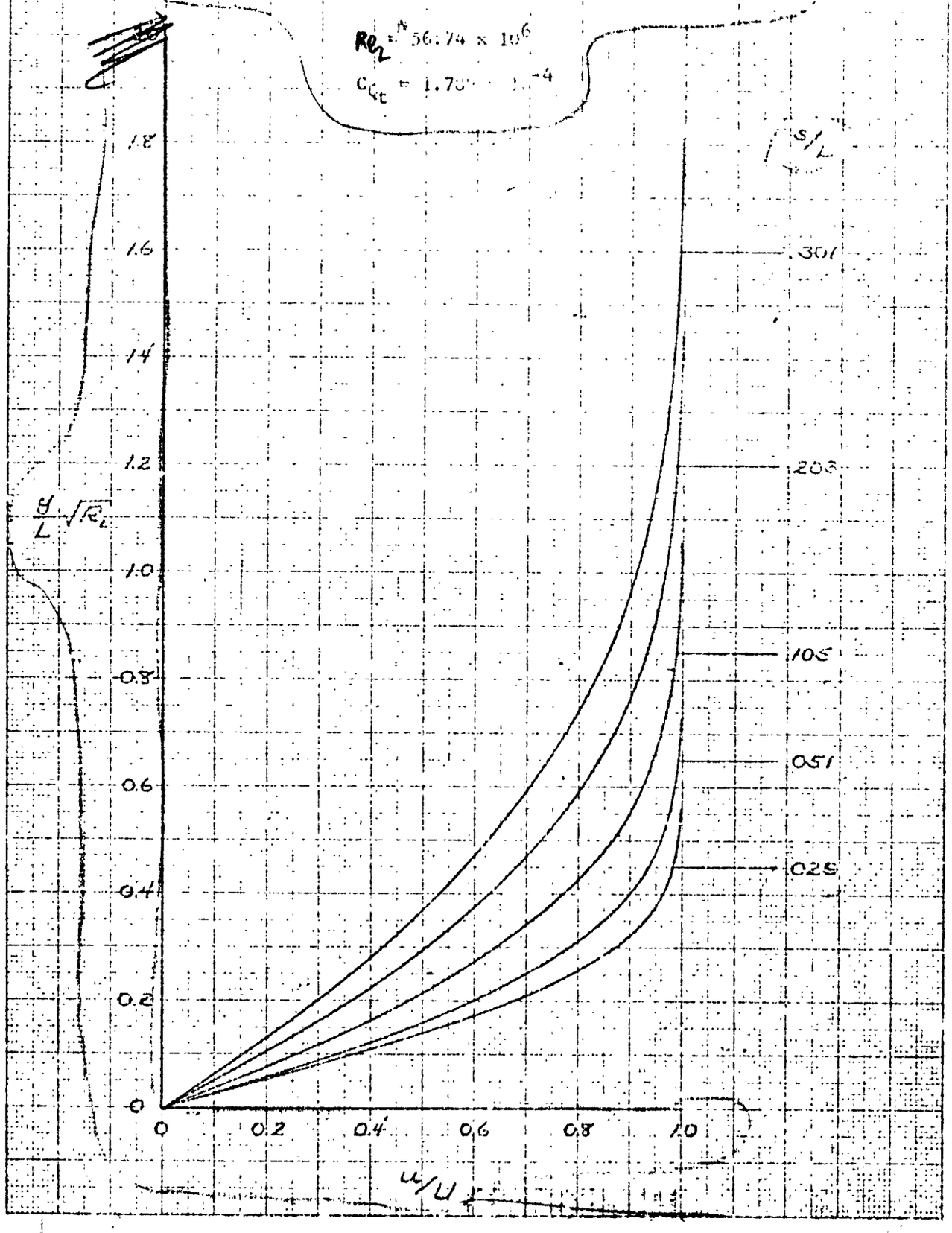

July 1963

Reichardt LFC body ($\frac{L}{D}=8$)

$Re_L = 56.74 \cdot 10^6$

$\alpha = 0°$

Reichardt LFC body ($\frac{L}{D}=8$)

$C_D = f(C_{Q_t})$, $\alpha = 0°$

$Re_L = 56.74 \cdot 10^6$

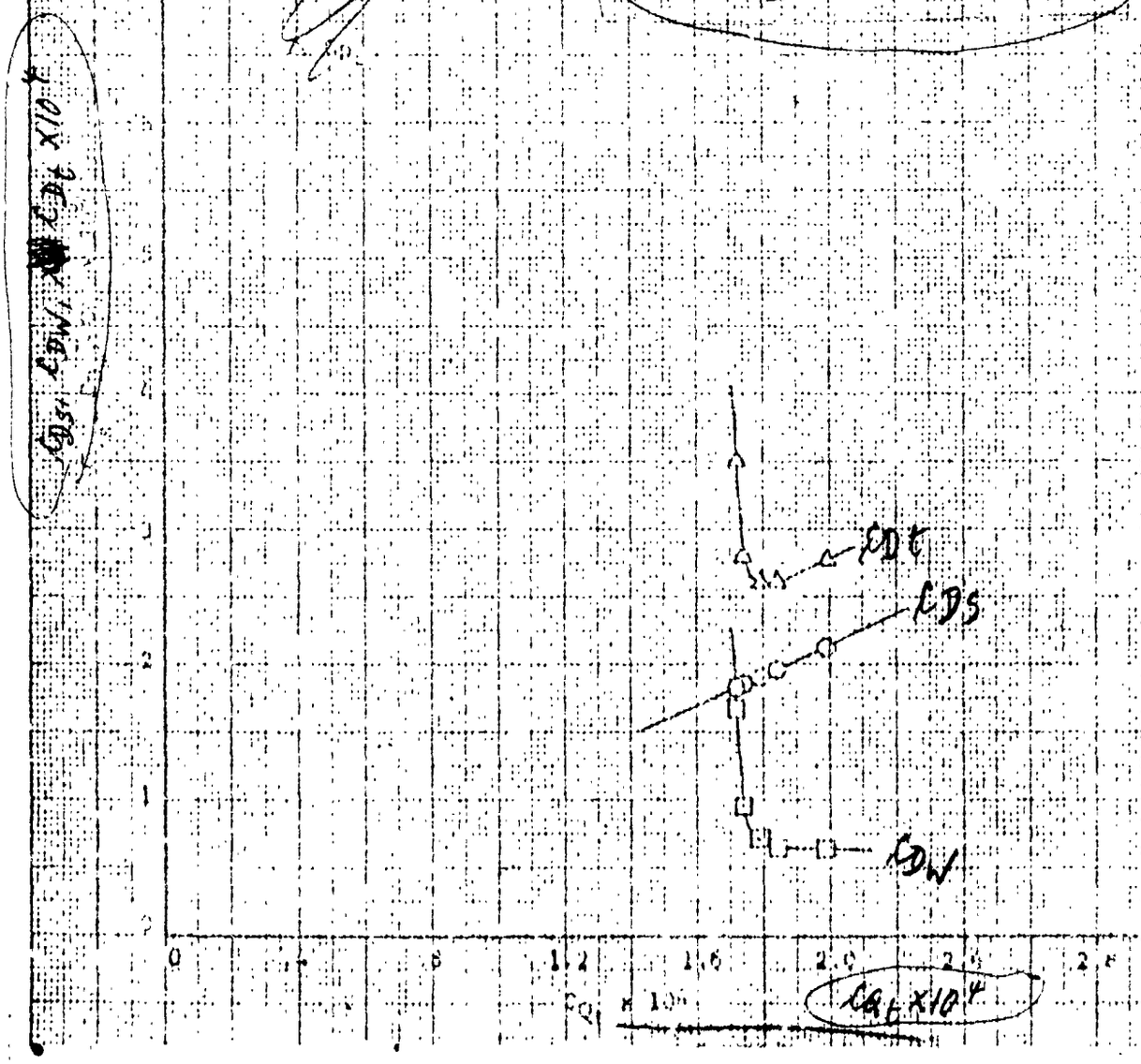

Reichardt LFC body ($\frac{L}{D}=8$)

Re_L 5571 · 10^6

0°

~~Reichardt LFC body ($\frac{L}{D}=8$)~~

$C_D = f(Re_t)$, ~~0°~~,

~~$Re_L = 5571 \cdot 10^6$~~

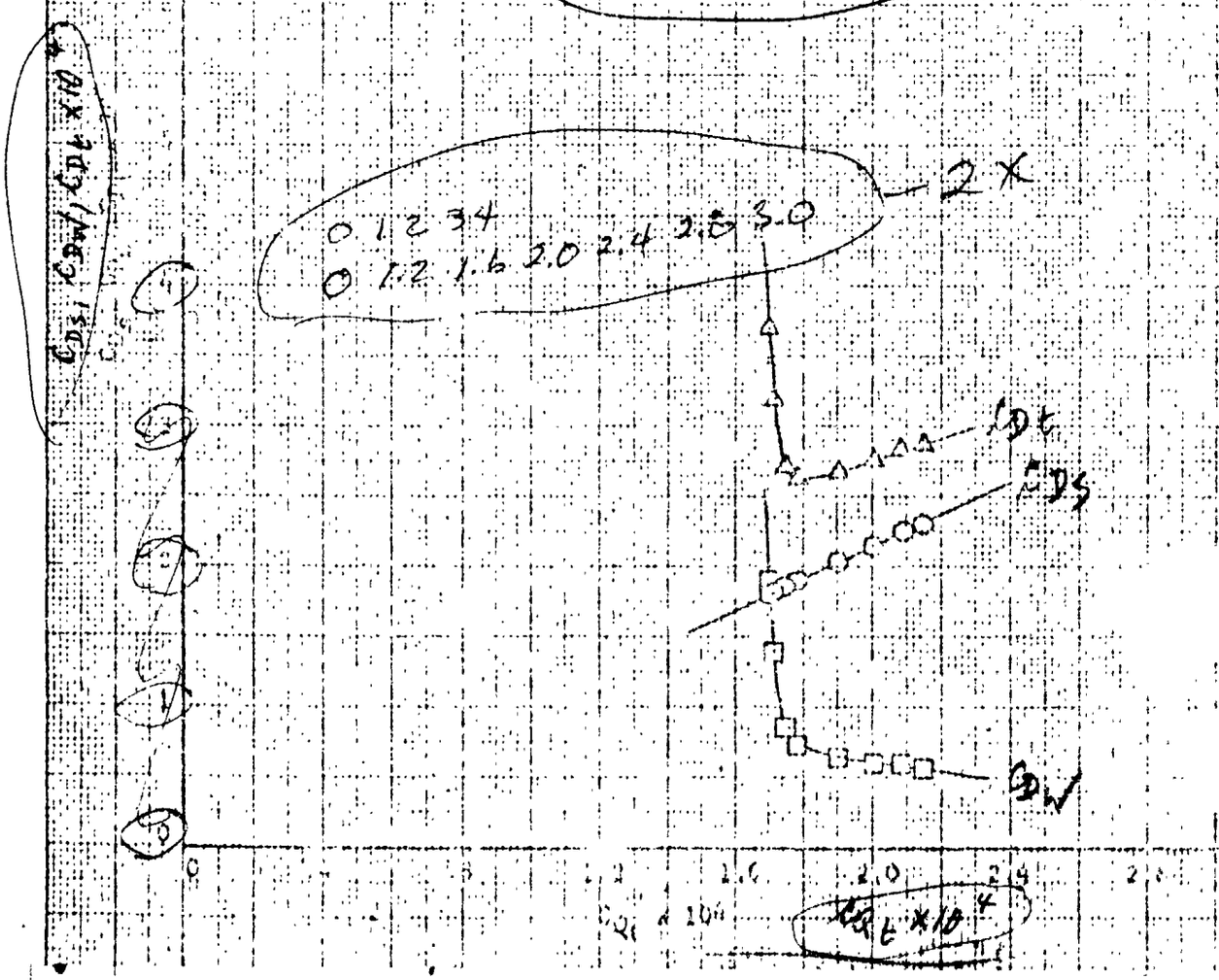

July 1963

→ Reichardt LFC body $\left(\frac{L}{D} = \ell\right)$

C_{Q_t}

Re_L

Re_L [illegible] $\times 10^6$

$\alpha = 0°$

fig. 25, 48, 49 on one sheet with scale as large

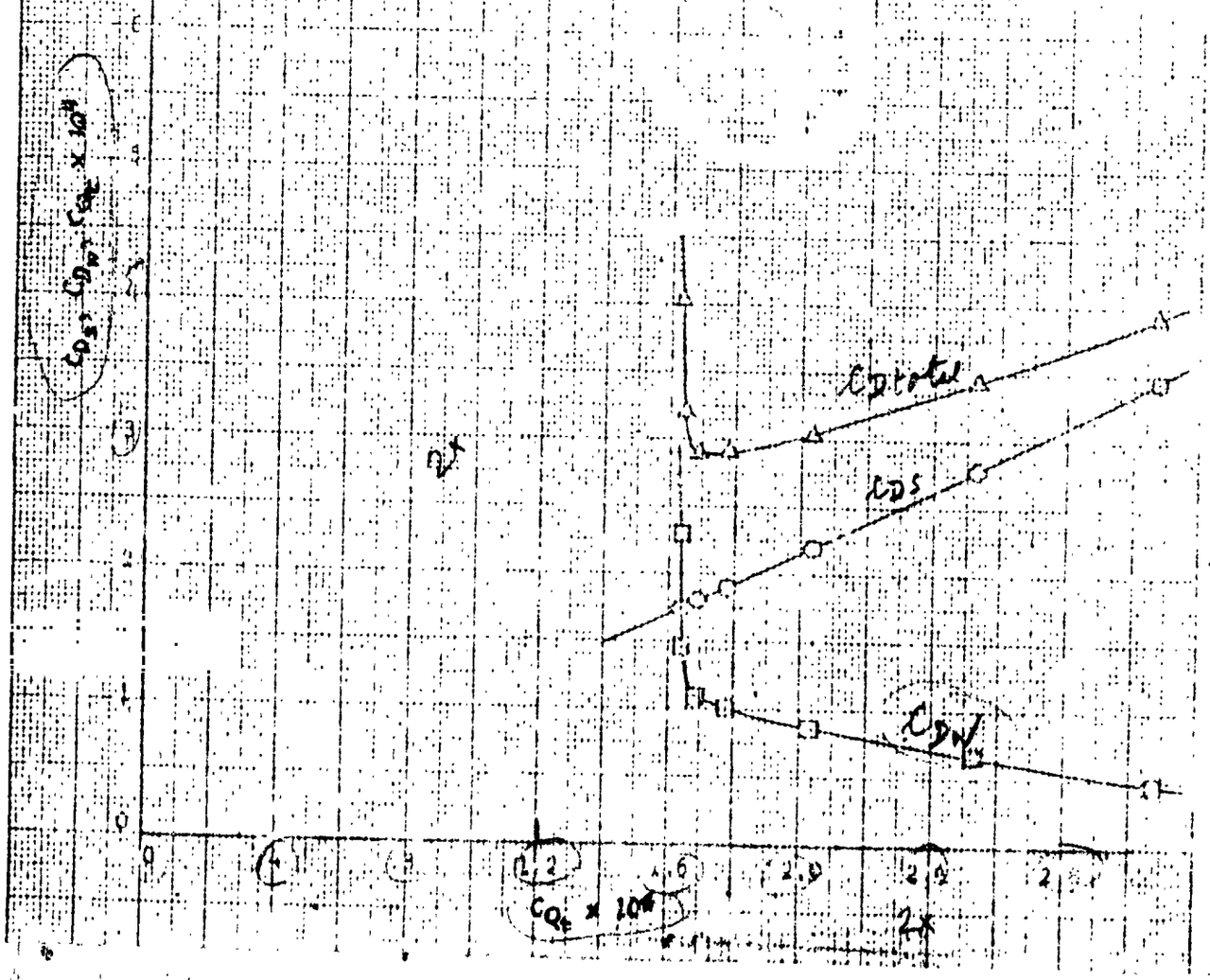

L. Gross	NORTHROP CORPORATION NORAIR DIVISION	83
CHECKED		REPORT NO. NOR 6[illegible] (BLC-[illegible])
DATE July 1963		MODEL

~~FIGURE 61~~ Reichardt LFC body (L/D = 8)

BOUNDARY LAYER VELOCITY PROFILES AS MEASURED

AT THE AFT END OF THE [illegible]

~~Run No. 237~~

$Re_{L} = 56.742 \times 10^{6}$

$Re_{C_{Q_t}} = 1.789 \times 10^{-4}$

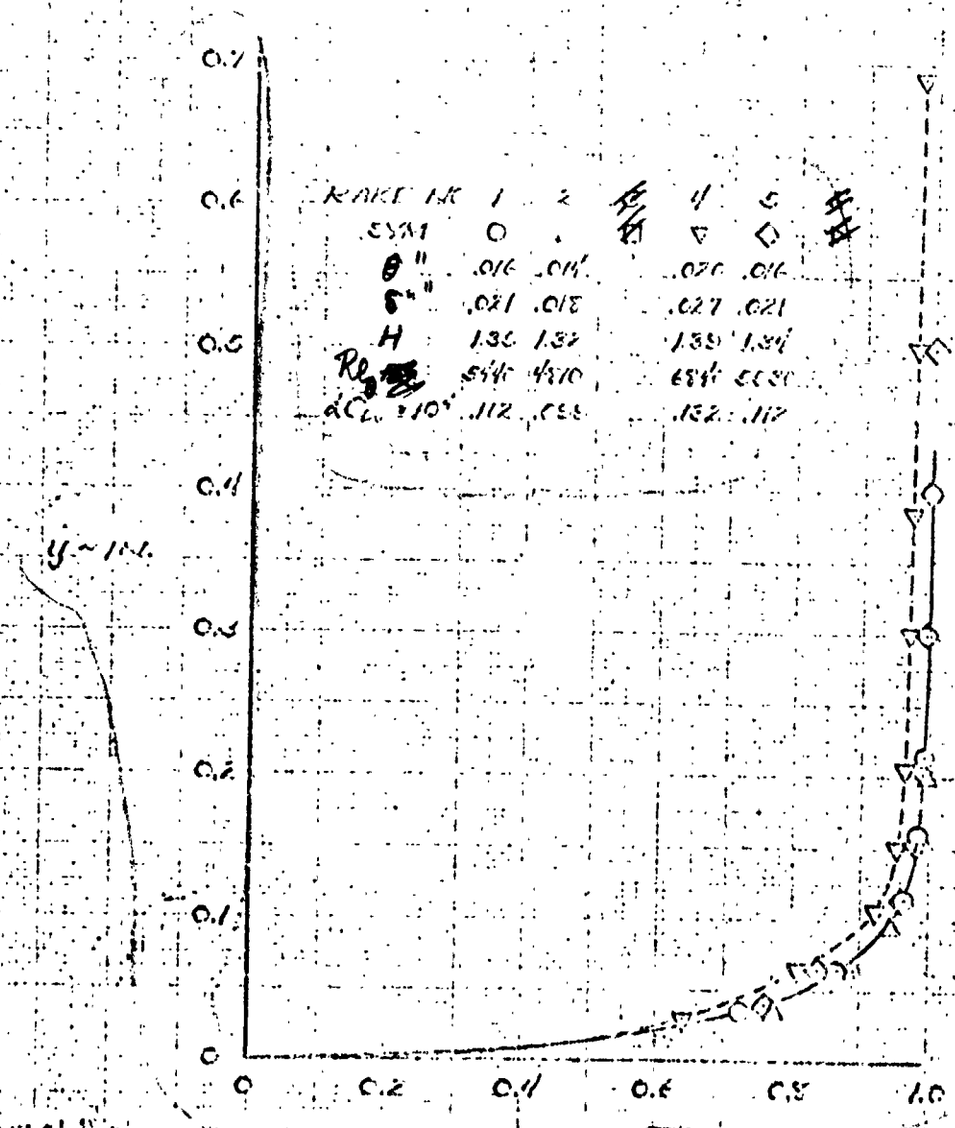

RAKE NO	1	2	~~3~~	4	5	~~6~~
SYM	○	•	~~□~~	▽	◇	~~△~~
θ"	.016	.014		.020	.016	
δ"	.021	.018		.027	.021	
H	1.35	1.32		1.39	1.34	
Re_θ	5440	4810		6840	5530	
$\alpha C_{L_0} \times 10^4$	.112	.099		.132	.112	

~~CONFIDENTIAL~~

Reichardt LFC body (L/D = 8)

FIGURE 3

COMPARISON OF MEASURED AND THEORETICAL VELOCITY DISTRIBUTIONS

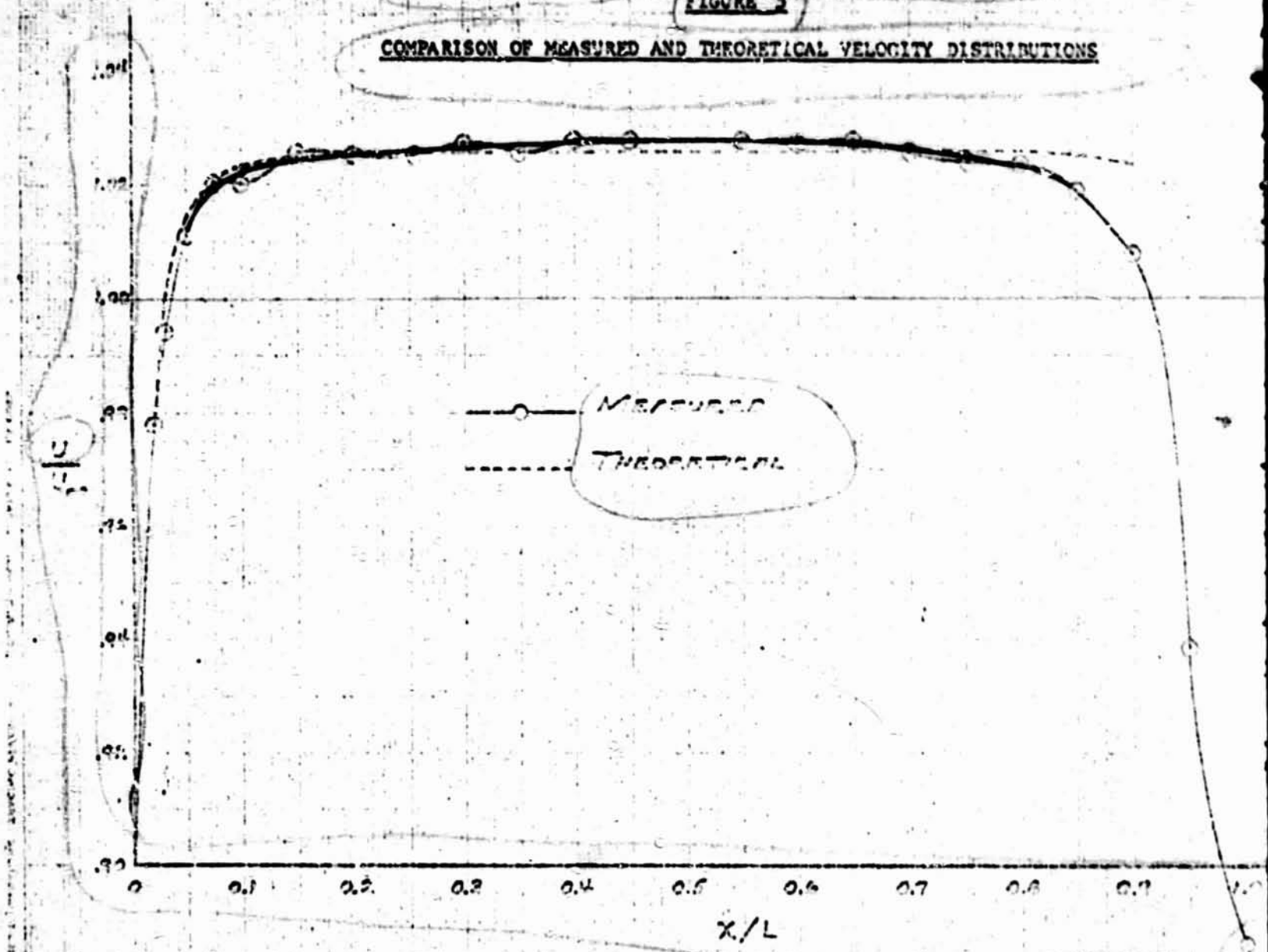

Reichardt LFC body ($L/D = 8$)

FIGURE [illegible]

VARIATION OF AFT END BOUNDARY LAYER VELOCITY
PROFILE WITH SUCTION COEFFICIENT

$Re_L = 56.740 \times 10^6$

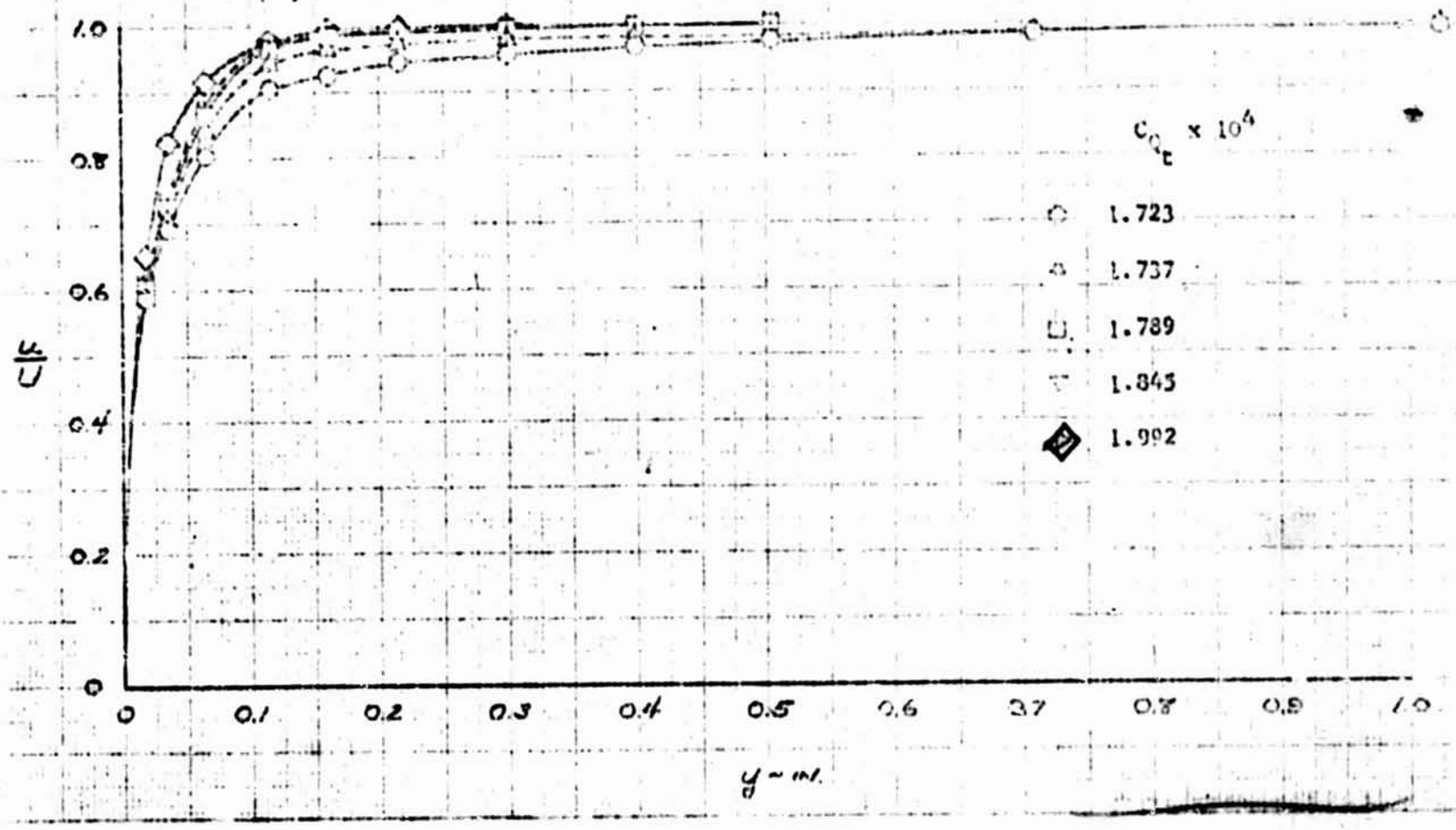

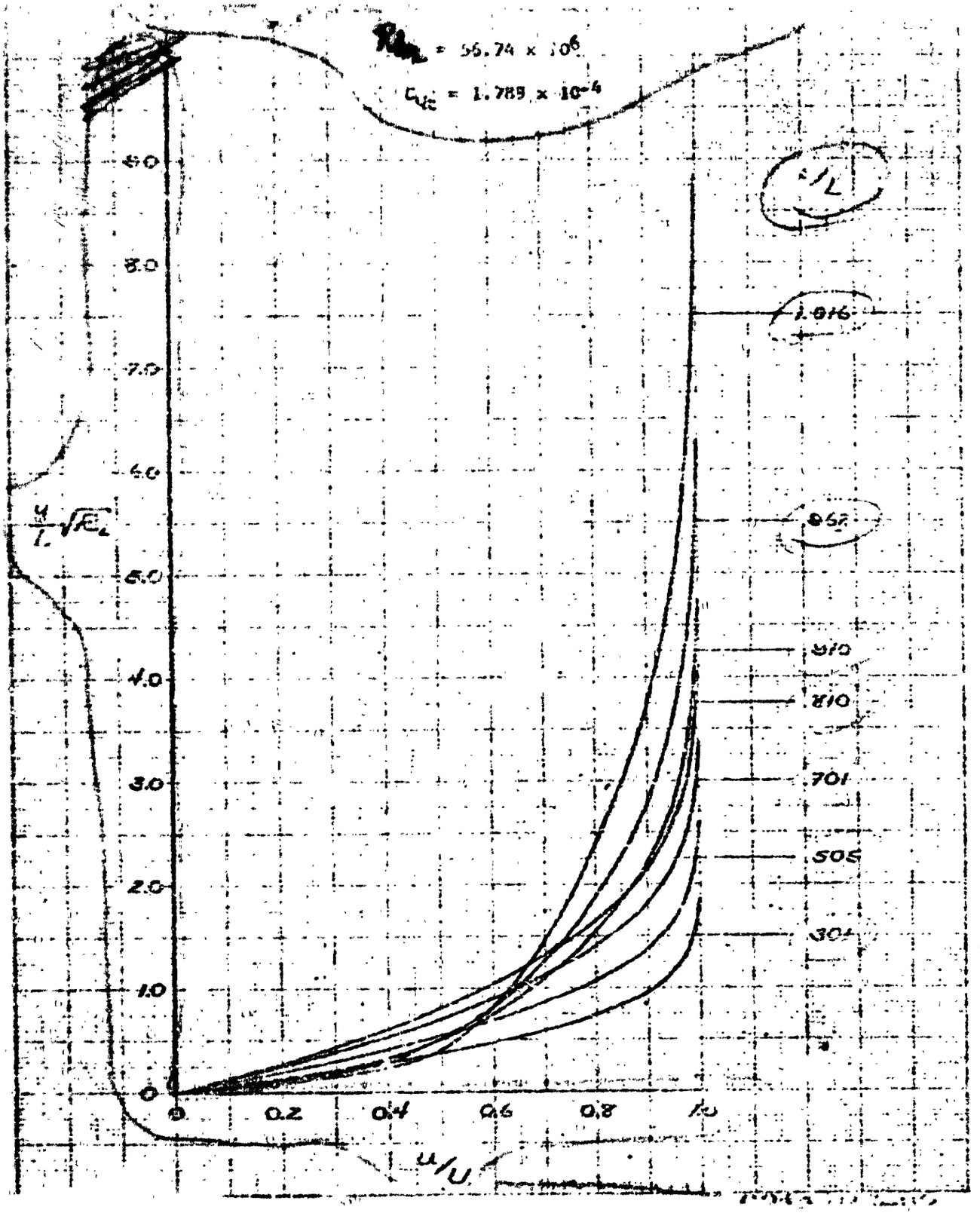

= 56.74 x 10^6
= 1.789 x 10^-4
9.0
8.0
7.0
6.0
5.0
4.0
3.0
2.0
1.0
0
0.2
0.4
0.6
0.8
1.0
u/U
1.016
.952
.910
.810
.701
.505
.304

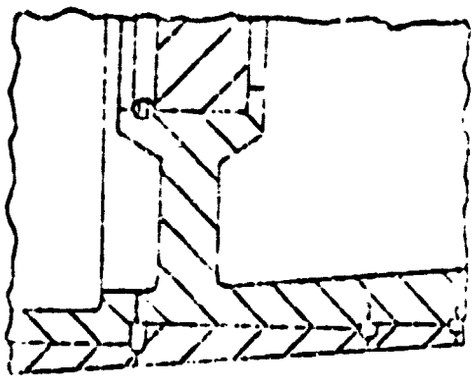

Schematic View Showing Typical Bulkhead Installation and Details of Suction Slot, Plenum Chamber and Suction Flow Metering Holes

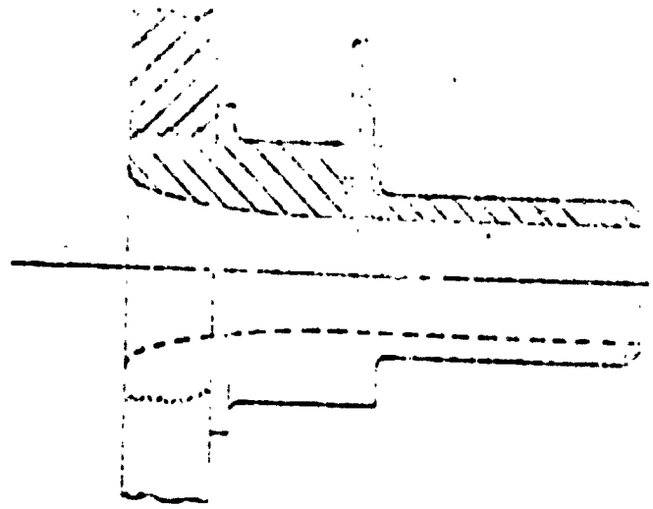

Schematic View of Typical Flow Measuring Nozzle Installation

Reichardt Absaugrotationskörper (L/D = 8) mit Absaugung durch 110 Schlitze

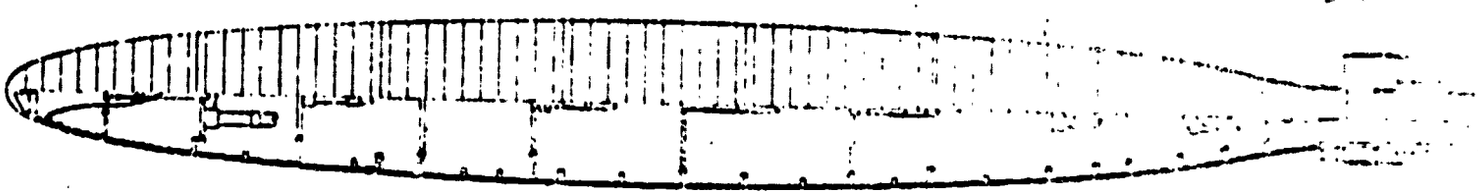

Körperlänge L = 12.5 ft
Durchmesser D = 1.5 ft
Schlitzweite = 0.003

FIGURE 1

MODEL CROSS SECTION WITH DETAILS OF SUCTION SLOTS

ref. 1

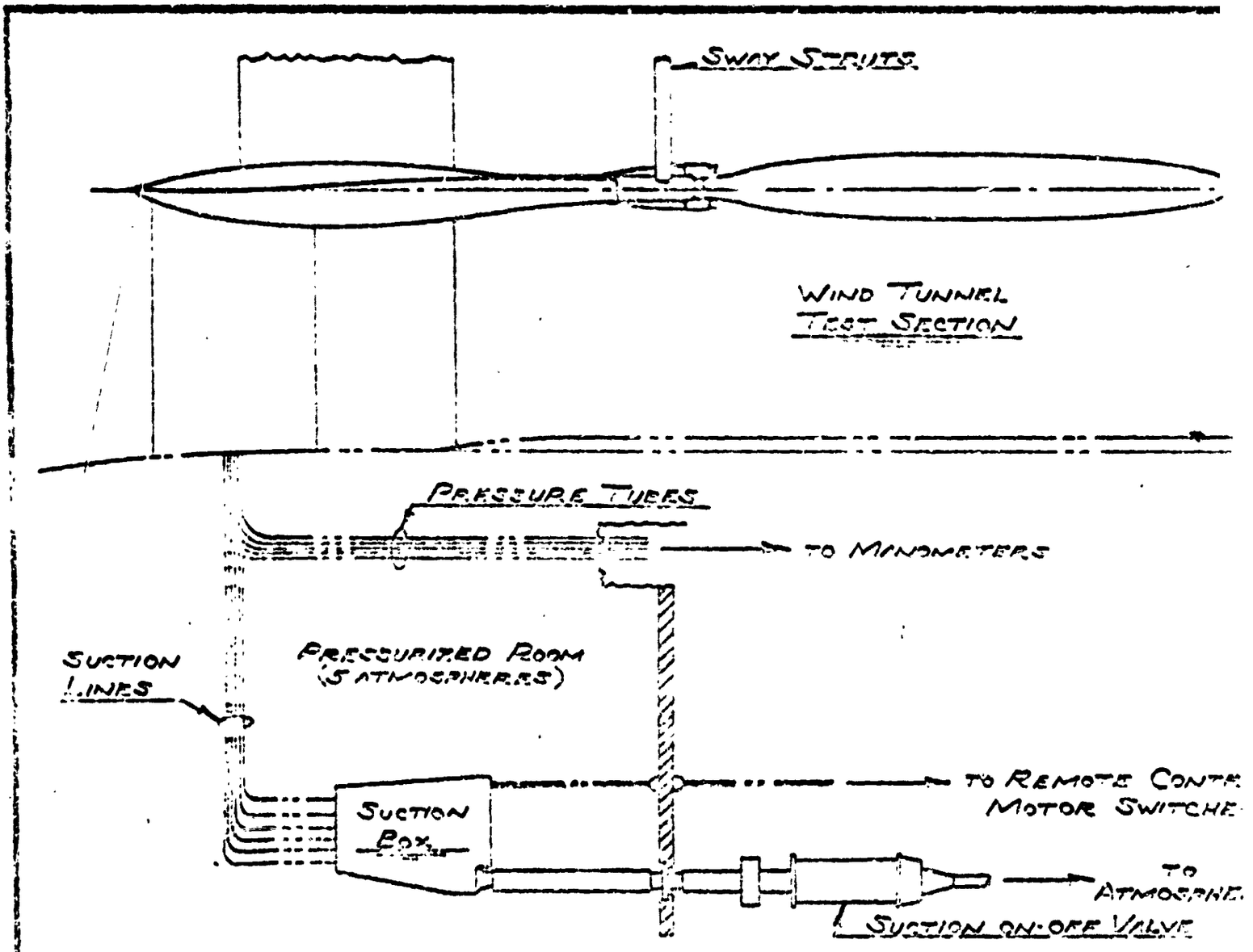

FIGURE 2
INSTALLATION DRAWING-REICHARDT BODY OF REVOLUTION WITH
LOW DRAG SUCTION IN NASA-AMES 12-FT. PRESSURE WIND TUNNEL

REICHARDT BODY OF REVOLUTION WITH LOW DRAG SUCTION IN NASA-AMES 12-FOOT PRESSURE WIND TUNNEL

FIGURE 3

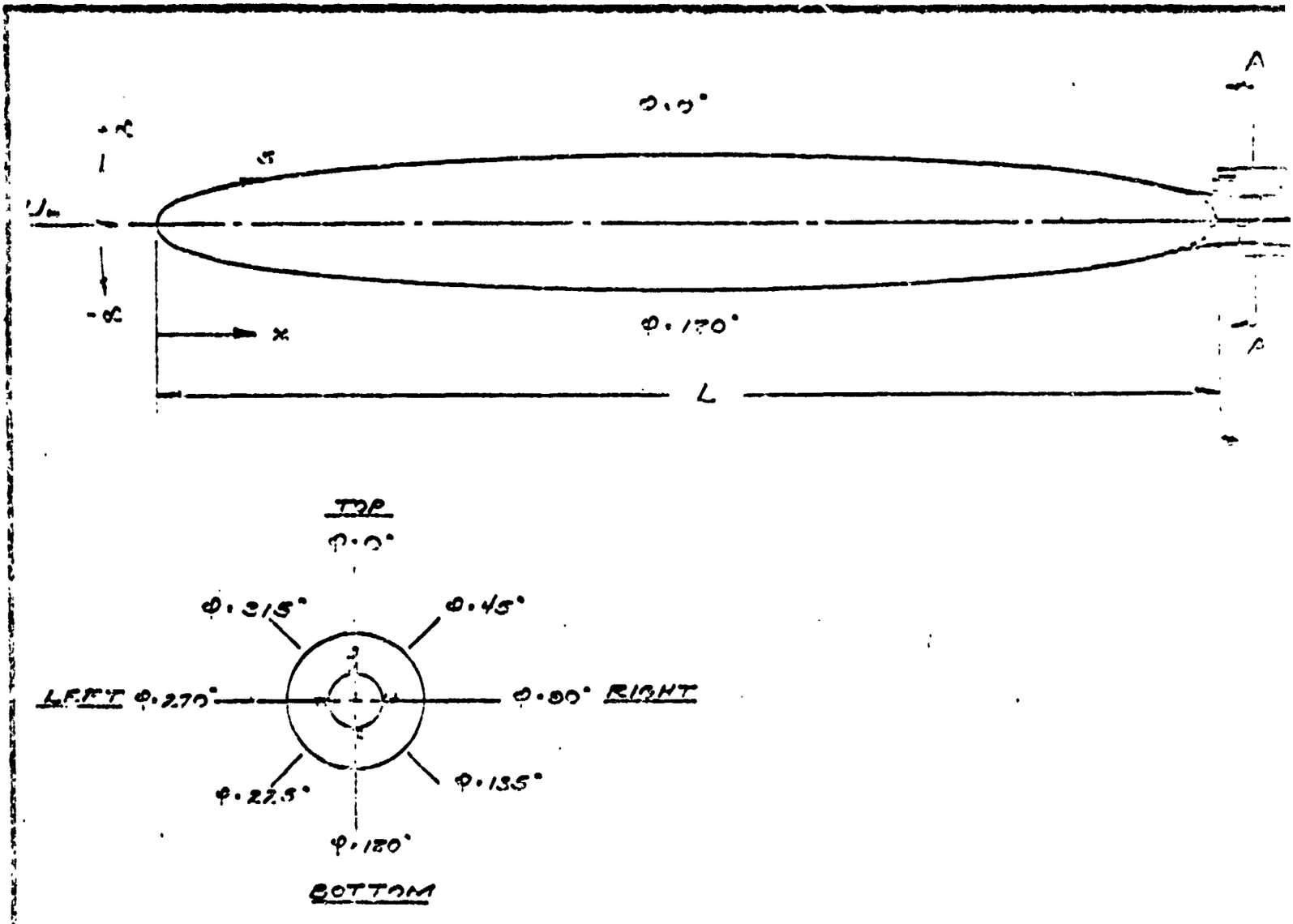

FIGURE 4

COORDINATE SYSTEM

FIGURE 6
DESIGN SUCTION VELOCITY DISTRIBUTION
AND BOUNDARY LAYER DEVELOPMENT

$R_L = 49 \times 10^6$

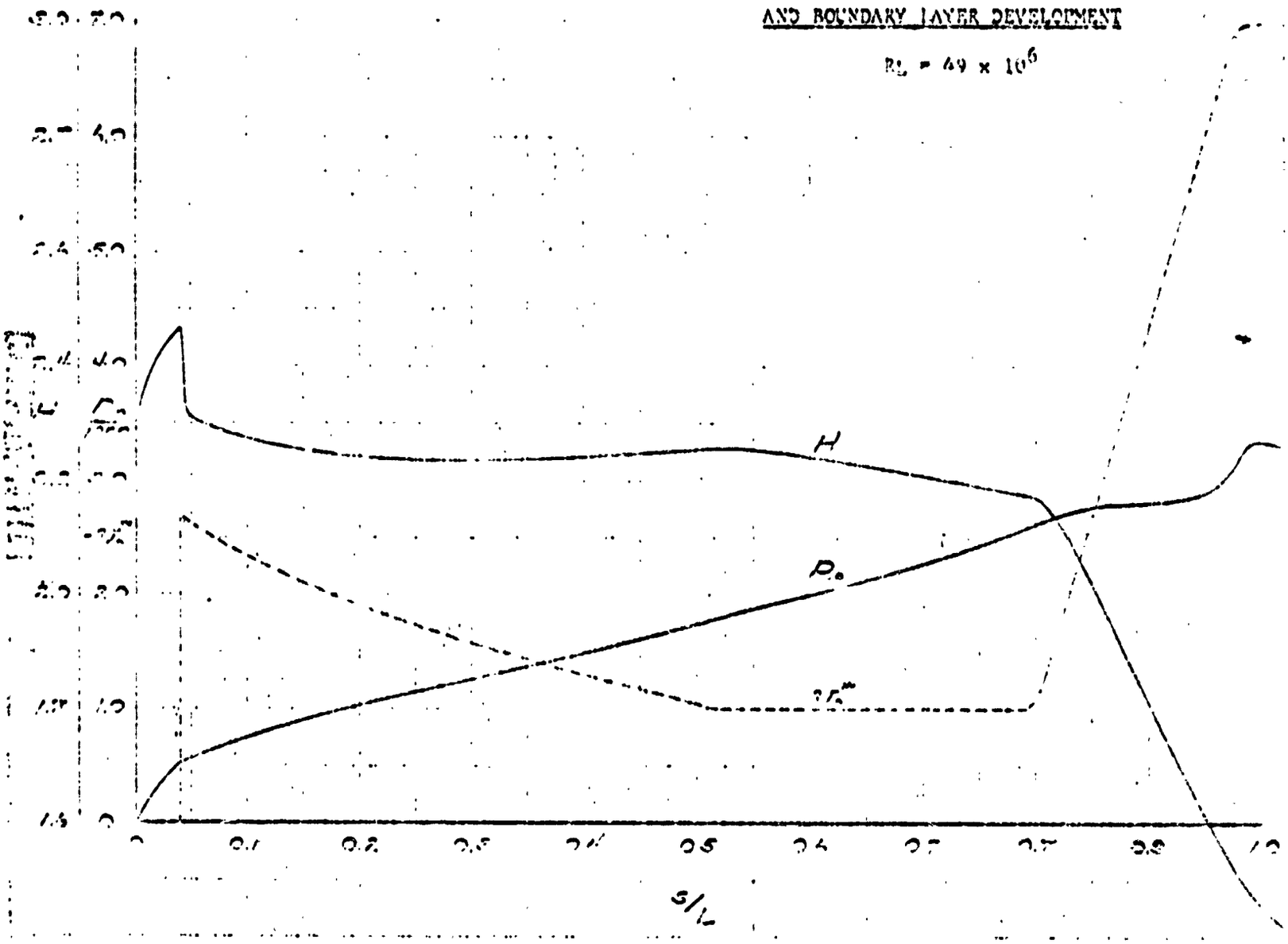

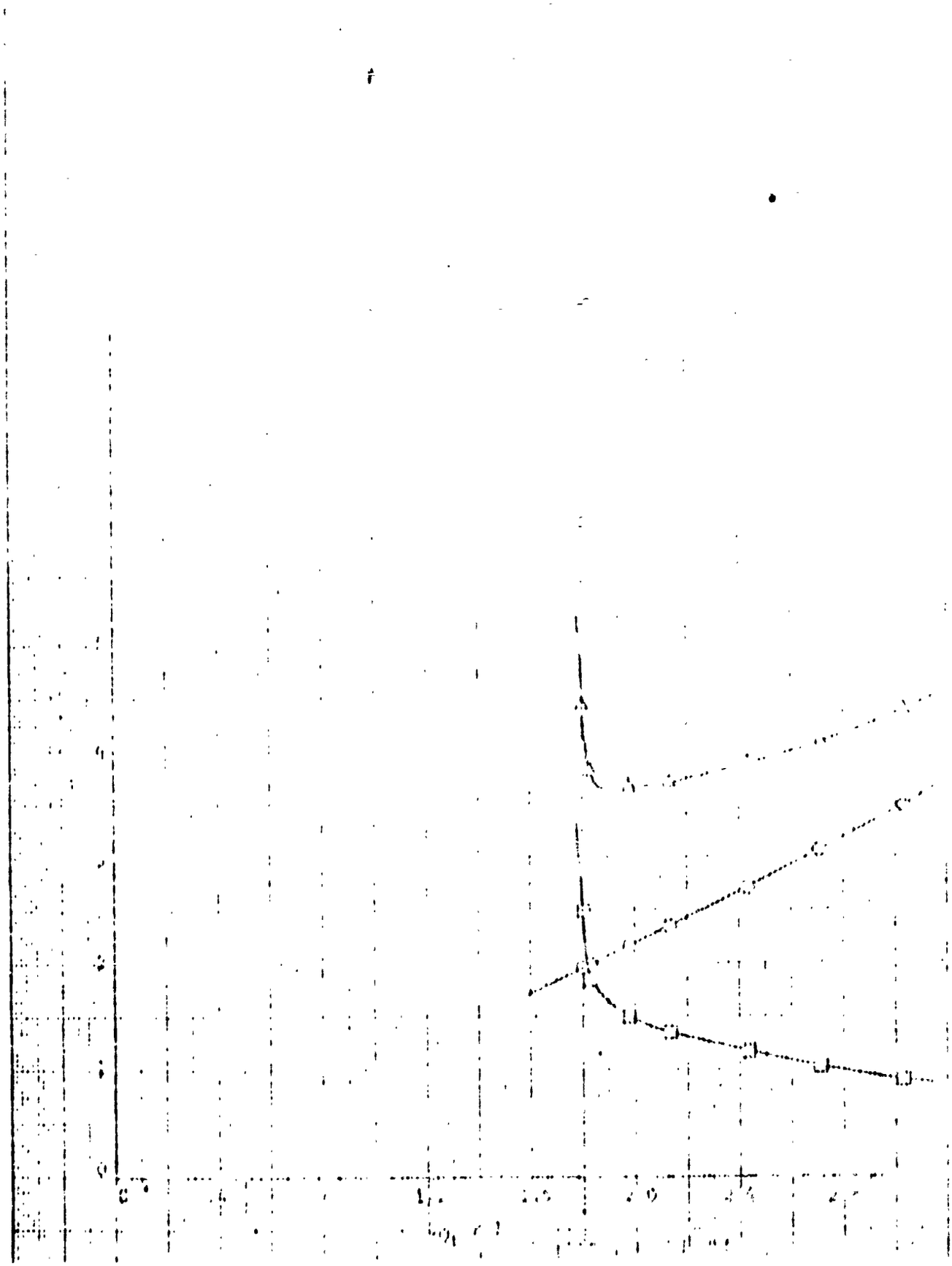

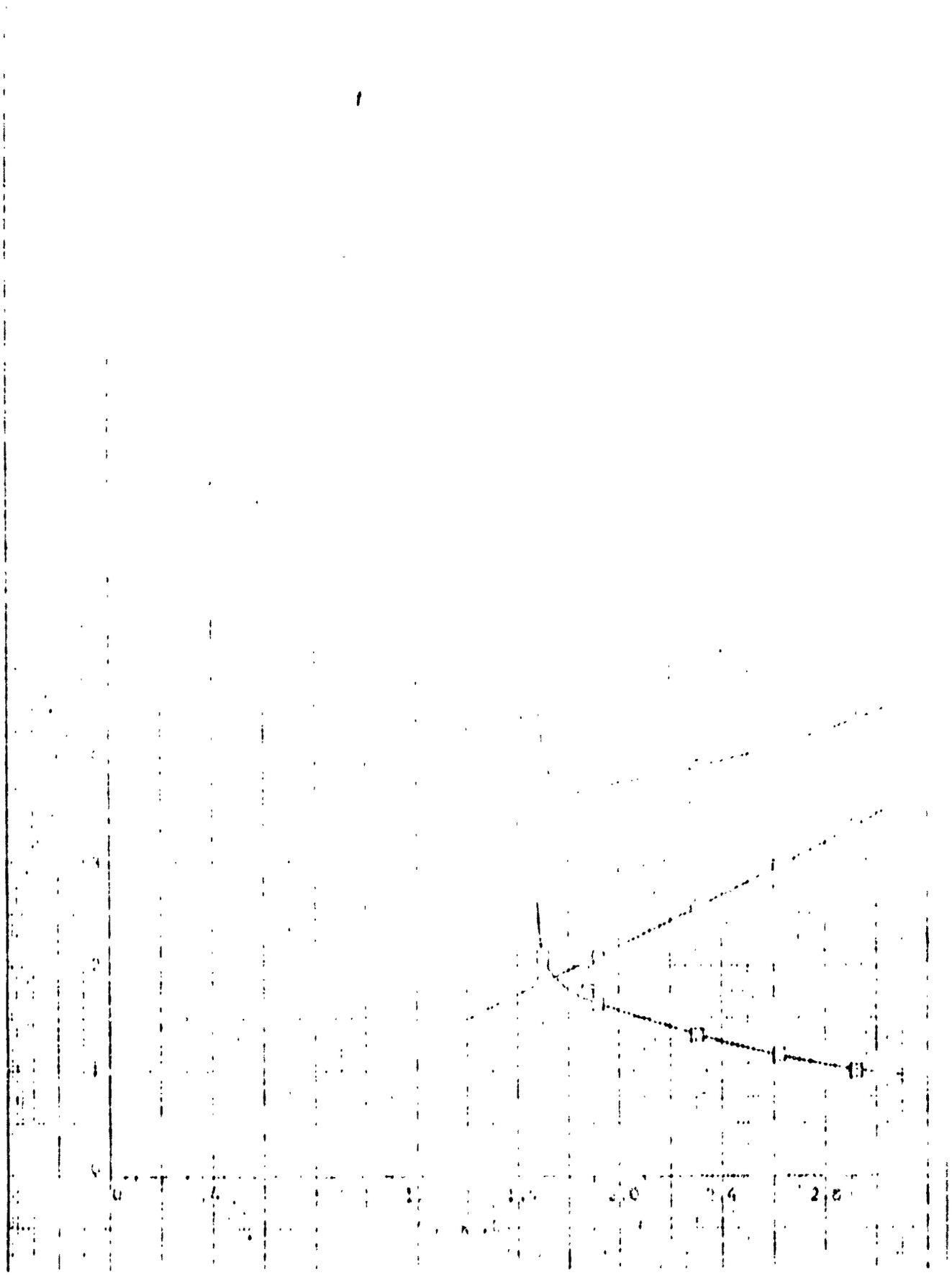

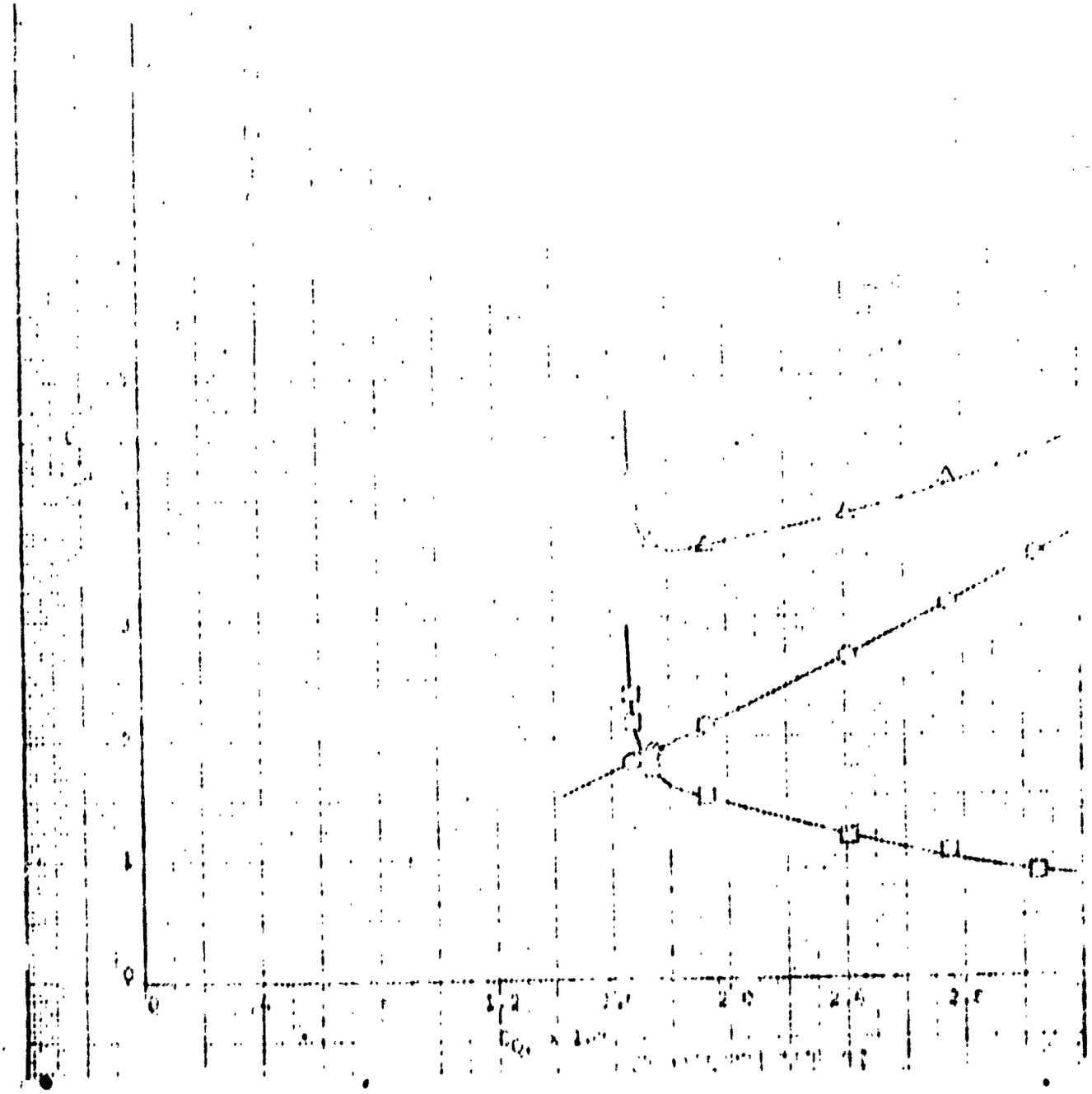

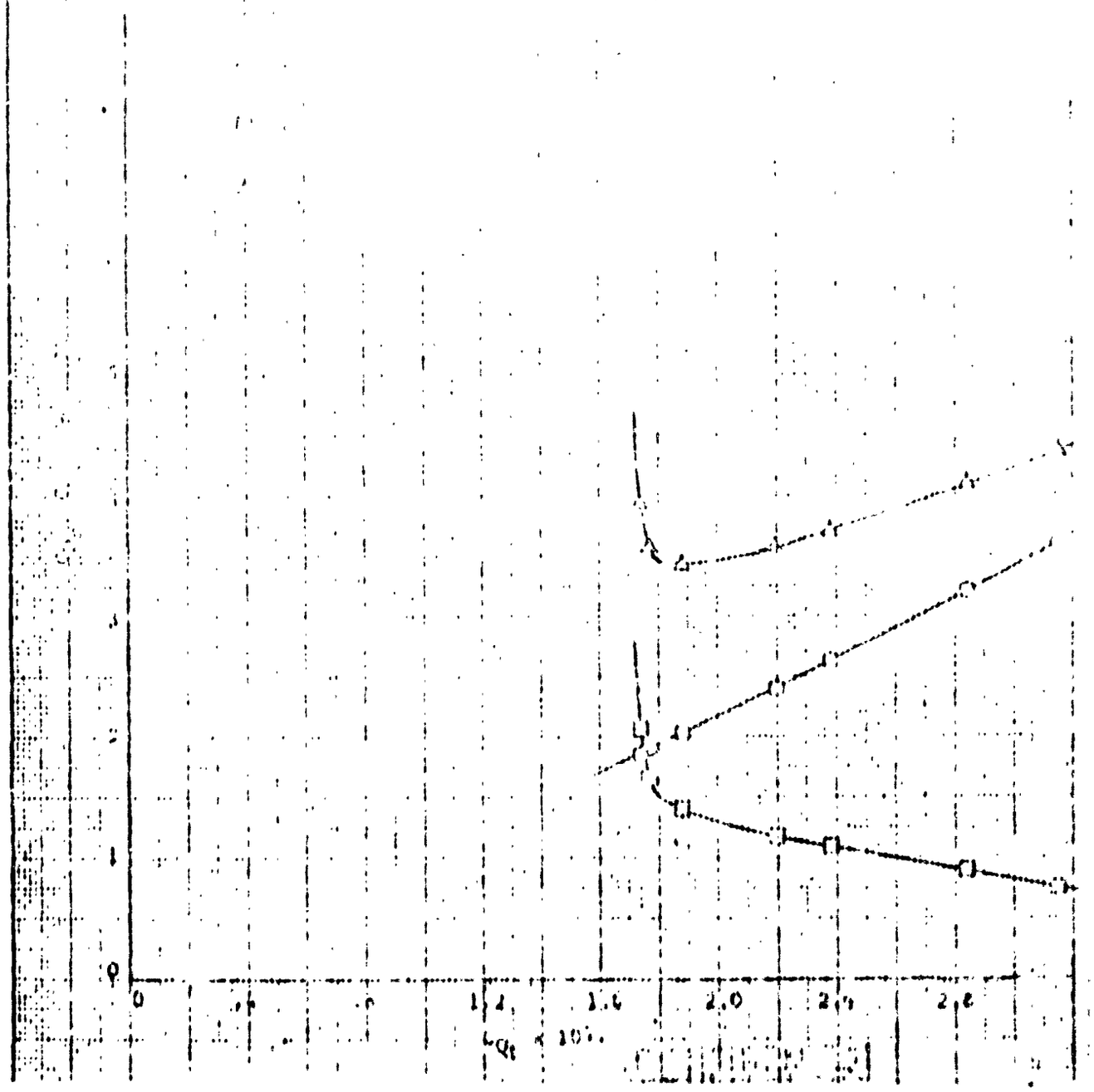

0
1
2
3
0
1.2
1.6
2.0
2.4
2.8

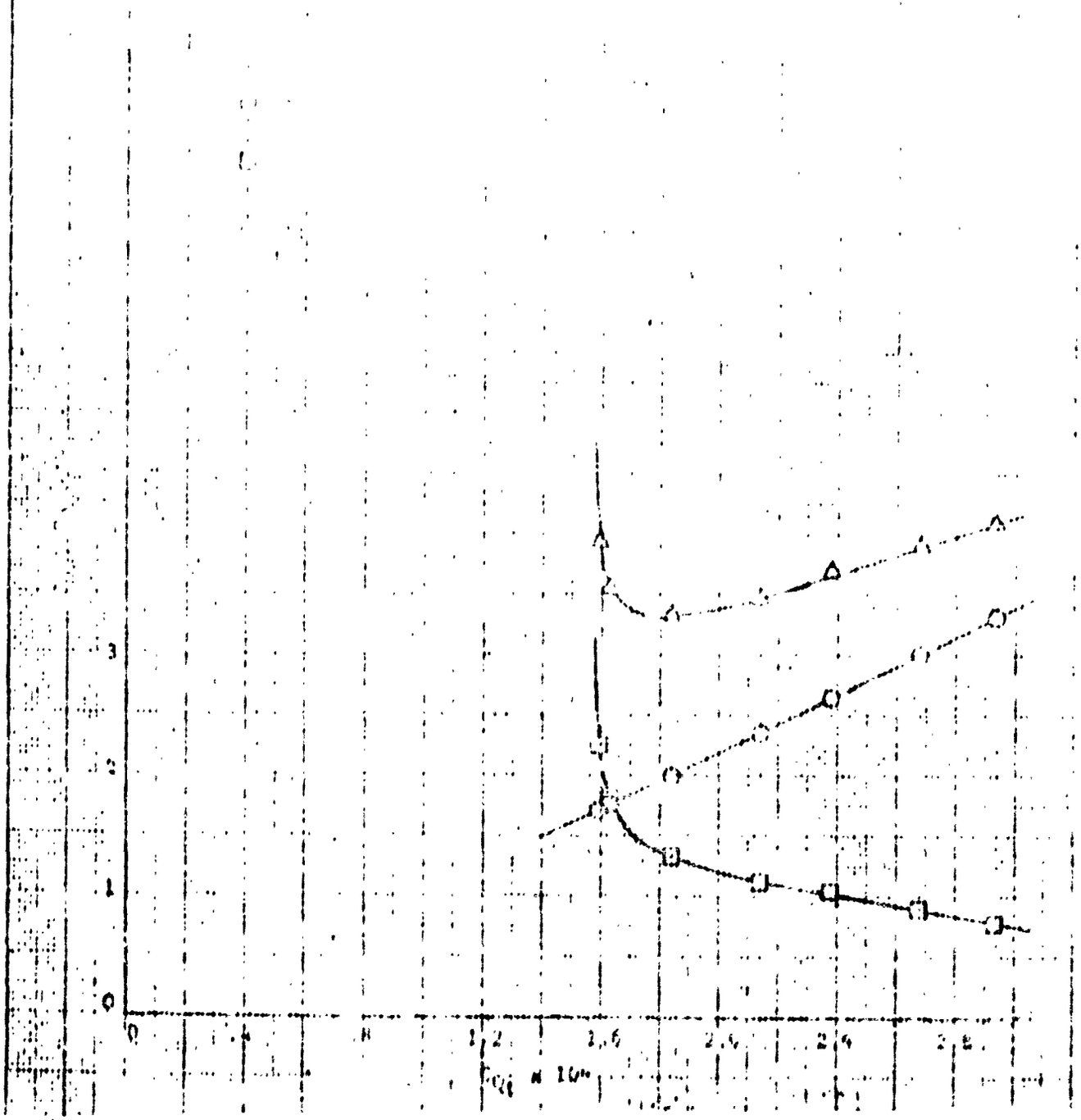

3
2
1
0
0
.4
.8
1.2
1.6
2.0
2.4
2.8

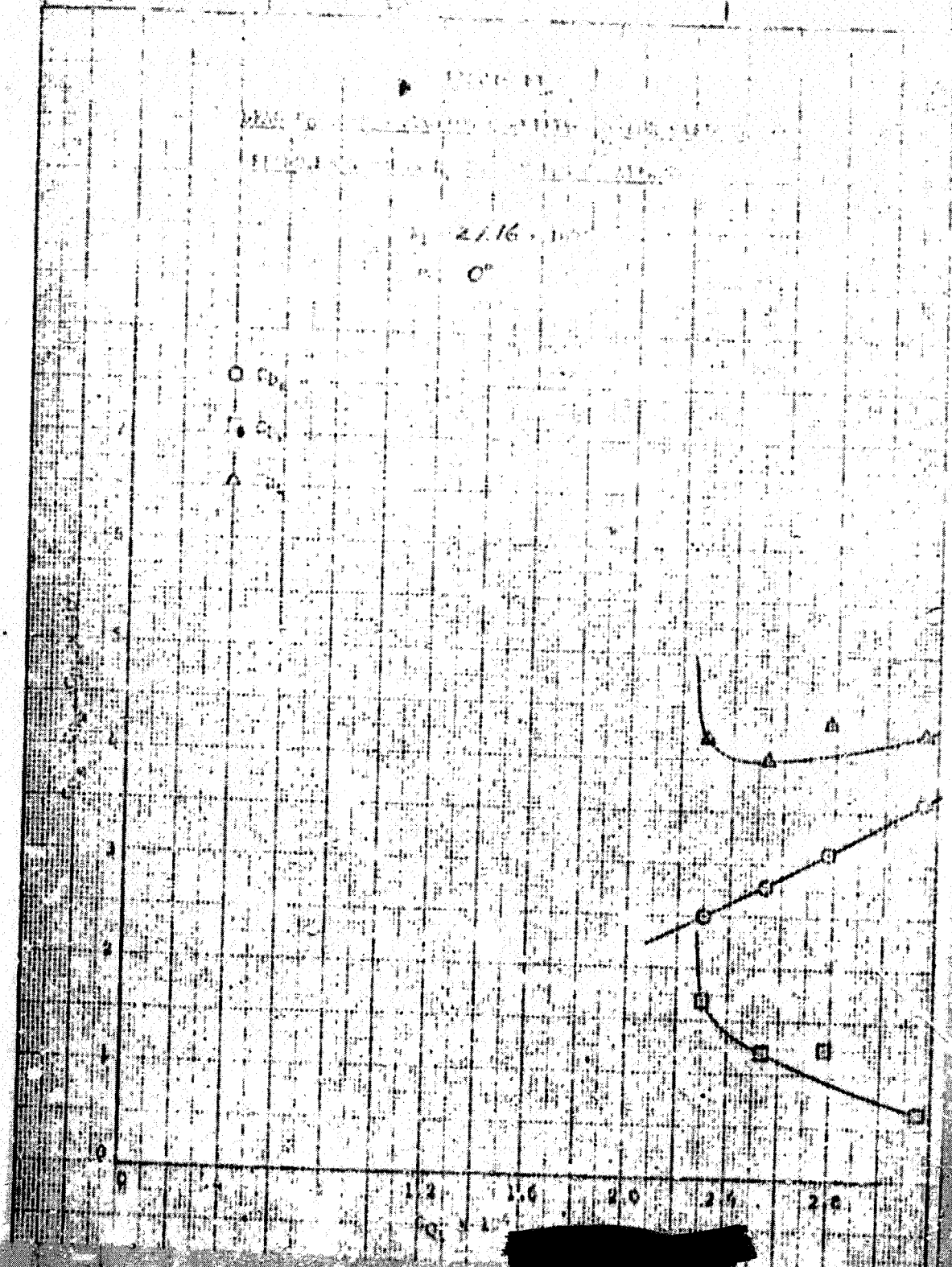

[redacted]

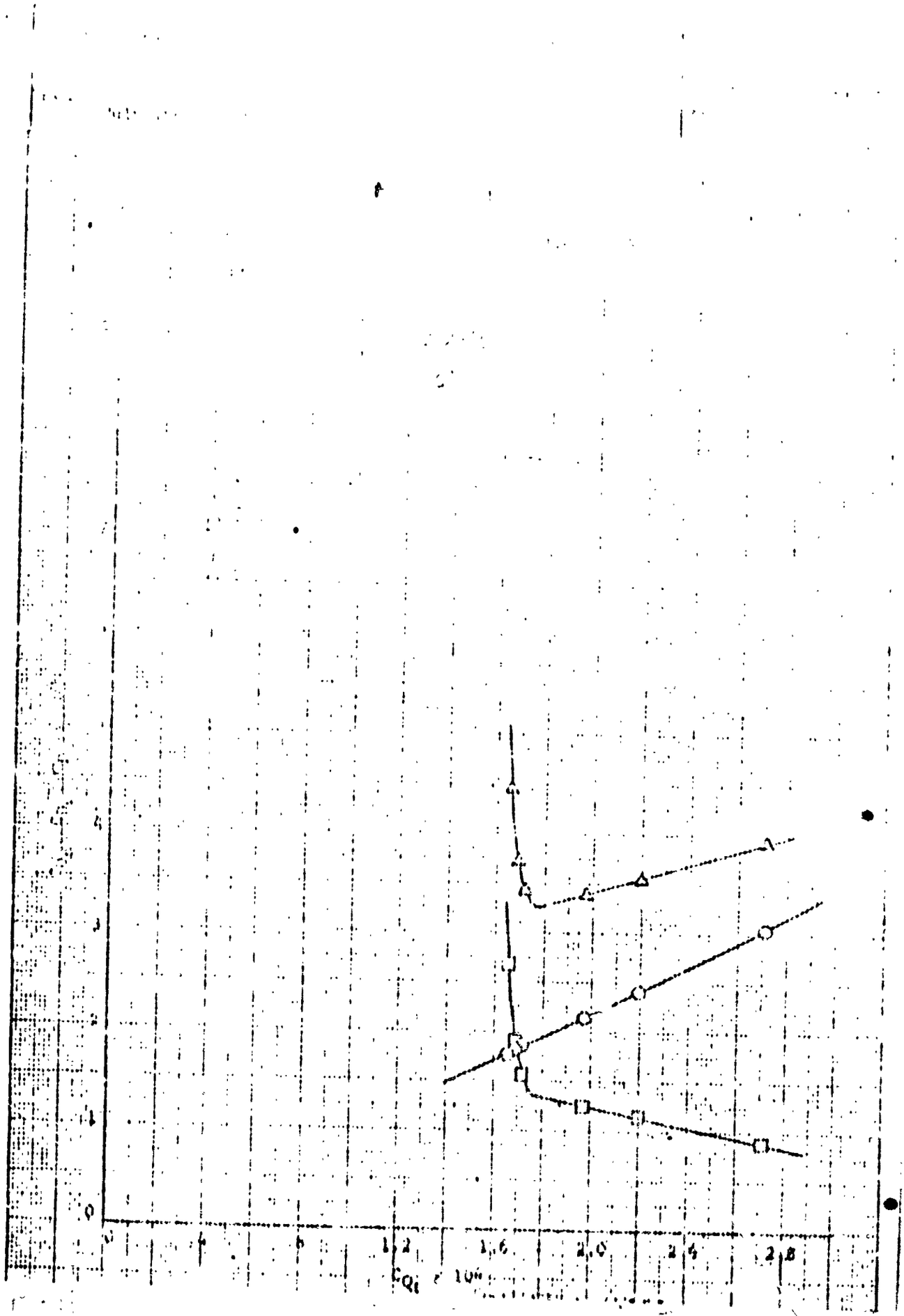
0
1
2
3
4
0
0.4
0.8
1.2
1.6
2.0
2.4
2.8
$Q_t \times 10^6$

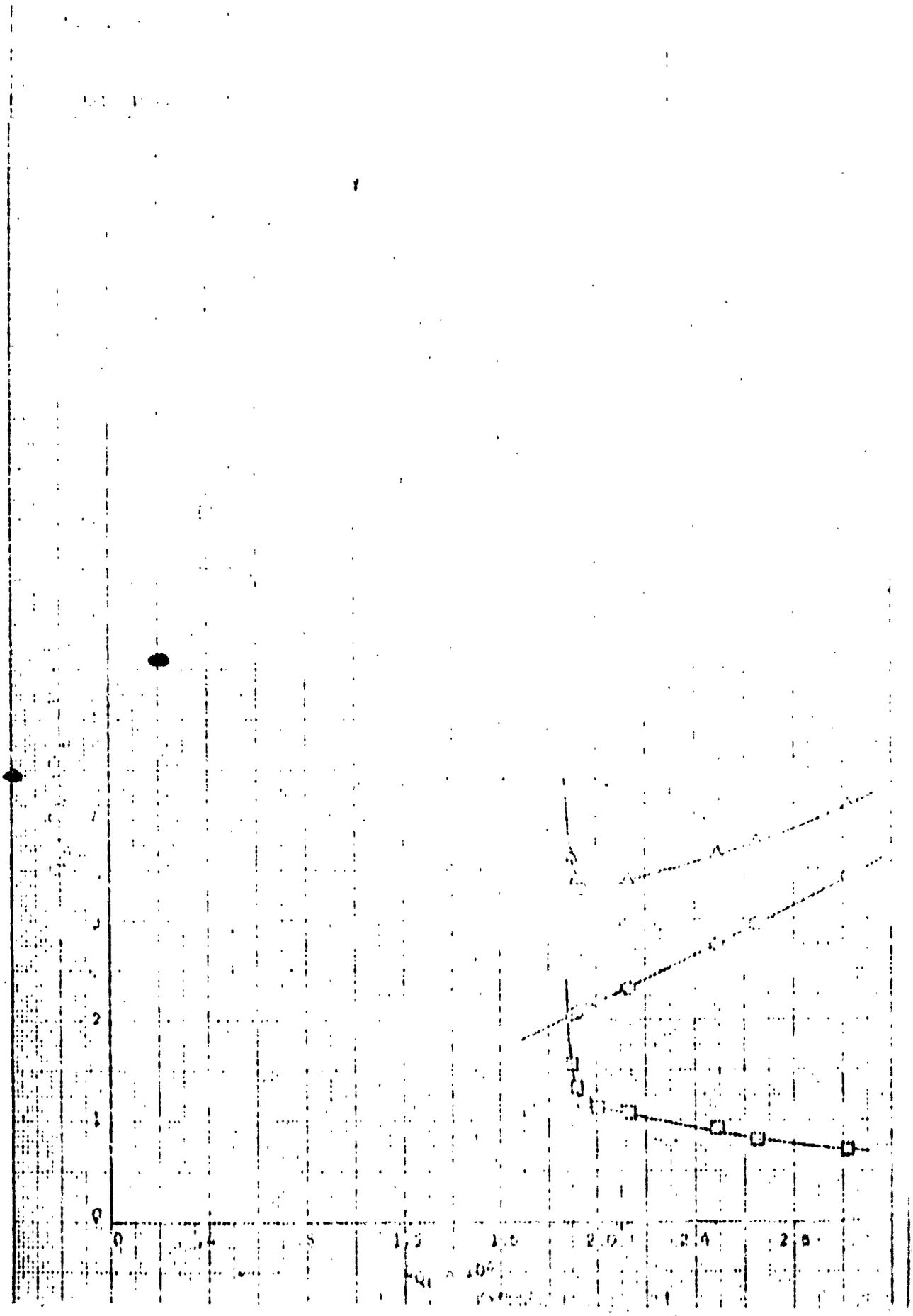
2
1
0
0
1.2
1.6
2.0
2.4
2.8

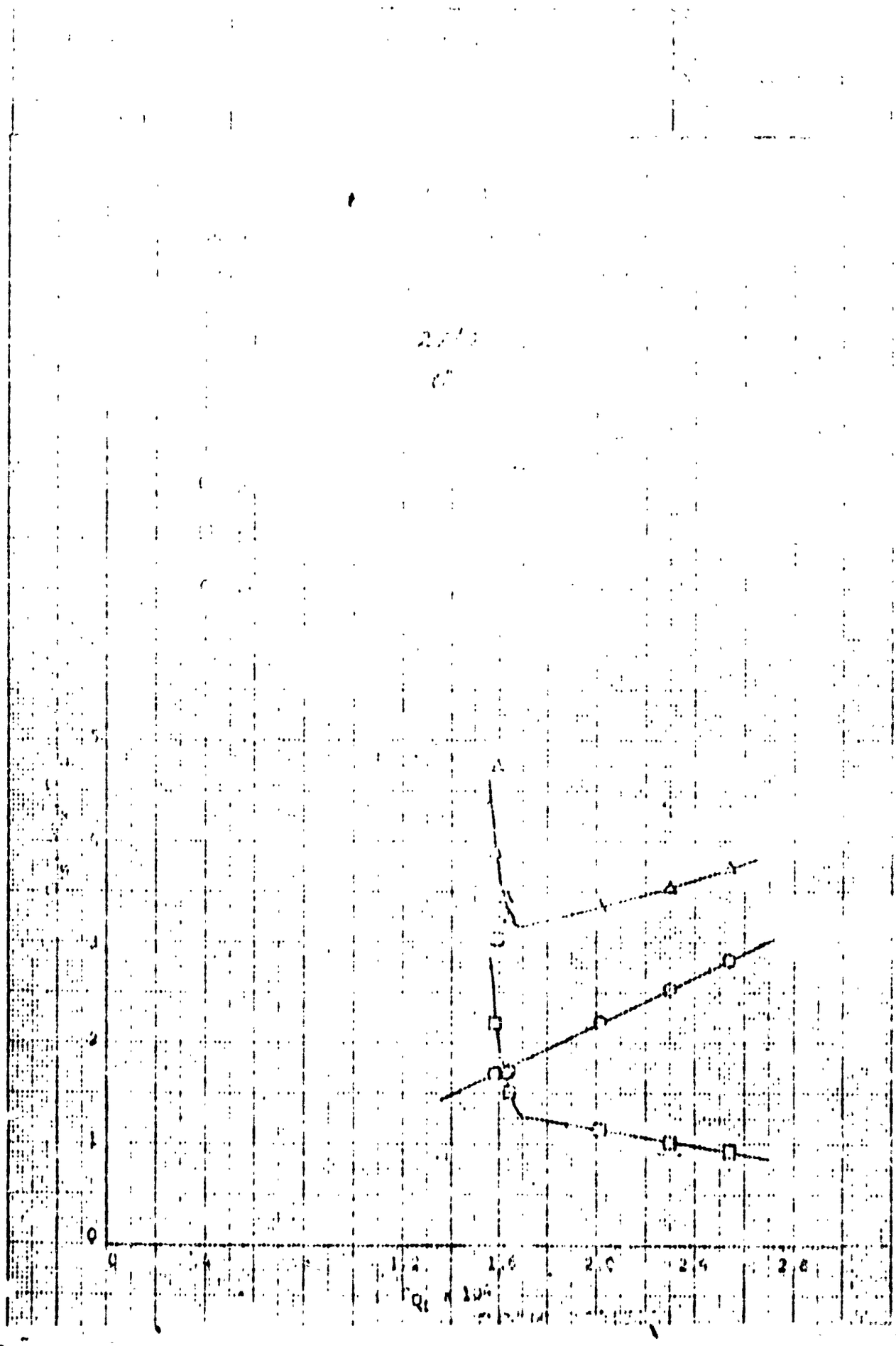
0
1
2
3
4
0
0.4
1.2
1.6
2.0
2.4
2.8

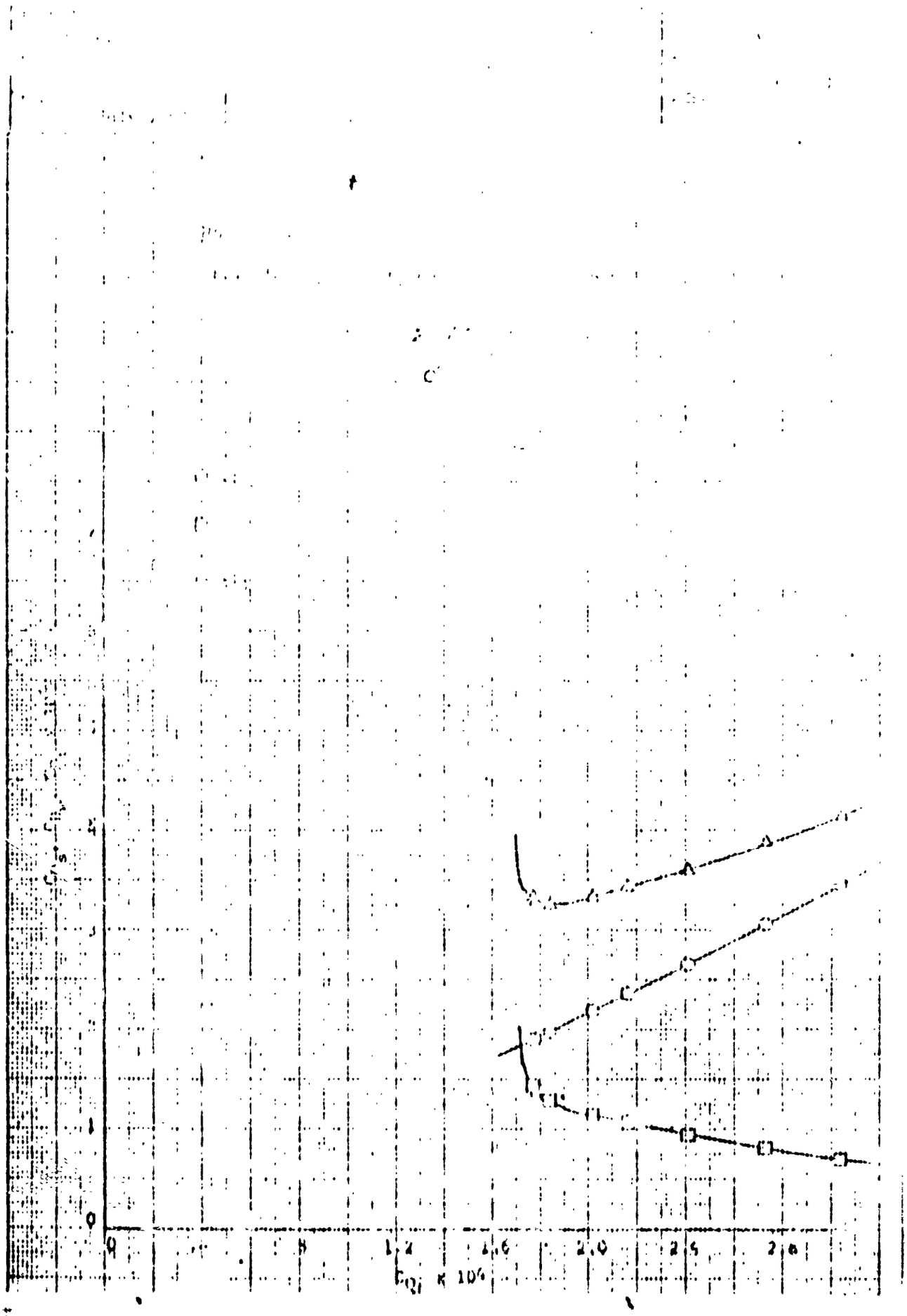
0
1
2
3
4
0
.8
1.2
1.6
2.0
2.4
2.8
$C_{Qi} \times 10^4$

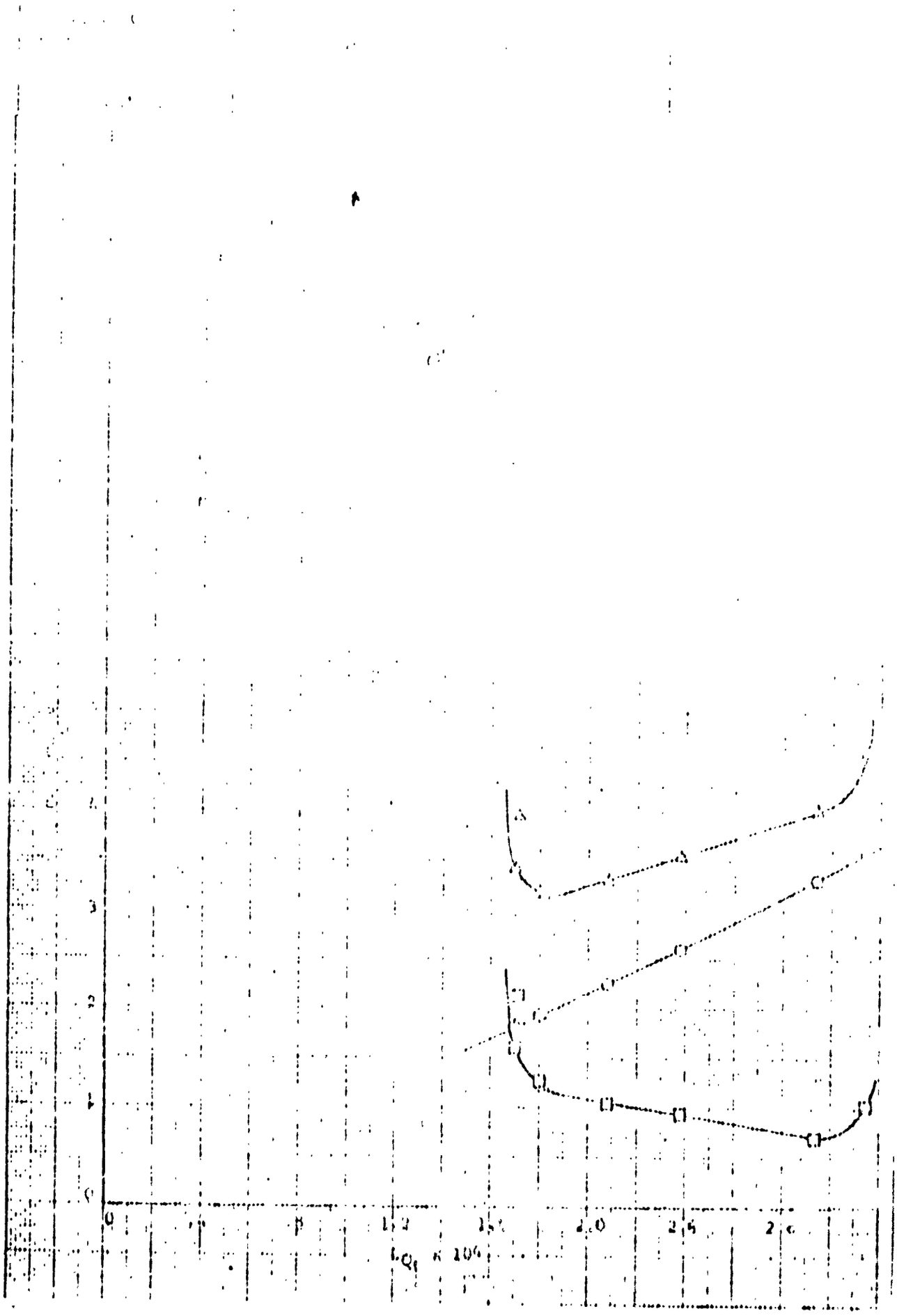

0
1
2
3
4
0
1.2
2.0
2.5

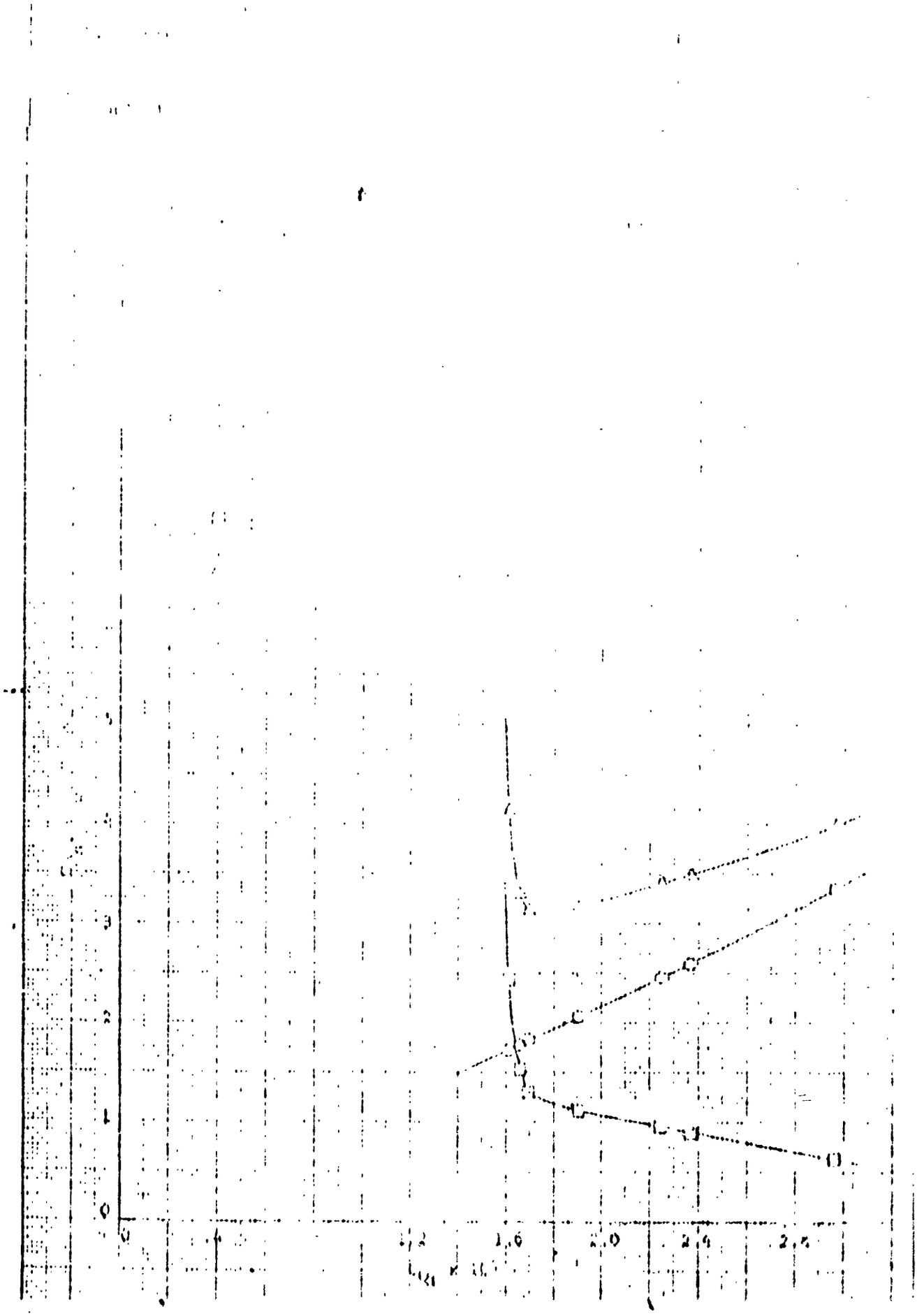
0
1
2
3
0
1.2
1.6
2.0
2.4
2.8

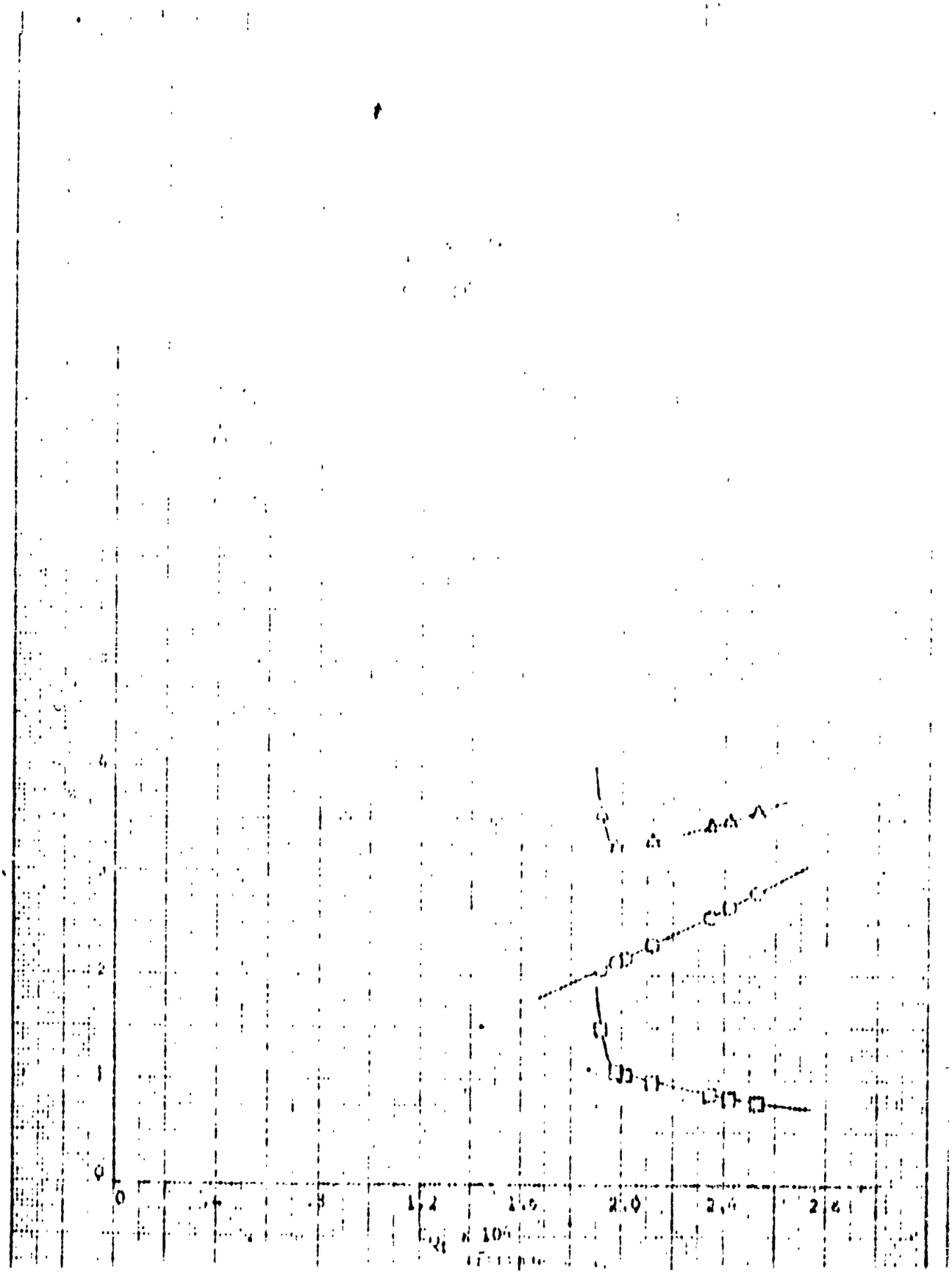
0
1
2
3
4
0
.4
.8
1.2
1.6
2.0
2.4
2.8

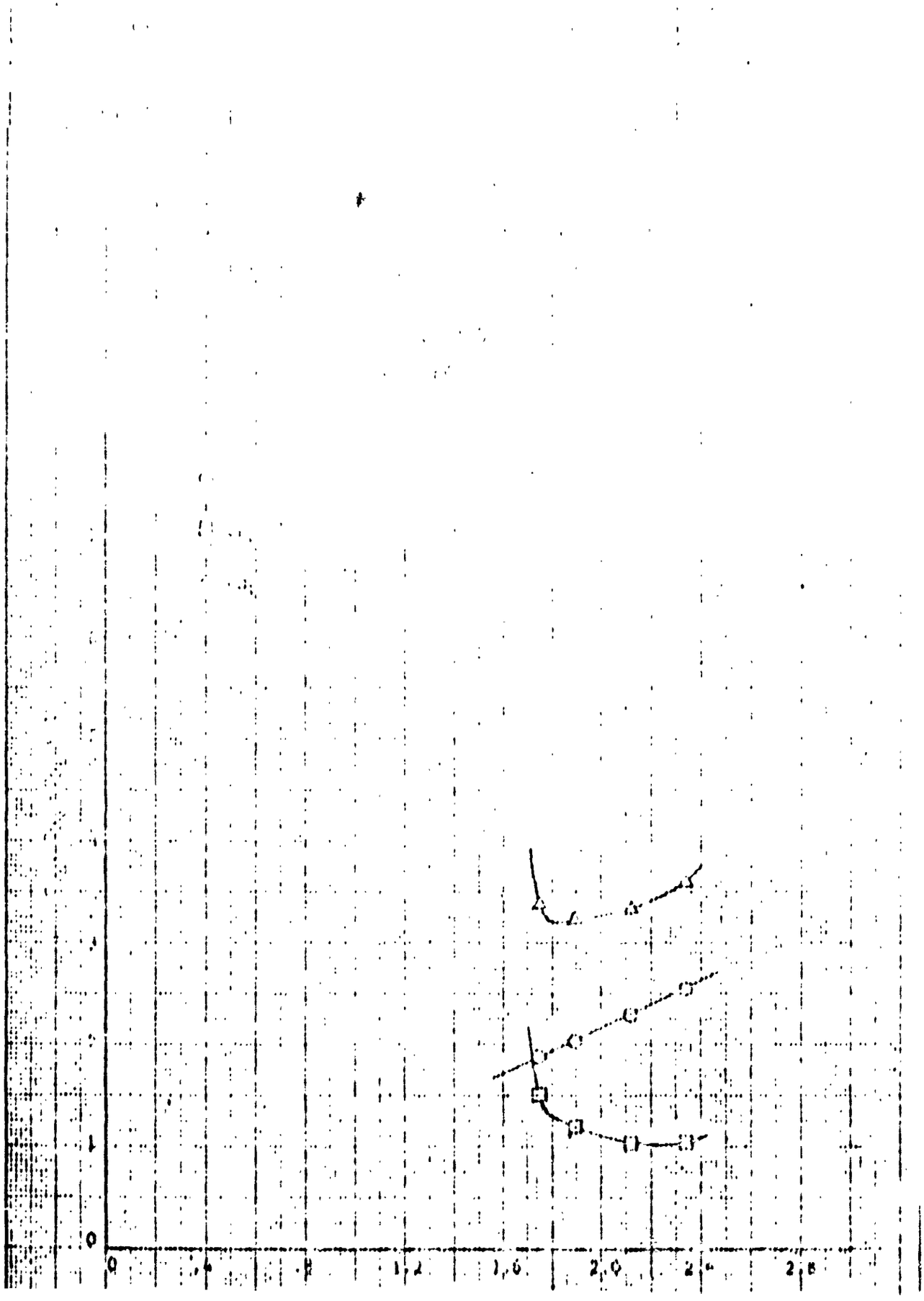
0
1
0
.4
.8
1.2
1.6
2.0
2.4
2.8

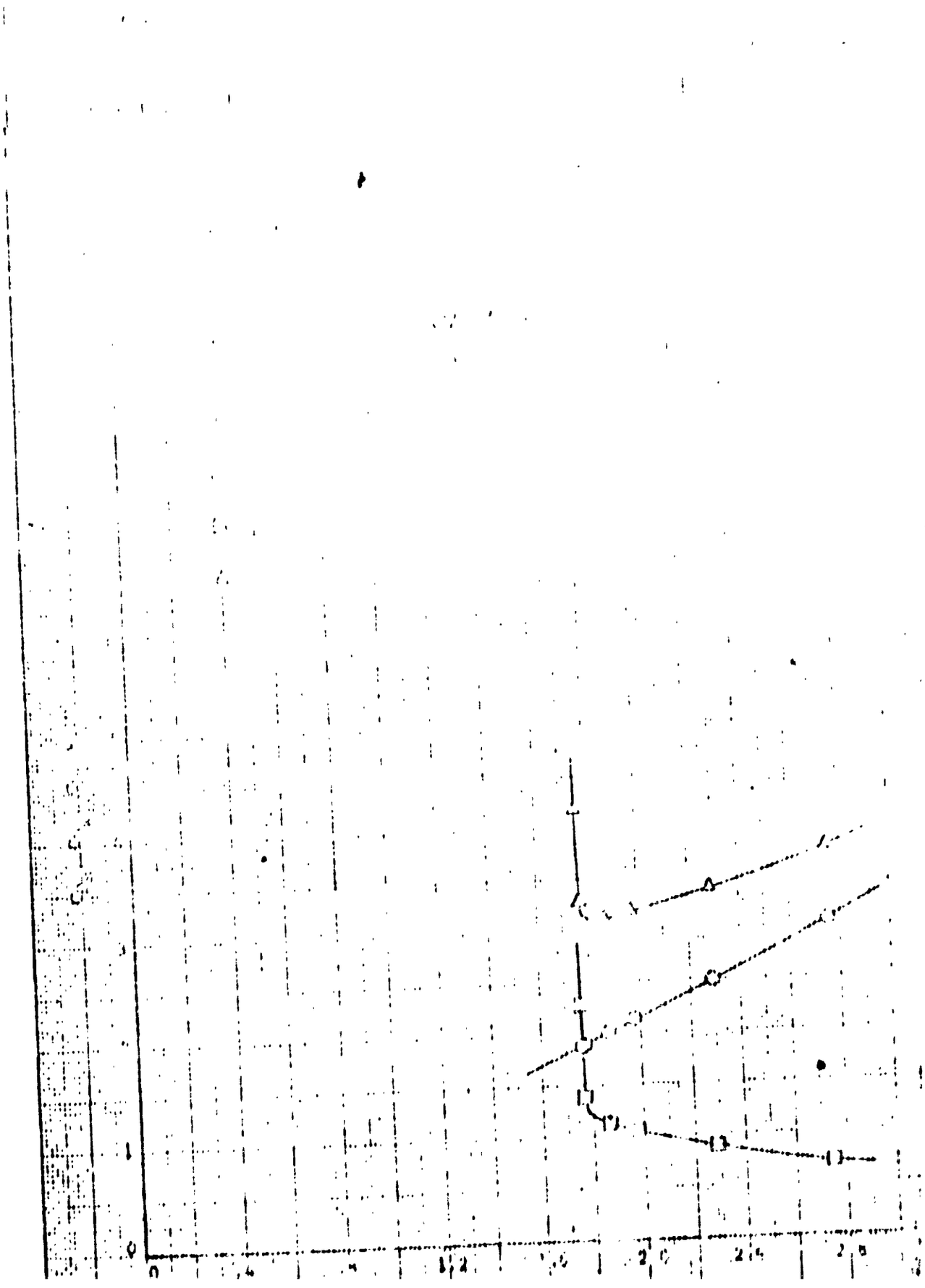

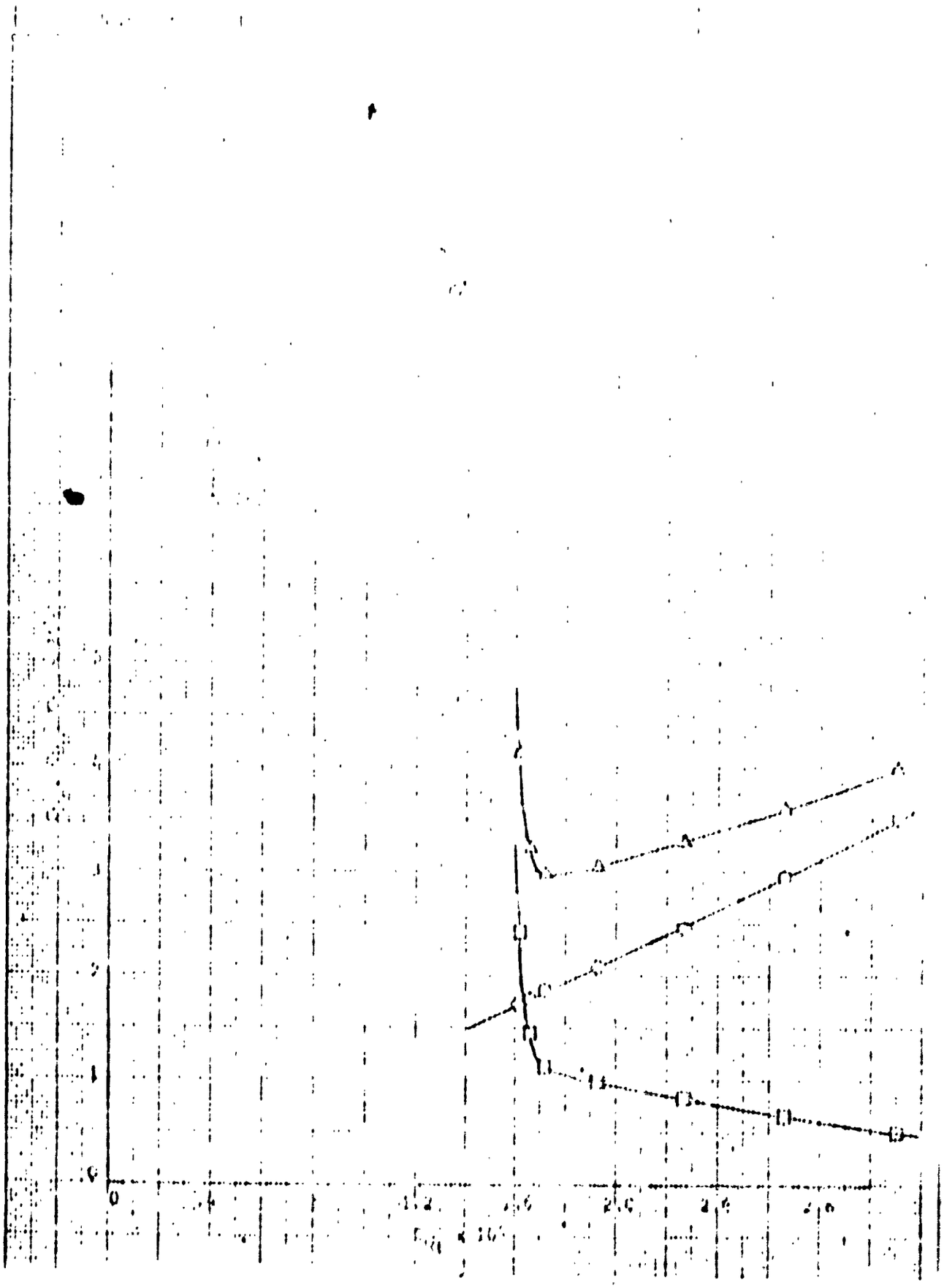

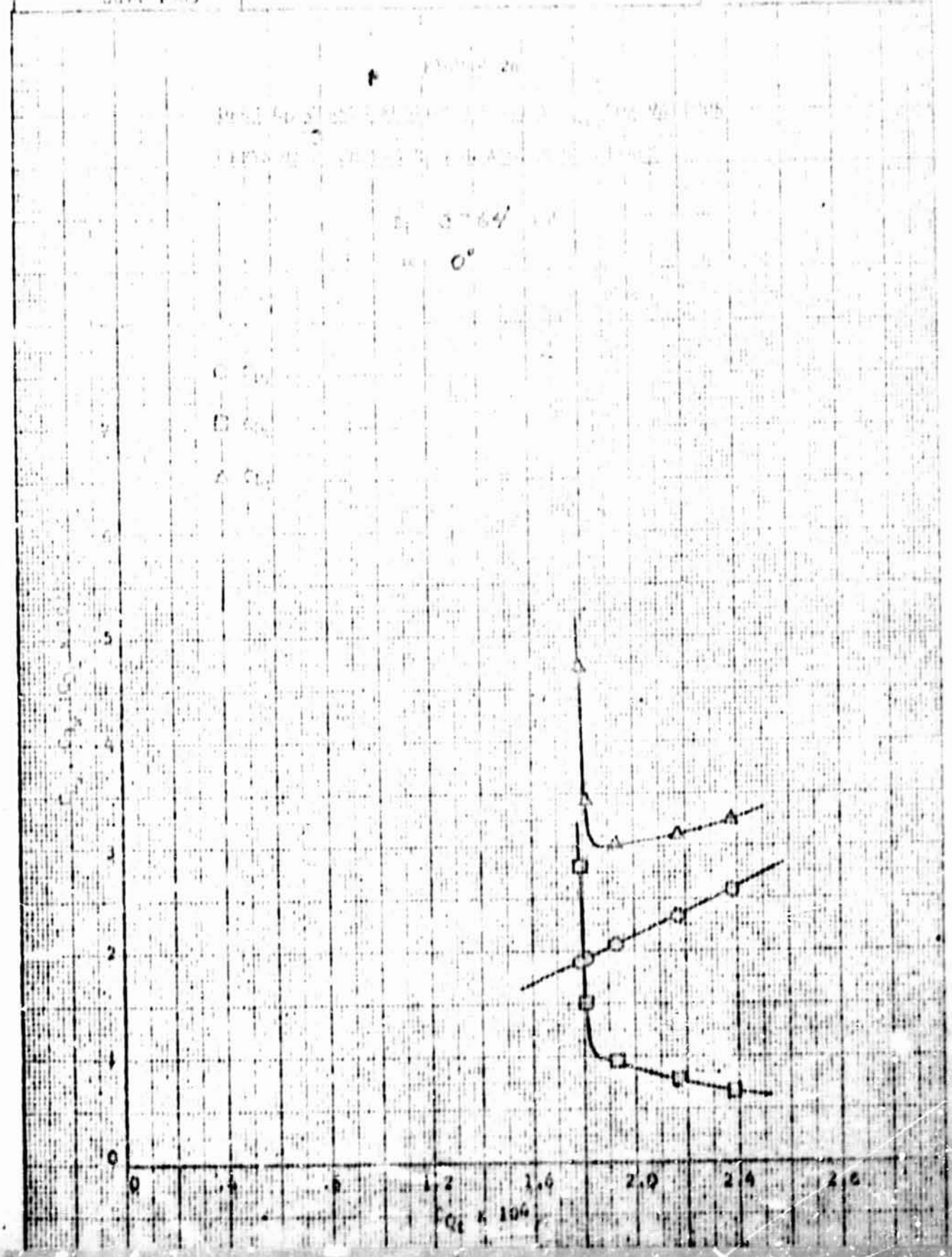
0°
.5
.4
.3
.2
.1
0
0
.4
.8
1.2
1.6
2.0
2.4
2.8

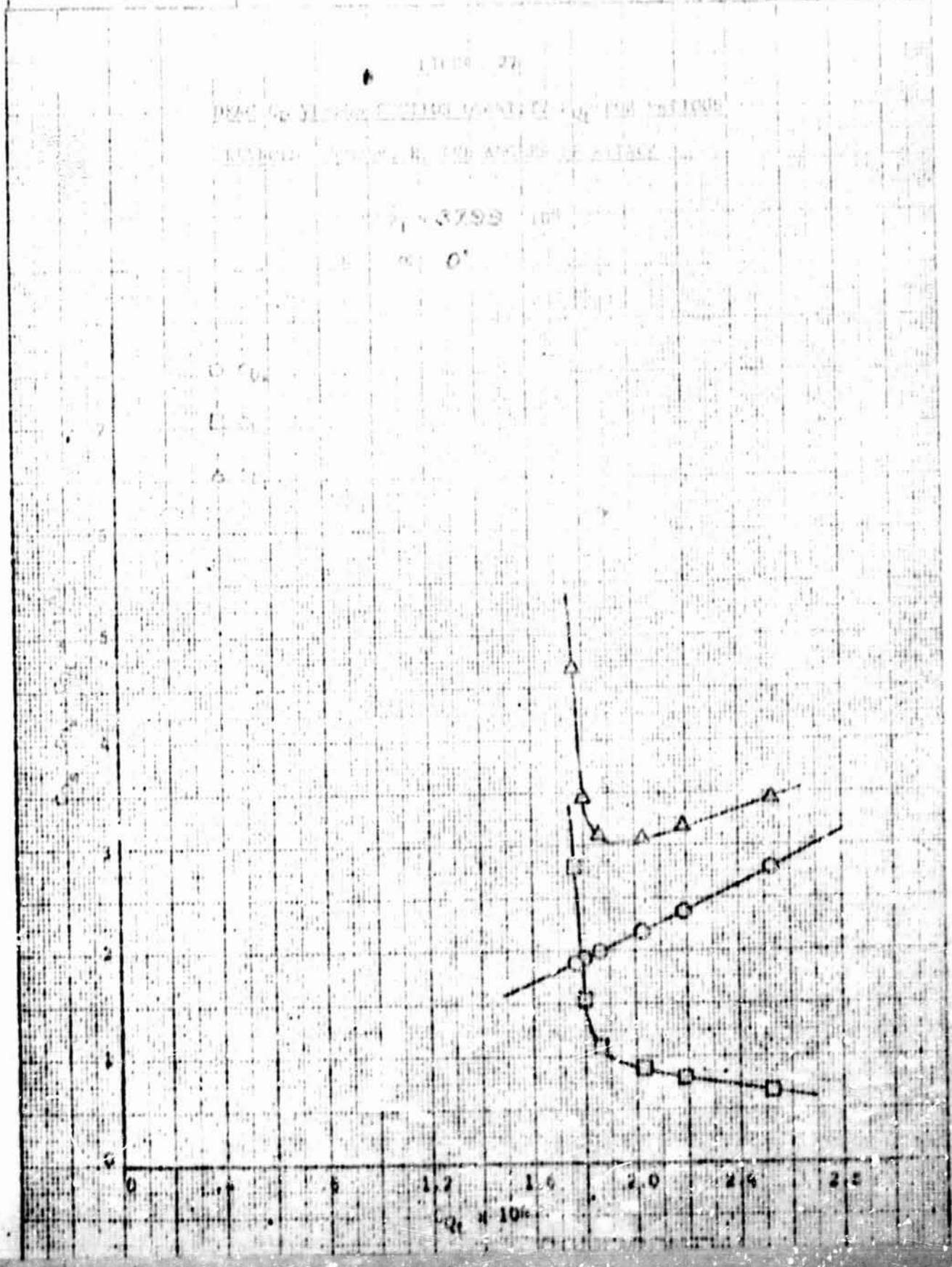

L. W. Grots
July 1963
0
.5
1.2
1.6
2.0
2.4
2.8

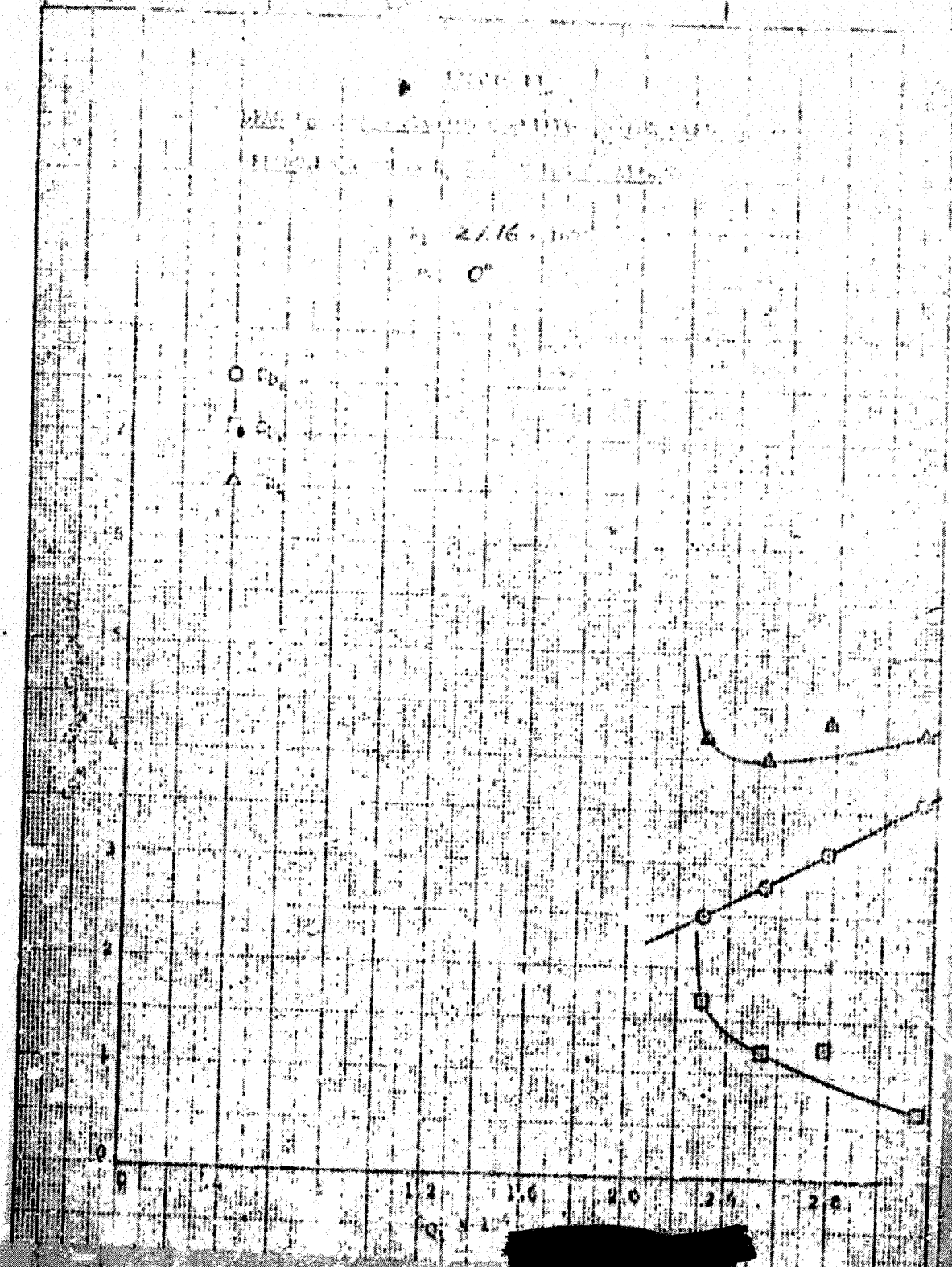

[redacted]

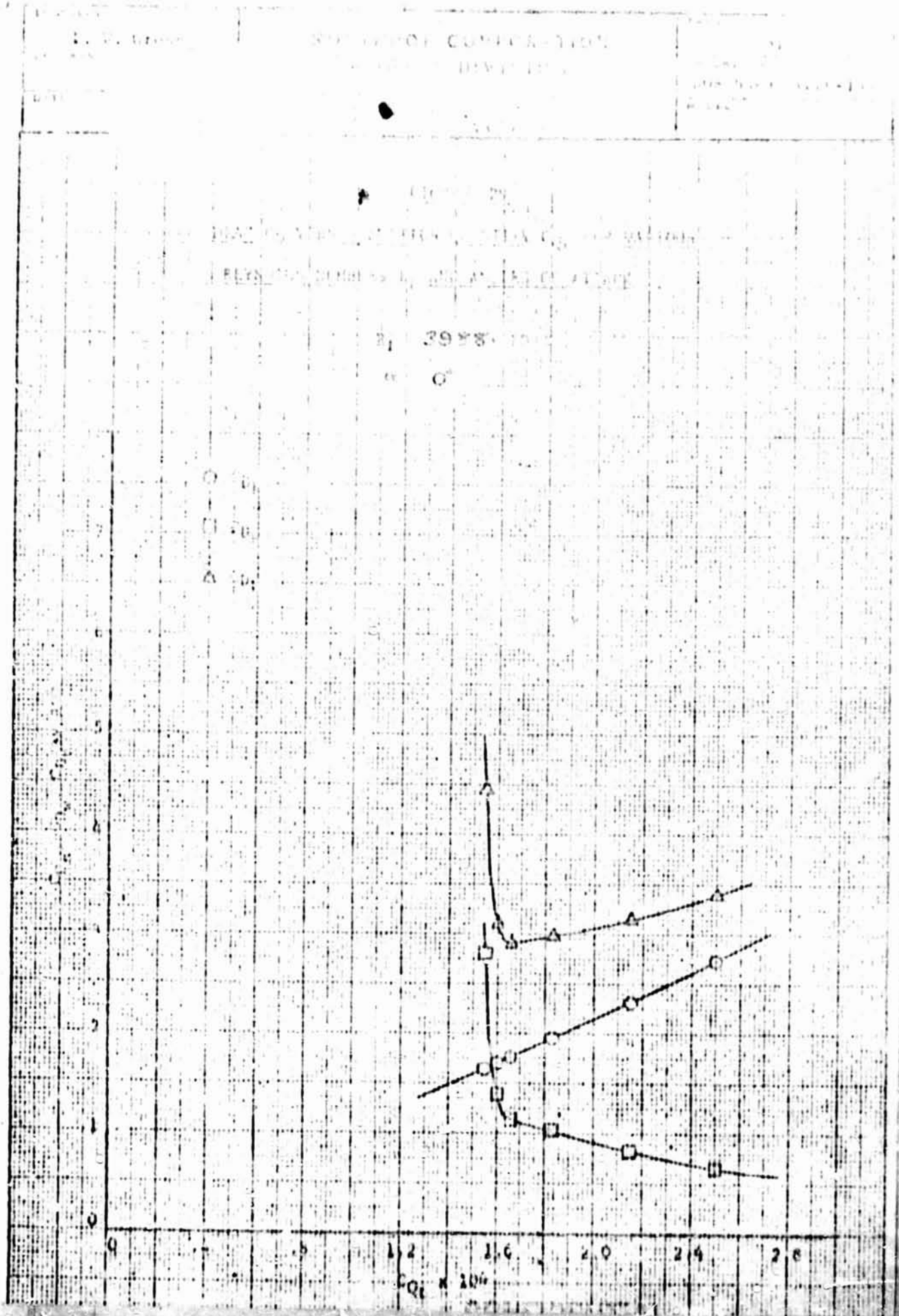

R_1 3988
α 0°
0
.5
1.2
1.6
2.0
2.4
2.8
$C_{Q_t} \times 10^4$

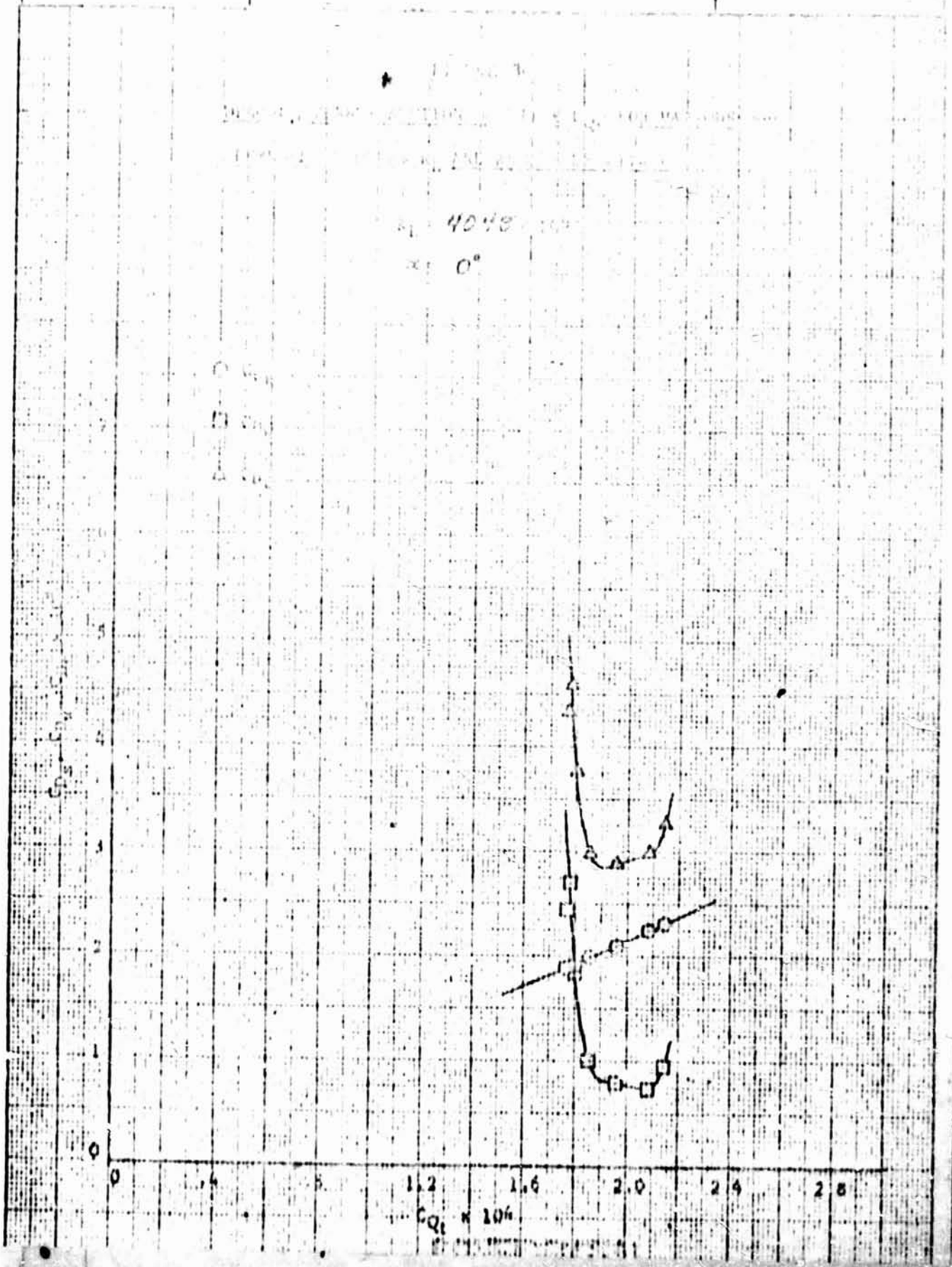
0
.4
.8
1.2
1.6
2.0
2.4
2.8
$C_{Q_t} \times 10^4$
0
1
2
3
4
5

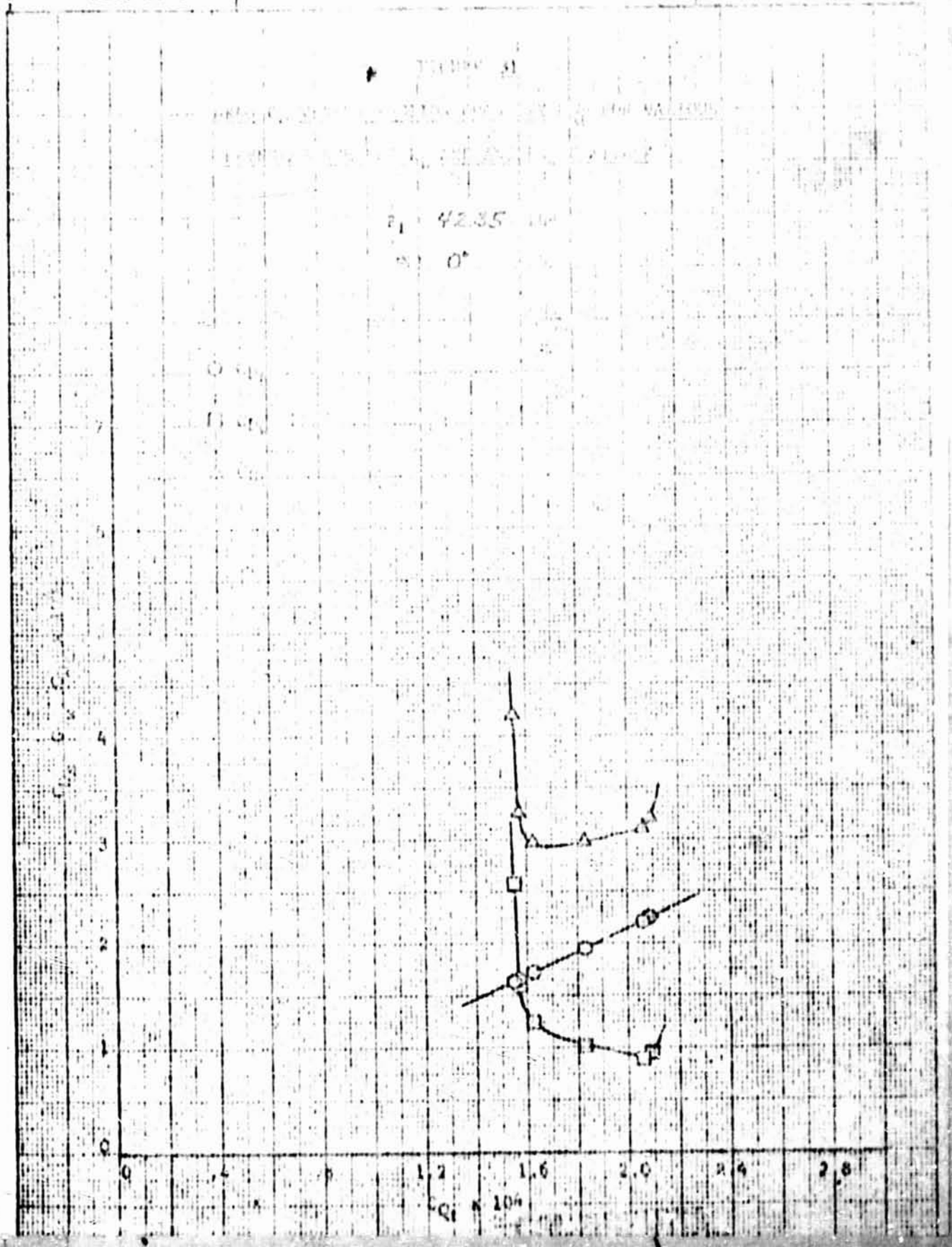
0
1
2
3
4
5
6
7
0
.4
.8
1.2
1.6
2.0
2.4
2.8

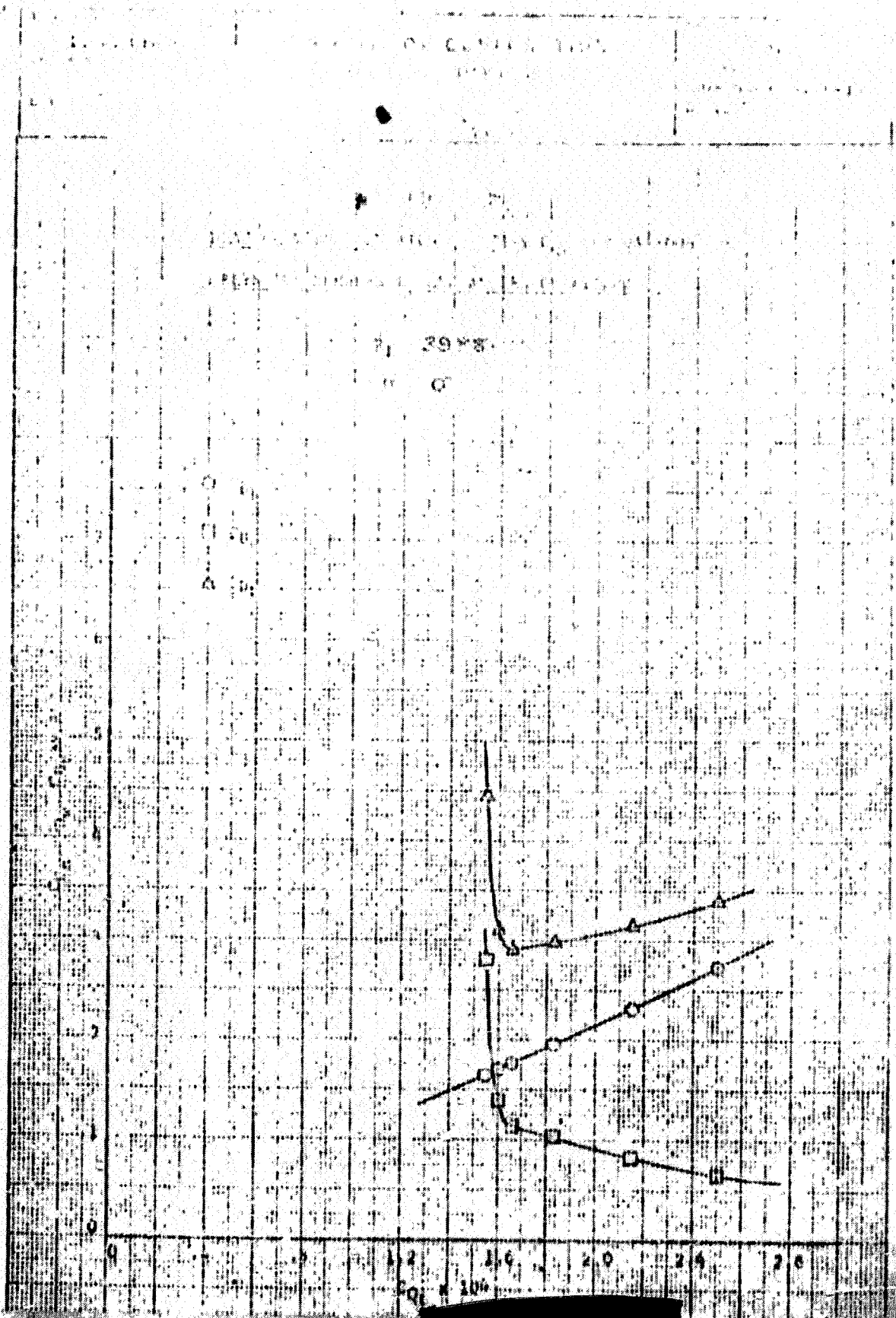

[redacted]

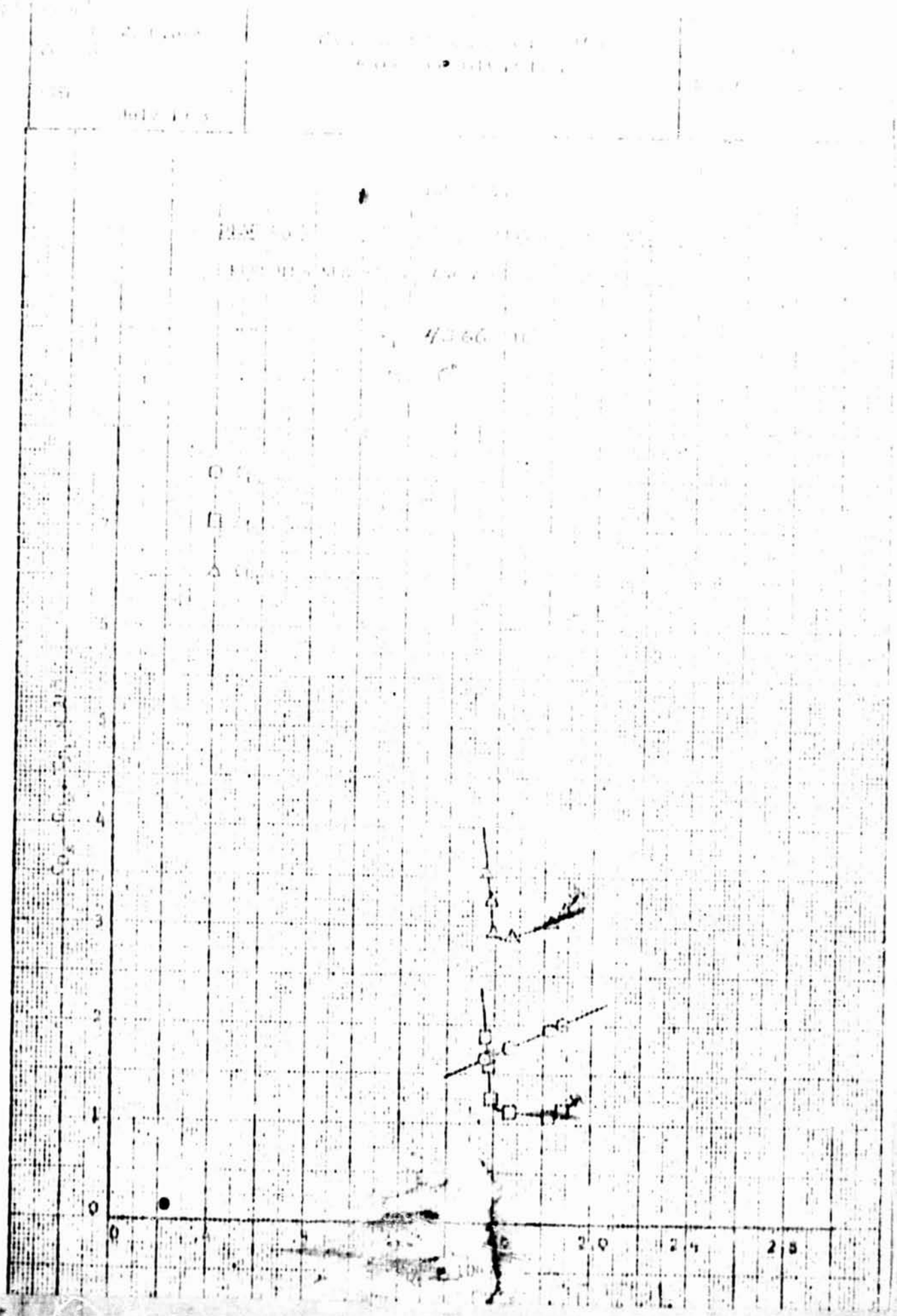
0
1
2
3
4
0
2.0
2.5

1
0
0
1.2
2.0
2.4
2.8

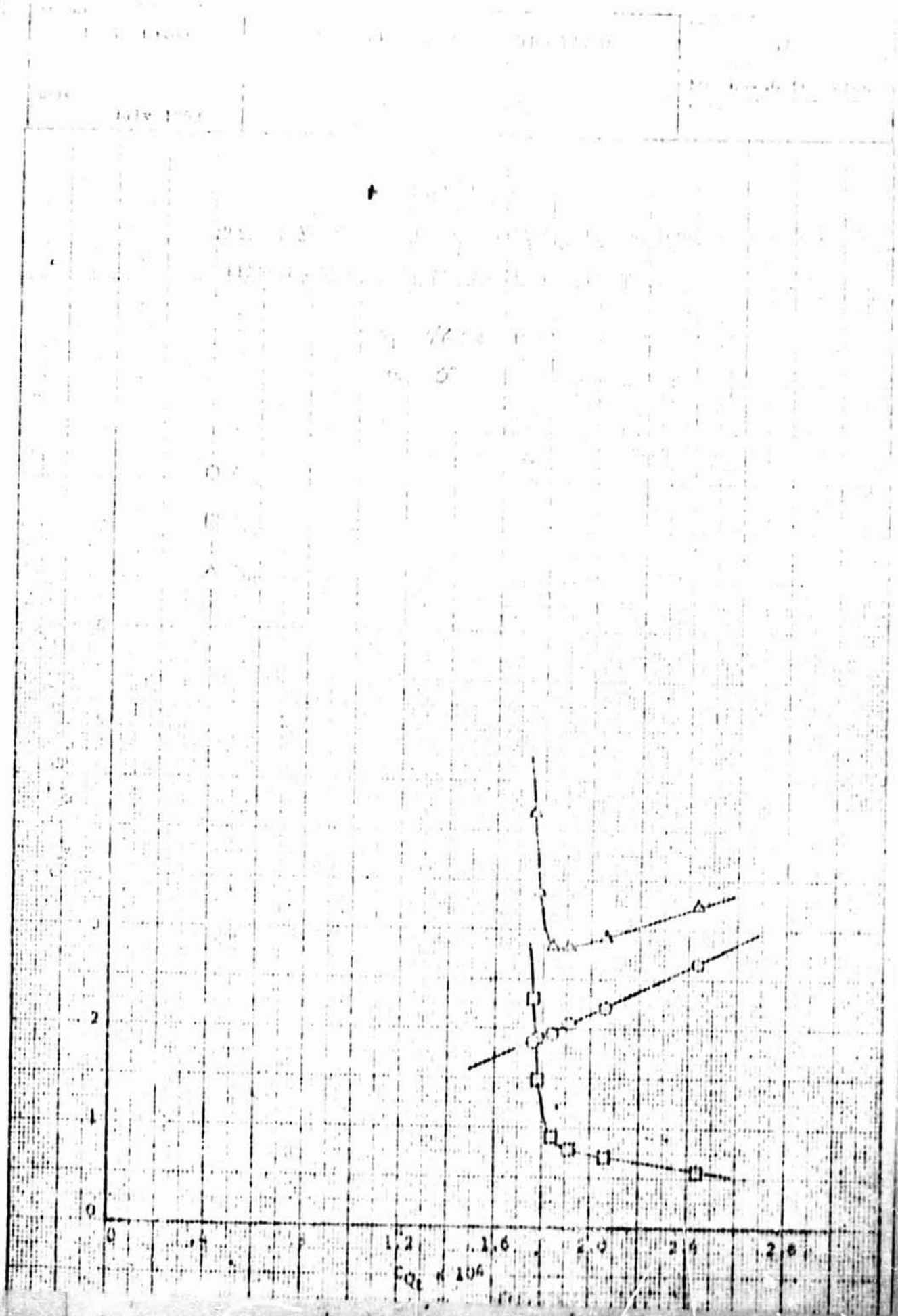

2
1
0
0
1.2
1.6
2.0
2.4
2.8

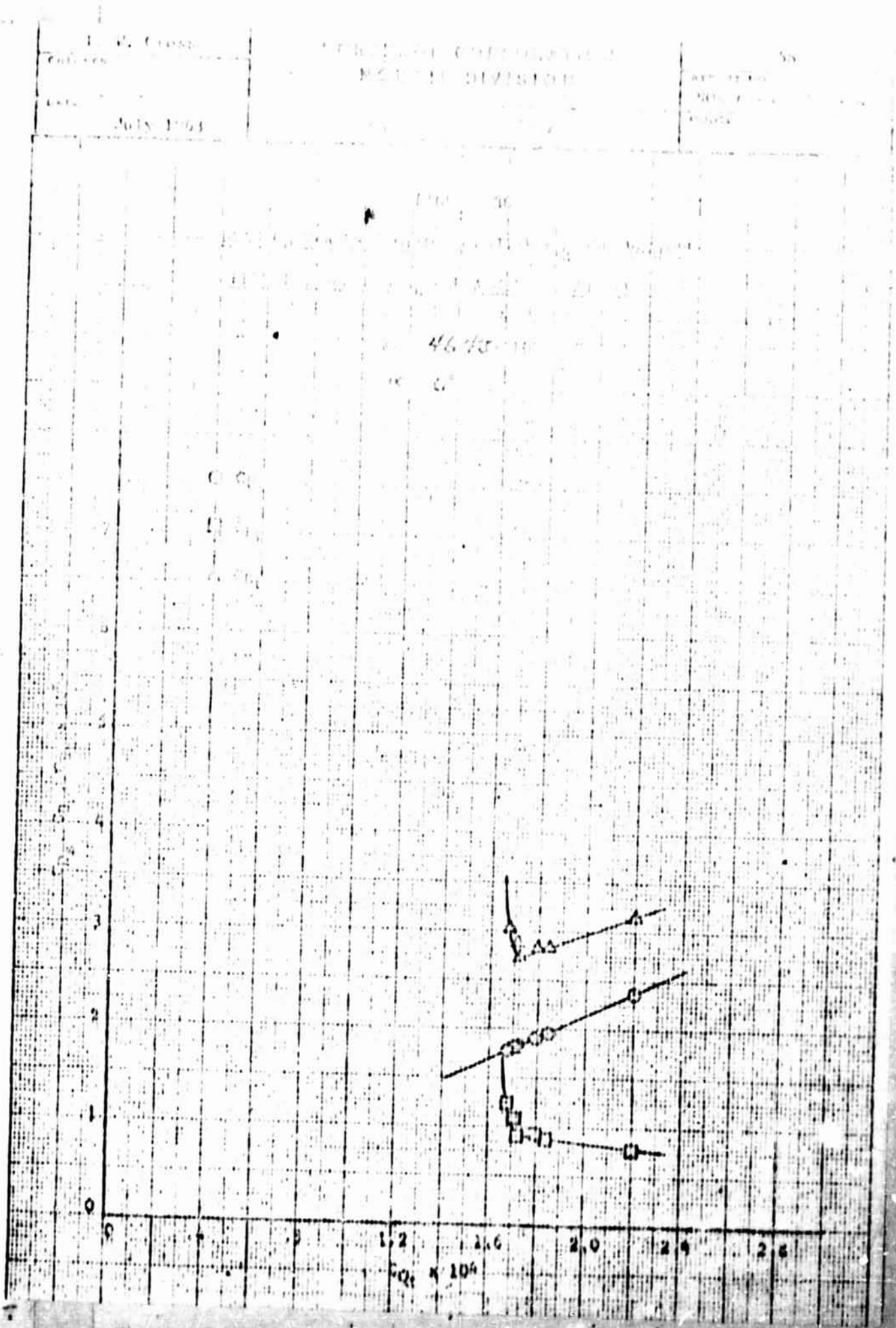

July 1963
0
1
2
3
4
1.2
1.6
2.0
2.4
2.8

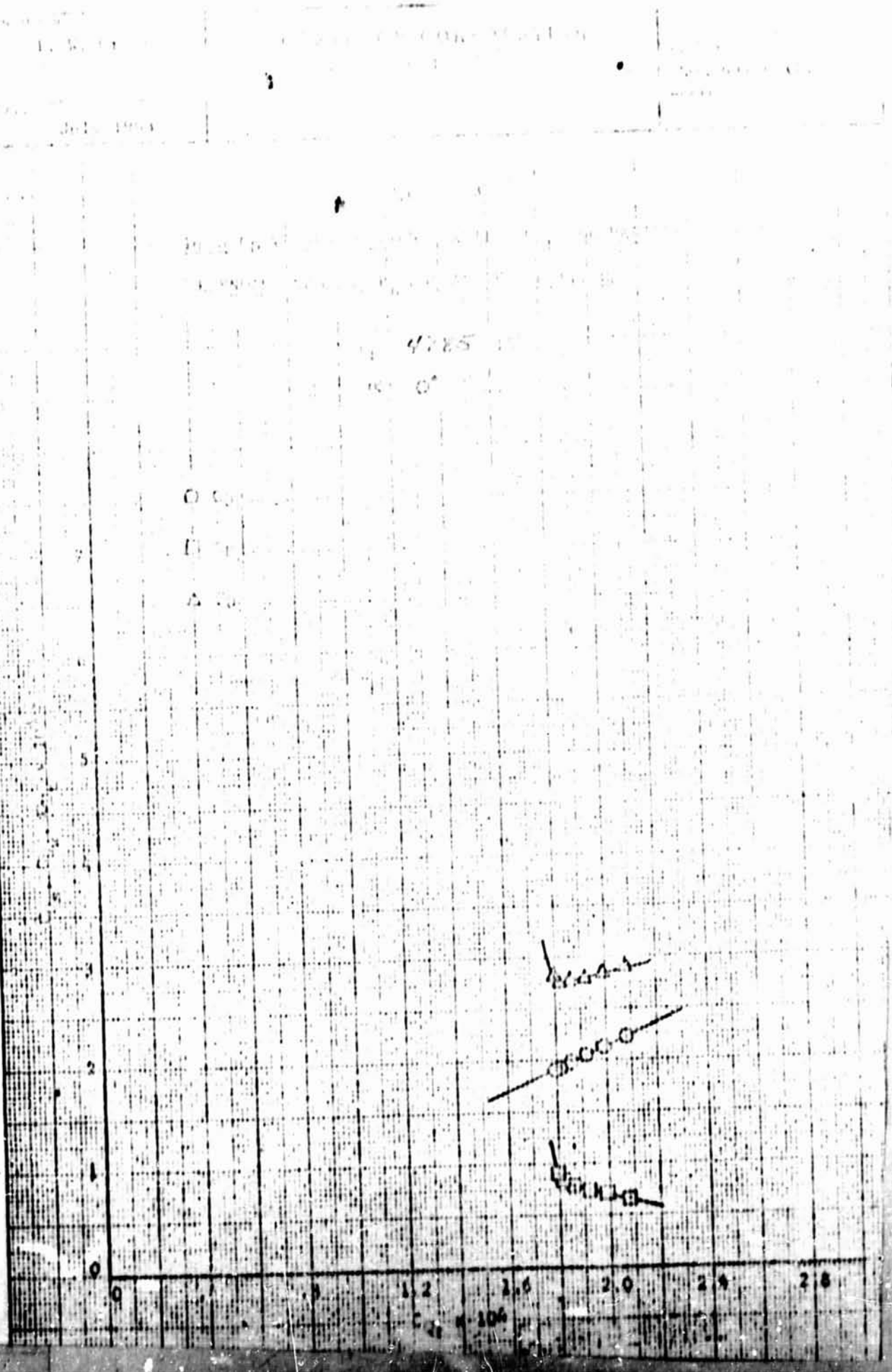
0
1
2
3
4
5
0
1.2
2.0
2.4
2.8